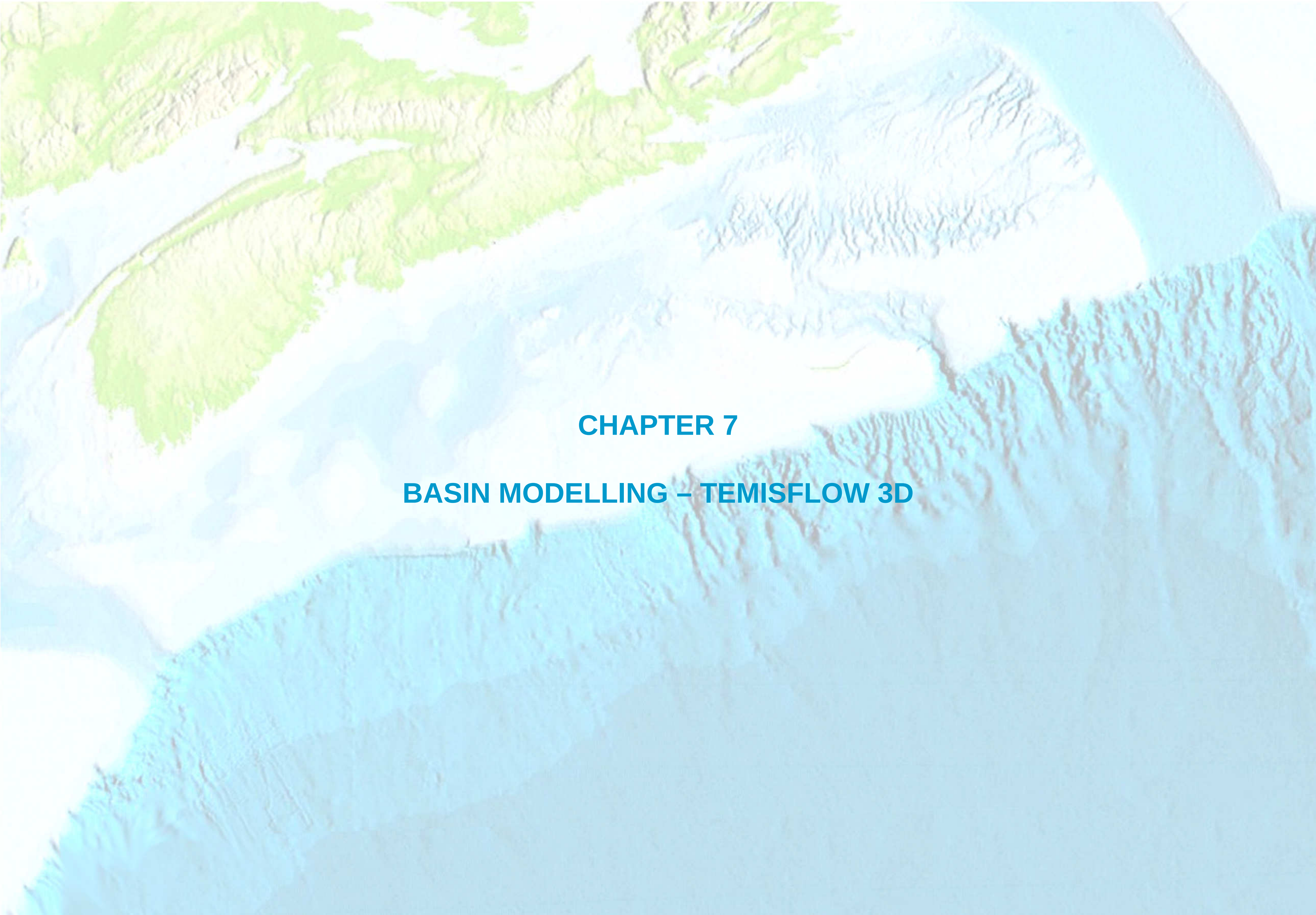

CHAPTER 7

BASIN MODELLING – TEMISFLOW 3D

Play Fairway Analysis Offshore Nova Scotia TEMIS 3D® Basin Modeling – INTRODUCTION

→ **Objectives**

- Active petroleum systems description
- Petroleum system chart definition
- Evaluation of basin scale source rock potential
- **In place hydrocarbon (HC) volume estimation**

Tools:

- The basin modeling software TemisFlow® to compute thermal, pressure and Darcy migration.
- Trap Charge Assessment (TCA®) tool to evaluate volumes in place.

→ **Input data:**

- Seismic data (chrono-structural interpretation in depth) from PFA 2011 + reinterpreted data (2016).
- Sedimentological data (Dionisos® results and other synthesis) from PFA 2011.
- Geological synthesis (geological history, petrophysics, geochemistry, etc.) from PFA 2011.
- Temis 3D® results (calibration data) from PFA2011.

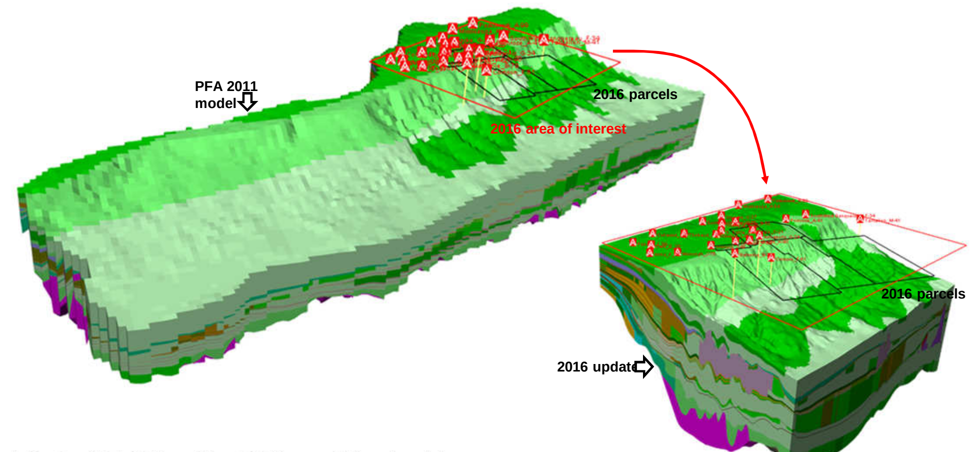

Figure 1: Regional PFA 2011 model and 2016 area of interest update.

Table of Contents

(1) Introduction to 3D Basin Modeling - 3D Block Building

Building of the 3D geological model. Compilation of structural data, sedimentological data, geochemical data, etc.

(2) 3D Maturity / Expulsion Modeling

1st modeling phase with Temis 3D®.

Modeling of the 3D block through the time (maturity and expulsion; migration not computed).
Analysis of Temis 3D® results for the definition of source rocks potential.

(3) 3D Migration Modelling / Trap Charge Assessment

2nd modeling phase with Temis 3D®.

Modeling of the 3D block through the time (migration)
Analysis of Temis 3D® results for the traps and volume estimates

Resolution of TemisFlow 3D Blocks used for this study

→Reference 3D Block, for Temperature/Pressure/Maturity Modeling

- 210*181 meshes.
- mesh resolution 1000 * 1000 m.
- 50 layers (51 horizons).
- 1750400 cells.

→ 3D Block for Darcy Migration

- 100*451 meshes .
- mesh resolution 2000 * 2000 m.
- 50 layers (51 horizons).
- 438600 cells.

Horizon	Age (Ma)	Petroleum System Element	Comment
Sea Bed	0		
Miocene	14.5		
Oligocene Unc	29		
Top Paleocene	50		
Top Wyandot	70		
Top Cenomanian Unc	94		Upper Logan Canyon
Cenomanian U. Albian	94.75		
Cenomanian U. Albian	95.5		
U. Albian	97		
Top Unc U. Albian	101		Lower Logan Canyon
Albian	104		
Albian	108		
Aptian	112		
Aptian	116		
Aptian	120		
Top Naskapi	122.5		Upper Missisauga
Top Barremian	125		
Barremian	126.3		
Barremian	127.5		
Barremian	128.8		
Top Hauterivian	130		Middle Missisauga
Hauterivian Valanginian	130.5		
Hauterivian Valanginian	131		
Hauterivian Valanginian	132		
Hauterivian Valanginian	133		
Hauterivian Valanginian	134		
Hauterivian Valanginian	135		
Top Allochtonous Salt	136.5		

Horizon	Age (Ma)	Petroleum System Element	Comment
BCU	137		Lower Missisauga
Valanginian Berriasian	139		
Valanginian Berriasian	142		
Valanginian Berriasian	145		
Top Allochtonous Salt	148		
Top Tithonian SR	149.5		
Tithonian	149.8		
Top Baccaro Mic Mac	150		
Base Baccaro	151		
Ind Baccaro	155		
Ind Baccaro	156.5		
Banquereau	158		
Top Allochtonous Salt	160.5		
Base Allochtonous Salt	161		
Top Scatarie	163		
Mid Jurassic	170		
Top Toarcian SR	182		
Base Toarcian	183		
Top Pliensbachian SR	189		
Base Pliensbachian	190		
Top Sinemurian SR	196		
Top Salt Autochtonous	197		
Top Basement	200		

— Seismic horizon

Syn rift sediments are present below the autochtonous salt but they have been included in the advanced basement as they are not interpreted.

Table 1: Stratigraphic Chart of the TemisFlow™ 3D Model.

CHAPTER 7.1

BASIN MODELLING – 3D BLOCK BUILDING

Structural Maps from Seismic Interpretation

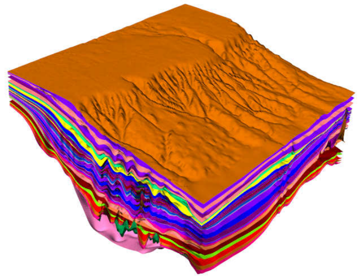

→ Update from the 2016 interpretation
→Correction and smoothing.
→ Identification of salt bodies.
→ Additional subdivisions for:
- Reservoirs
- Source rocks (with effective thickness maps)
- Refining of sedimentary sequences (automatic subdivisions proportional to age)
- Technical subdivisions (refining time steps)
→ Restoration through time.

PFA 2011

→ Coherency between the two models (data and results)
→ Crust model and rifting

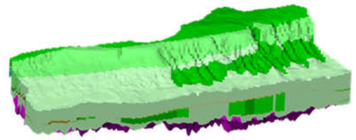

Geological Data

→ Geological context
→ Geological history
→ Deep geophysics
→ Geochemical data
→ Well log data
→ Petroleum field data

Source Rocks Parameter

- Kerogen types
- Chemical kinetics
- TOC

Thermal boundaries

- Surface temperature history
- Thermal basement (lithosphere modelling)
- Rifting history

TEMISFLOW 3D® Block

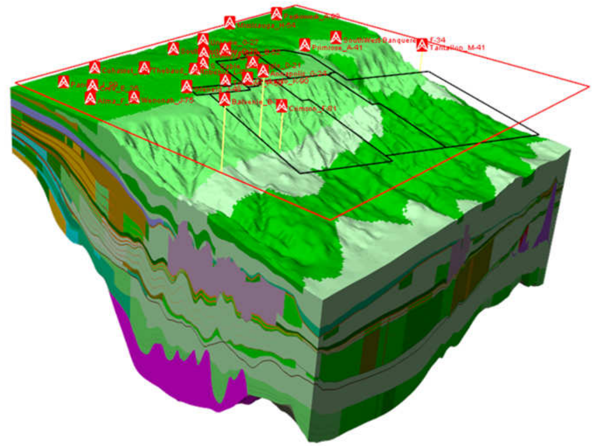

*GRID RESOLUTION = 1 * 1km*

PRESSURE / TEMPERATURE / MATURITY MODELLING

Calibration Phase

- Pressure
- Temperature
- Maturity

SR Modelling

- Present day maturity level
- Maturity history
- Expelled volumes

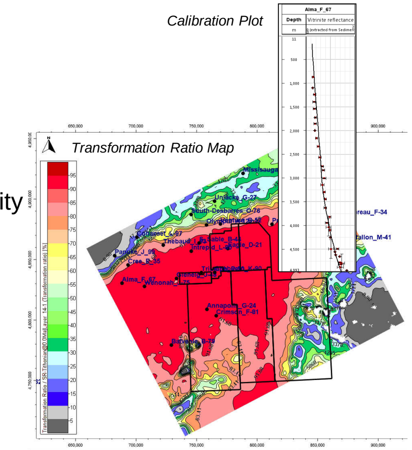

1st Modelling Phase

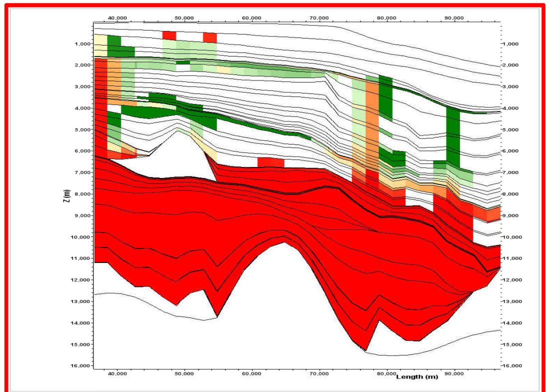

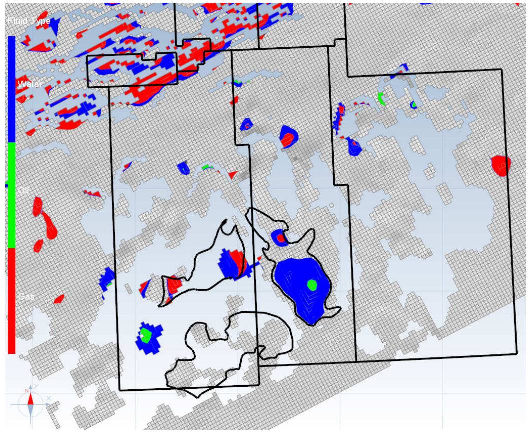

HC MIGRATION MODELLING

Traps and Hydrocarbon Volume Estimate

- Complete Darcy Migration taking into account all of the model on an upscaled version (2 * 2km resolution).
- Redistribution of HC volumes with the Trap Charge Assessment tool.
- In place hydrocarbons (mass, volume, composition, etc.)

2nd Modelling Phase

Model Building - Salt

- Dimension: 1 * 1km.
- Model skeleton was built using depth-interpreted horizons corrected from crossings and canopies.
- Allochthonous and autochthonous salt were built as specific horizons, honoring the seismic horizon geometry.
- Salt canopy was built using specific lithology with editing of certain horizons to fit the top/base canopy from seismic horizons. This was done due to the complexity of the salt canopy.
- Uplift under salt diapirs were corrected using an interpolation algorithm.
- Three levels of allochthonous salt + canopy (see Figures 2 and 3).

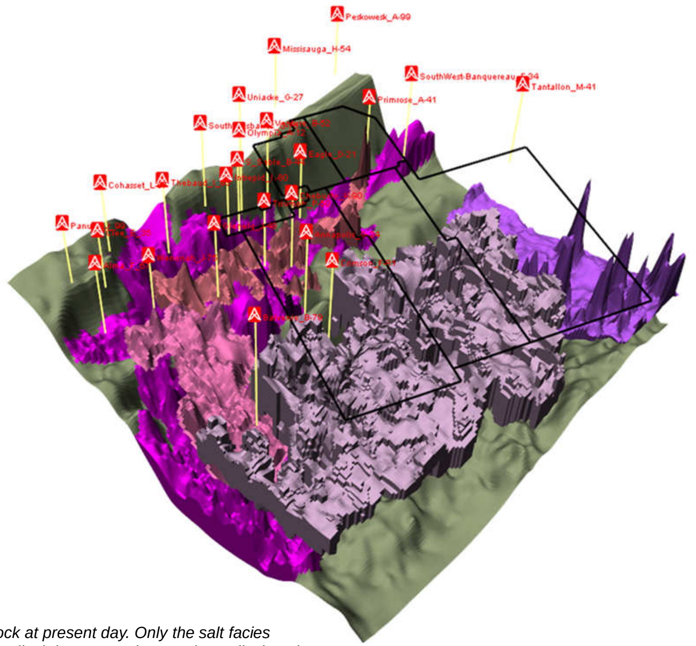

Figure 2: 3D Block at present day. Only the salt facies (autochthonous, allochthonous and canopy) are displayed.

Salt Restoration

- Salt restoration was completed according to tectonic evolution (Weston et al., 2012), sedimentation and paleobathymetry.
- Salt volume is considered approximately constant through time (42*E12 m^3), summing the volumes of all present day salt bodies. However, the canopy volume is an approximation due to geometric uncertainties (seismic resolution).
- Structures under the salt were maintained through time.
- Three allochthonous salt levels:160My (Banquereau Wedge), 147My and 137My.
- Canopy formation starts at 101 Ma and ends at 50 Ma where no additional salt movement is assumed.

Figure 3: Salt evolution through time with diapirism and salt canopy formation.

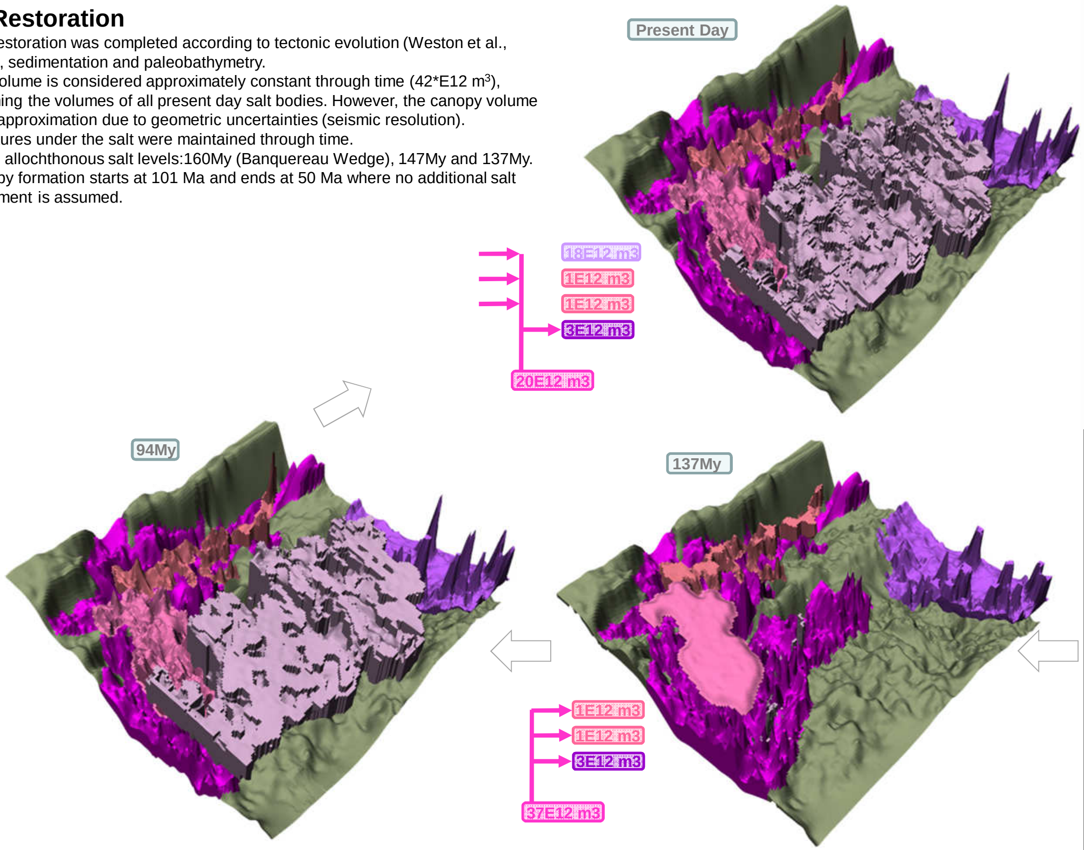

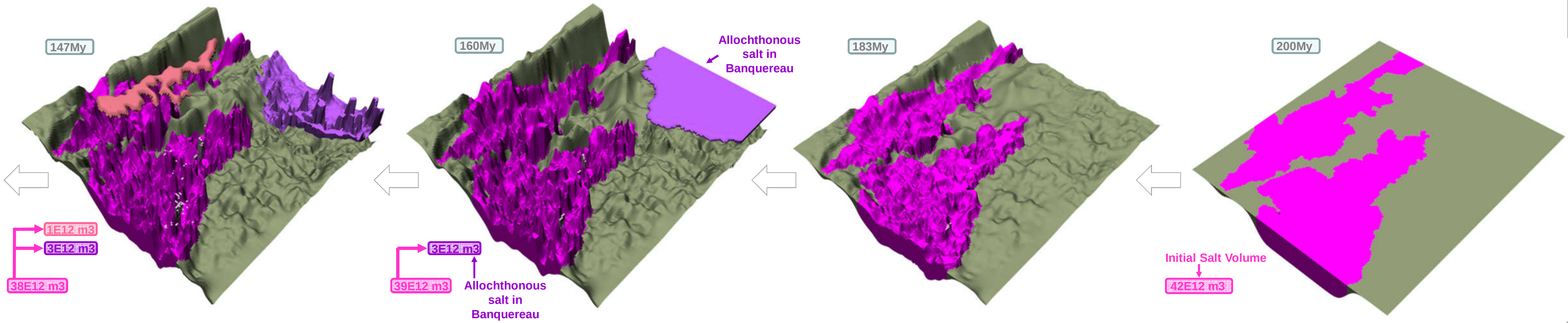

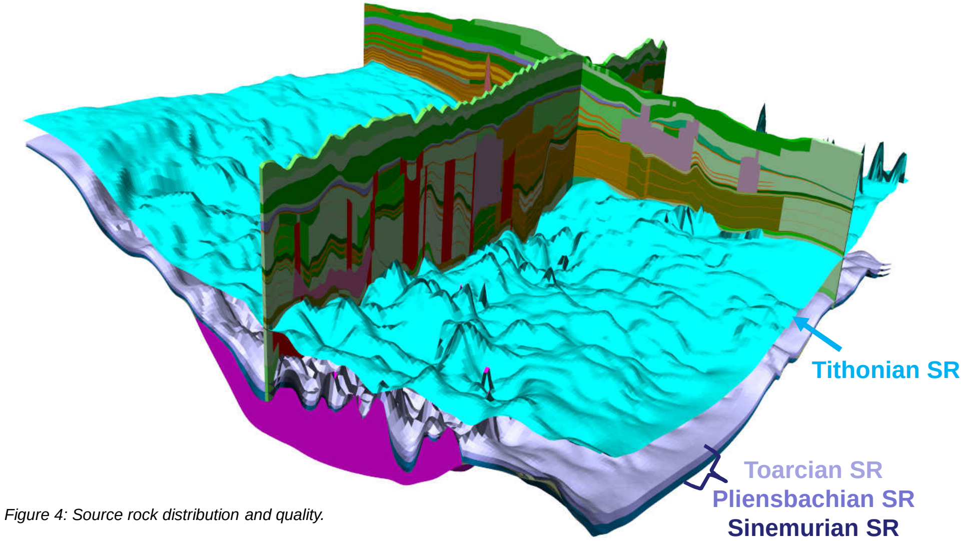

Figure 4: Source rock distribution and quality.

Four Source Rocks in the 3D Block.

The thickness and richness of the different source rocks considered in the model are presented in the Figure 4.

For each source rock (SR), the "Source Rock Thickness" corresponds to the cumulative thicknesses of organic-rich intervals ("effective source rock thickness"). This thickness is estimated with well geochemical data (rock eval. data) and structural data from the 2011 PFA study. The thickness of the Lower Jurassic Complex SR is speculative.

With respect to the depositional context, each SR is considered as a single organic-rich layer with a constant thickness in the 3D model.

Source rock petrophysical facies were defined as a specific shaly facies (to help expulsion).

Total Organic Carbon (TOC) is assumed to be a constant value (see table below) where the depositional context allows the presence of a source rock.

	Source Rock	Age	Type	Thickness	TOC	IH	Distribution
Upper Jurassic	Tithonian	150Ma	TYII-III	20 meters	5%	424mg/gC	homogeneous
Lower Jurassic Complex	Toarcian	182Ma	TYII	10 meters	2,5%	600mg/gC	homogeneous
	Pliensbachian	189Ma	TYII	10 meters	2,5%	600mg/gC	homogeneous
	Sinemurian	198Ma	TYII-S	10 meters	5%	600mg/gC	homogeneous

Table 2: Source Rock (SR) description with deposition age, TOC, IH and kerogen type.

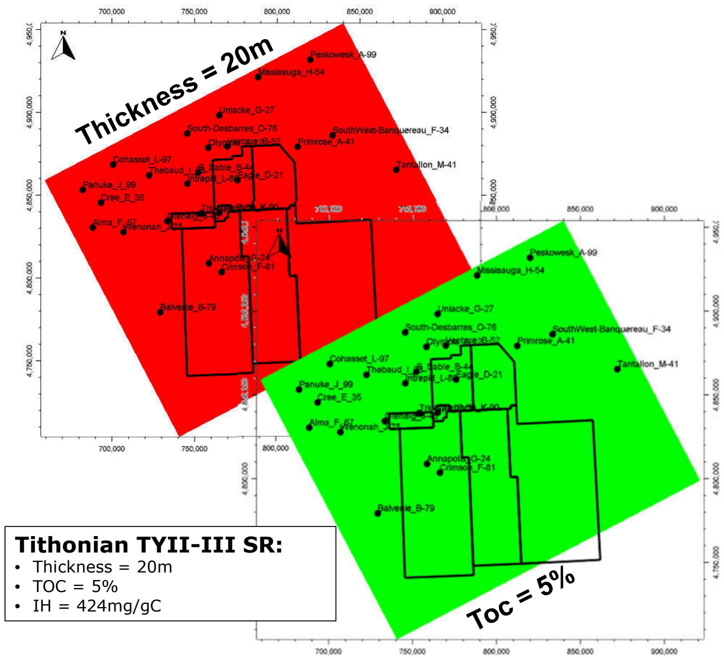

Tithonian TYII-III SR:
- Thickness = 20m
- TOC = 5%
- IH = 424mg/gC

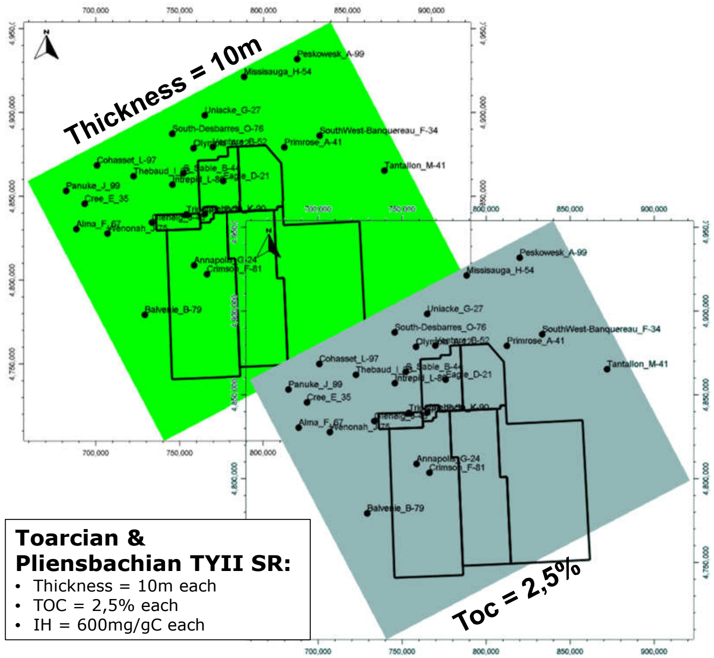

Toarcian & Pliensbachian TYII SR:
- Thickness = 10m each
- TOC = 2,5% each
- IH = 600mg/gC each

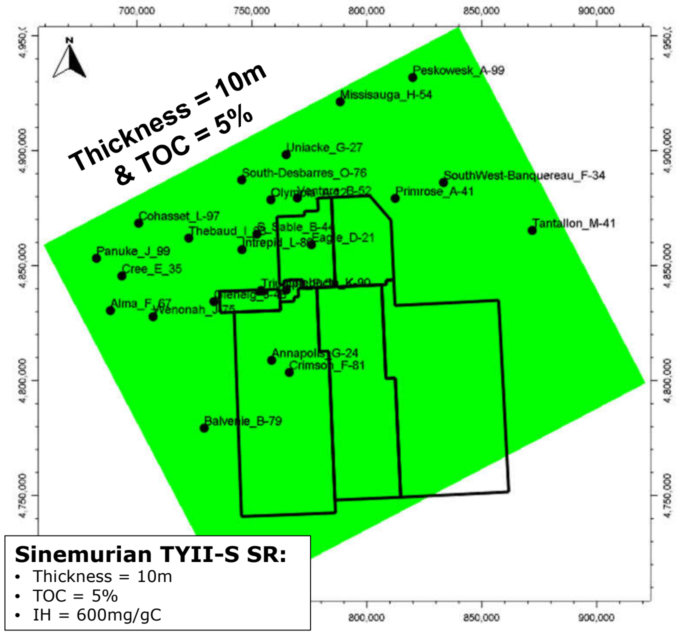

Sinemurian TYII-S SR:
- Thickness = 10m
- TOC = 5%
- IH = 600mg/gC

Name	Kerogen	Molar Weight[g/mol]	Compound Type	Mobility	Default Phase	Thermal Stability
6_Coke		18.04	SOLID_OM	IMMOBILE	LIQUID	STABLE
5_C1-biogenique		16.0	HYDROCARBON	MOBILE	VAPOR	STABLE
4_GAS-Thermogenic		18.0	HYDROCARBON	MOBILE	VAPOR	STABLE
3_OIL-Condensate		120	HYDROCARBON	MOBILE	LIQUID	UNSTABLE
2_OIL-Normal		230	HYDROCARBON	MOBILE	LIQUID	UNSTABLE
1_OIL-Heavy		300	HYDROCARBON	MOBILE	LIQUID	UNSTABLE

Table 3: Six class scheme used in the study.

Chemical Scheme

- IFP 6 classes – 5 mobile fractions, edited from IFPEN default library and from the 2011 PFA study, used in the model (Table 3).
- Maturation of initial kerogens can generate six families of chemical components.
- Two gas families (thermogenic and biogenic if necessary), three oil families (from the heavier compounds to the lighter) and coke (considered only in the secondary cracking).
- A "mobile" fraction can migrate in reservoir layers, while an "immobile" fraction is solid or very viscous and remains in the layer where it was generated.
- An "unstable" chemical fraction can be altered by secondary cracking. The secondary cracking generates lighter mobile compounds and immobile residual coke.

Name	Reference density[kg/m^3]
5_C1-biogenique	0.6678
4_GAS-Thermogenic	50.0
3_OIL-Condensate	780
2_OIL-Normal	860
1_OIL-Heavy	980

Table 4: HC class densities at surface conditions.

Average Densities at Surface Conditions (for the five mobile hydrocarbons classes)

Density is empirically defined for each fraction, and calibrated with API gravity observed in the Nova Scotia Basin (PFA 2011).

- The gas densities are clearly affected by the presence of methane which is dominant in the Sable Sub-basin where calibration is possible.
- Note that densities (and other parameters not presented here such as PVT parameters) are averaged values for each fraction.
- These values are used for the calculation of volumes in surface conditions (0.1 MPa, 20°C).

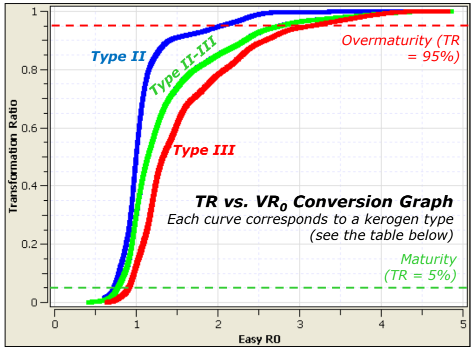

Relationship TR/Vitrinite	TR=5% Oil Window	TR=50%	TR=95% Overmaturity
Kerogen Type II	VR_0 = 0.7	VR_0 = 0.9	VR_0 = 2
Kerogen Type II-III	VR_0 = 0.75	VR_0 = 1	VR_0 = 2.7
Kerogen Type III	VR_0 = 0.8	VR_0 = 1.2	VR_0 = 3.2

Graph and Table 5: Relation Between TR and Vitrinite by Kerogen Types.

Transformation Ratio vs. Vitrinite Reflectance

The Transformation Ratio (TR) corresponds to the fraction of initial kerogen that has been affected by maturation reactions. It is expressed in percent:

TR = observed HI / initial HI

The TR is representative of the maturity level of a given kerogen (and consequently of a source rock), while the vitrinite reflectance/EasyRo is an absolute maturity index, not specific to a kerogen type.

The correspondence by kerogen type is shown in the graph and Table 5.

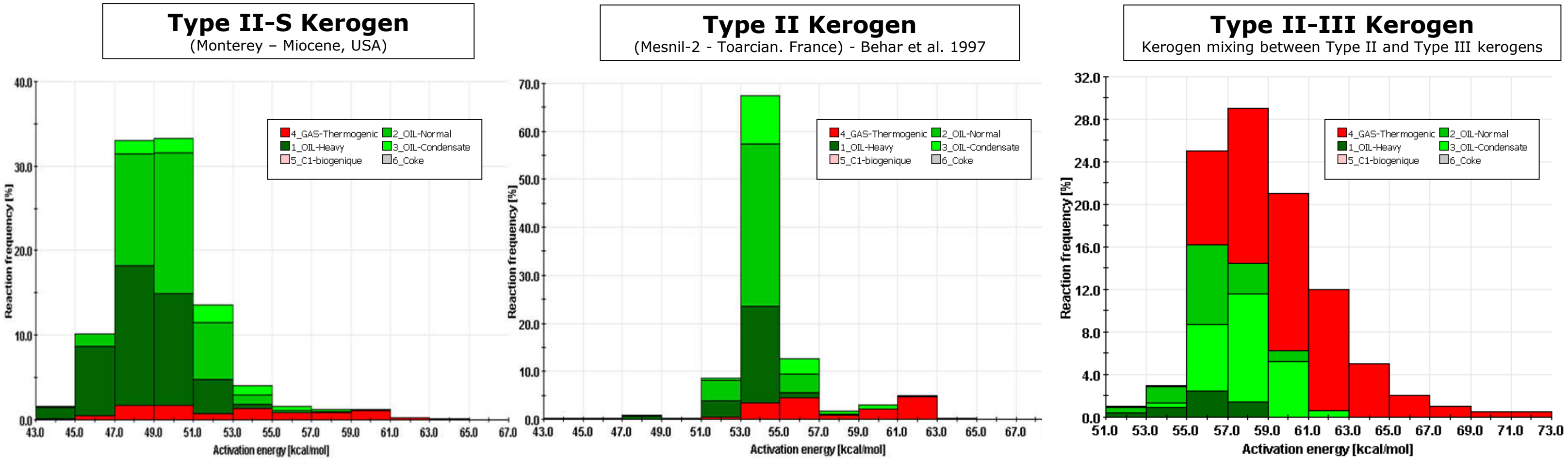

Figure 5: Different kinetic schemes used in the study.

Compositional Kinetic Scheme

- Kerogen maturation follows "kinetic schemes" specific to each kerogen type.
- The maturation process is divided into "n" parallel chemical reactions which have their own reaction speeds. Reaction speed is calculated using Arrhenius' Law and depends on the Activation Energy, the Arrhenius Coefficient (specific to each chemical reaction), and the temperature. Each reaction generates chemical fractions defined by the chemical scheme.
- Figure 5 details the three kinetic schemes used in this study (Type III, Type II-III, Type II). These schemes were edited from the IFPEN Default Library (specific data is not available for Nova Scotia).
- Secondary cracking reactions follow the same kinetics laws.

Secondary Cracking

Following Arrhenius' Law, each unstable component can generate new chemical fractions that can be stable or unstable (and so may generate lighter components until complete secondary cracking if the conditions are favorable).
Table 6 details the three kinetic schemes used in this study (heavy oil, normal oil and condensate). These schemes were edited from the IFPEN Default Library (specific data not available for Nova Scotia).

Name	Activation Energy[kcal/mol]	Pre-exponential Factor[1/s]	1_OIL-Heavy[%]	2_OIL-Normal[%]	3_OIL-Condensate[%]	4_GAS-Thermogenic[%]	5_C1-biogenique[%]	6_Coke[%]
1_OIL-Heavy	48	1E10		40	15	5	0	40
2_OIL-Normal	50.5	1E10	0		55	30	0	15
3_OIL-Condensate	66.5	3.85E16	0	0		75	0	25

Table 6: Secondary cracking scheme for heavy oil, normal oil and condensates.

Paleo surfaces temperatures were calculated from paleo-bathymetries using the following equation:

$$T = Tmin + A \times e^{\left(\frac{-z}{B}\right)}$$

Where:

- T is temperature
- A is a regional coefficient
- Tmin is the minimum attained temperature
- z is the depth
- B is the curvature (empirical calibration of the depth at which To is reached)
- Tmin + A when z = 0 is the maximum temperature

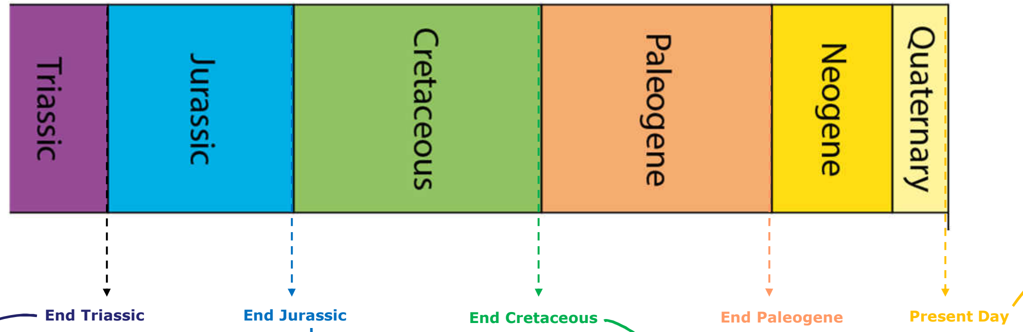

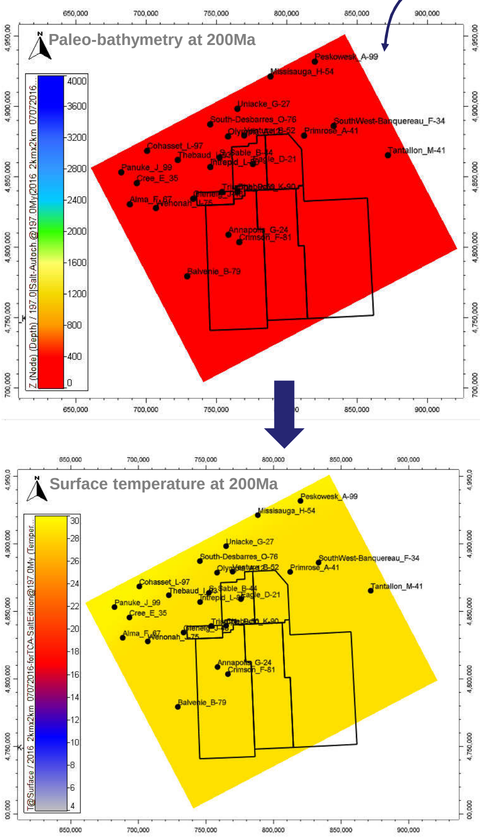

Figure 6: Paleo-bathymetry and paleo-surface temperature maps at end Triassic.

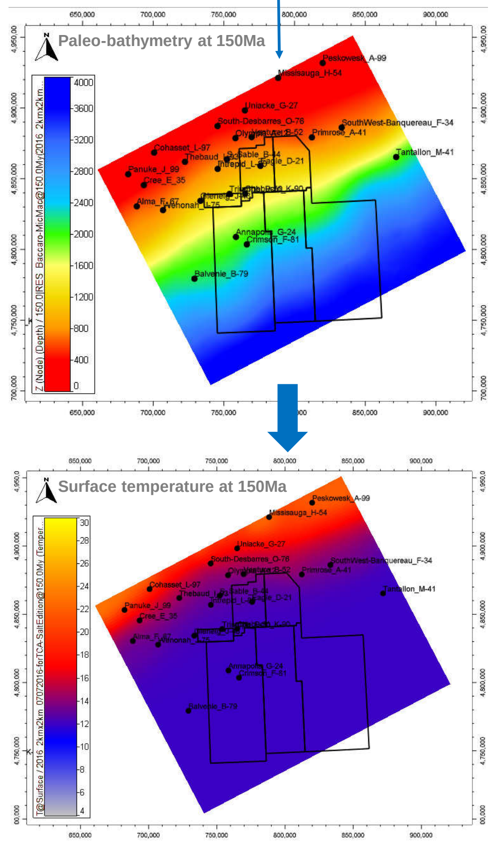

Figure 7: Paleo-bathymetry and paleo-surface temperature maps at end Jurassic.

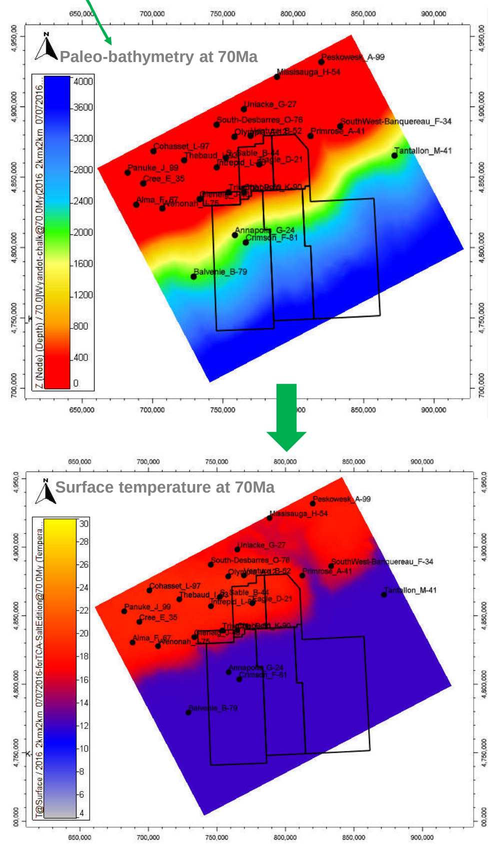

Figure 8: Paleo-bathymetry and paleo-surface temperature maps at end Cretaceous.

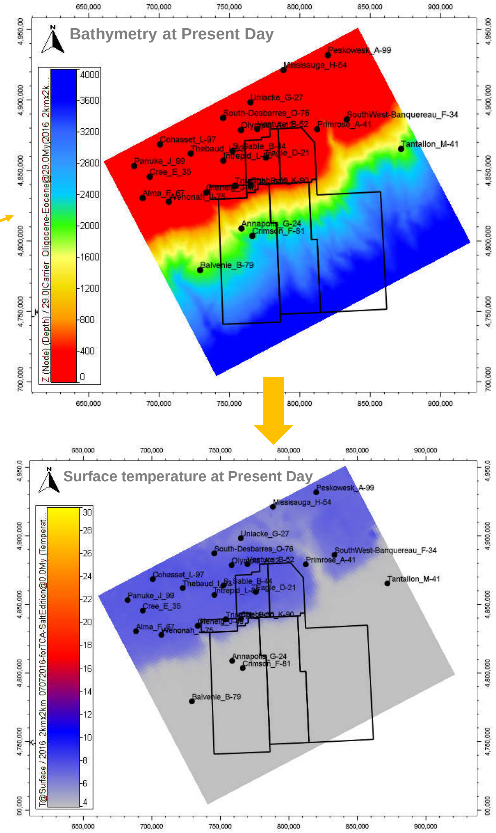

Figure 9: Bathymetry and surface temperature maps at present day.

Surface temperature maps show the evolution of surface temperature through time, based on paleo-bathymetries, paleo-climate and thermohaline circulation in oceans for the end Triassic (Figure 6), end Jurassic (Figure 7), end Cretaceous (Figure 8) and present day (Figure 9).

Surface temperature maps are applied on the model for several events with paleo-bathymetry maps and used for computation. For events with undefined paleo-bathymetry maps and thus temperature maps, a linear interpolation is applied to simulate temperature evolution through times.

Starting from a warm continental setting at the end of the Triassic, the rest of the Mesozoic shows no significant climatic variations. Temperature distribution is controlled by the position of the shelf relative to the basin. Tertiary climatic evolution is marked by a drastic cooling after the Paleogene.

Moho Depth

The Moho depth (Figure 10) varies between 17 and 32 km in the study area (After Dehler and Welford 2013).

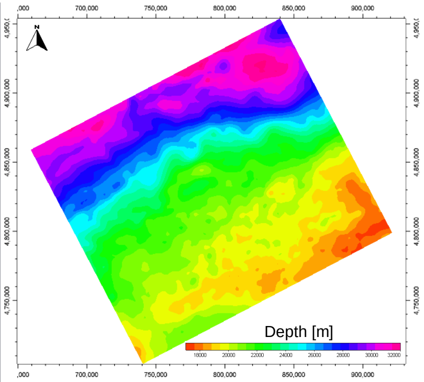

Figure 10: Moho depth.

Crust Thickness

The thickness of the crust (Figure 11) in the model is calculated with the Moho depth map (after S. Dehler from the GSC) and the Top Basement depth map provided by seismic interpretation. Crustal thickness ranges between 4.5 and 32 km.

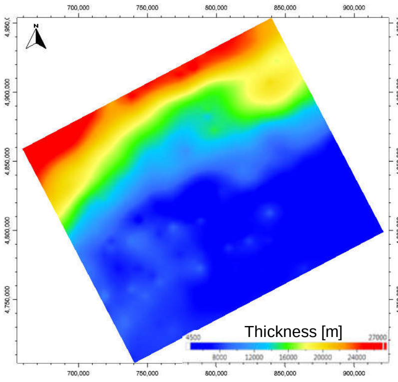

Figure 11: Crust thickness.

Upper Crust Lithology

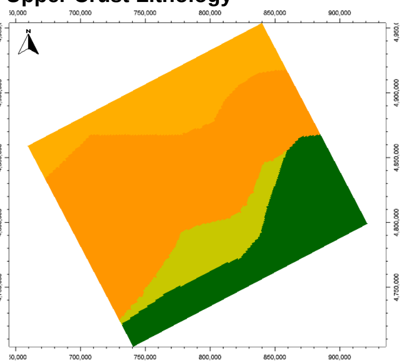

Figure 12: Upper Crust facies distribution.

	Upper continental crust	+ Average Crust Radiogenic Heat Flow -
	Upper+ middle continental crust	
	Transition crust	
	Oceanic crust	

The upper crust lithology has a strong influence on the thermal modelling: the continental crust is usually rich in radiogenic elements while the oceanic crust does not generate radiogenic heat. Different types of continental crust with differing radiogenic element contents are considered.

The distribution of crustal lithologies (Figure 12) is estimated using geophysical data (estimated rock densities, seaward dipping reflectors) and thermal calibration with well data (from this study and PFA 2011).

Rifting Definition

Rifting events are defined by the thinning of the crust, from which derives the isotherms rise in the TemisFlow® basement, and its duration.

- Beta Factor map (Figure 13):
  - Initial crust thickness before rifting H0: 42 km.
  - Crust thickness after rifting (should be equal to present-day thickness if no other events affected the basement) H1: Figure 6
- Rifting starts at 220My and ends at 198My:
  - The Beta Factor map was applied during this interval to simulate crustal thinning and asthenospheric uplift.
  - Continental crust was replaced by transitional and oceanic crust seaward to simulate oceanization (Lithoswitch tool of TemisFlow®).
- Total lithosphere thickness: 120km.

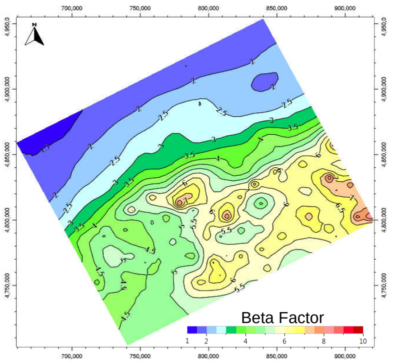

Figure 13: Beta factor map used for the 220-197My rifting.

Before Rifting (220 Ma)

Relatively uniform temperature field. 1330°C at the base of the lithosphere (base of the model).

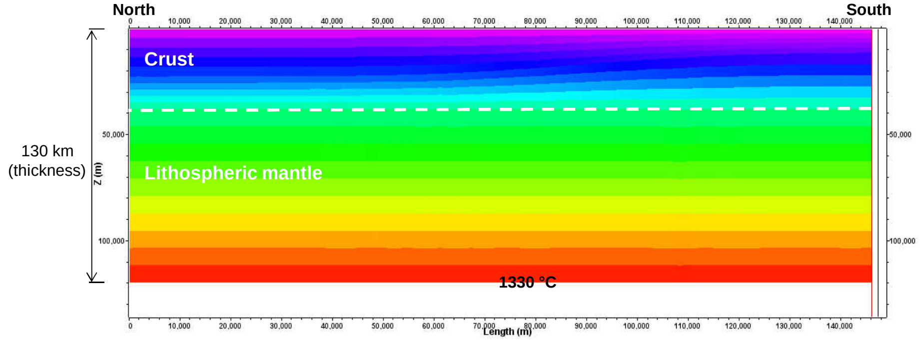

After Rifting (197 Ma)

Heating due to the rifting. The thinning of the crust is stronger seaward (ocean opening). The 1330°C isotherm is decoupled from the geometric base of the model. The mantle plume is also bigger seaward, to the south.

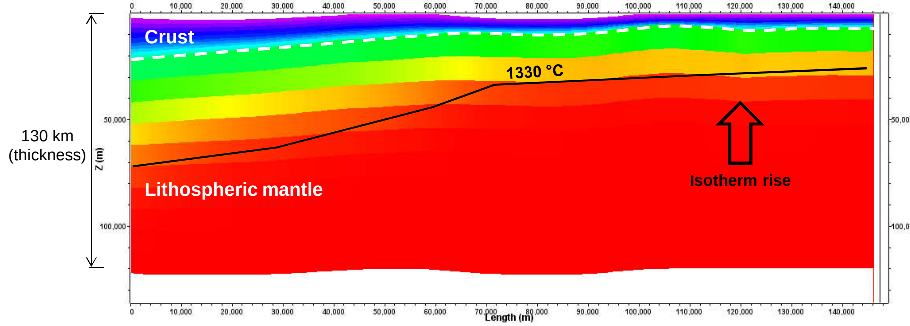

Present Day (0 Ma)

Slow cooling after the rifting. At the same depth below the surface and above 50 km, temperature is lower seaward than on the shelf at present day.

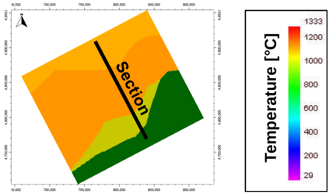

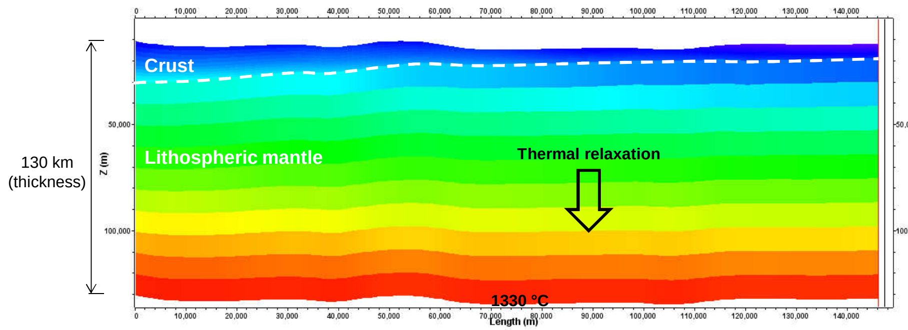

- Upper continental crust
- Upper + Middle continental crust
- Transitional crust
- Oceanic crust
- Lower crust
- Mantle

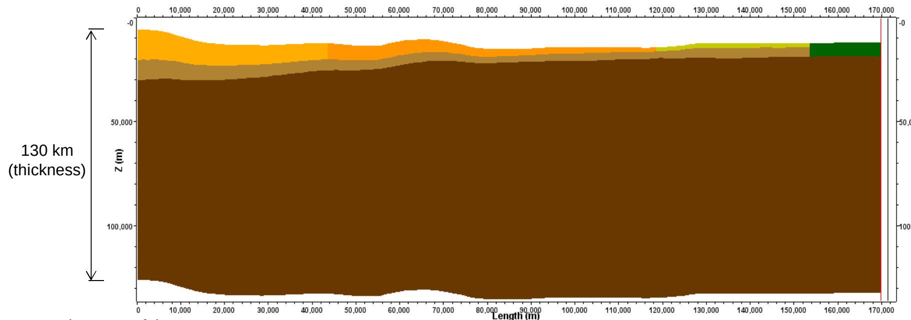

Figure 14: Thermal evolution through time and present-day state of the crust

CHAPTER 7.2

BASIN MODELLING – MATURATION/EXPULSION SIMULATION

The **1st modelling stage** consists of temperature, pressure, maturity, and expulsion modelling using the basin modelling software TemisFlow 3D®.

The evolution of the entire 3D block (i.e., the geological model) is simulated through geological time:

→ Modelling of progressive burial due to sedimentation.
→ Sediment compaction with the "backstripping method".
→ Structural evolution (uplift, subsidence, normal faulting, salt deformation, etc.).
→ Water flow modelling.
→ Rifting of the lithosphere and resulting thermal effects on the sedimentary basin.
→ Computation of temperature and pressure through time in the entire 3D block.
→ Computation of Source Rock (SR) maturity through time.
→ Computation of hydrocarbon (HC) expulsion through time (primary migration).

Results will be used for the migration modelling and analysis (maturity, porosity, etc.).

Calibration

The 3D model was calibrated in pressure / temperature / maturity (vitrinite reflectance) using available data from 24 wells (see Figure 15 for well locations).

The modeling of a basin's temperature history results from integrating different heat sources in the subsurface such as heat flow from the mantle and crustal and sedimentary radiogenic production. The resulting heat flow is then modulated by the sediment's heat transmissibility and the surface temperature. Simulation results were obtained by finely tuning these different parameters and an accurate calibration of temperature and pressure was achieved as demonstrated by the comparison between simulation results and well data (Figure 16, 17 and 18). The simulation results are in agreement with those obtained in the 2011 PFA.

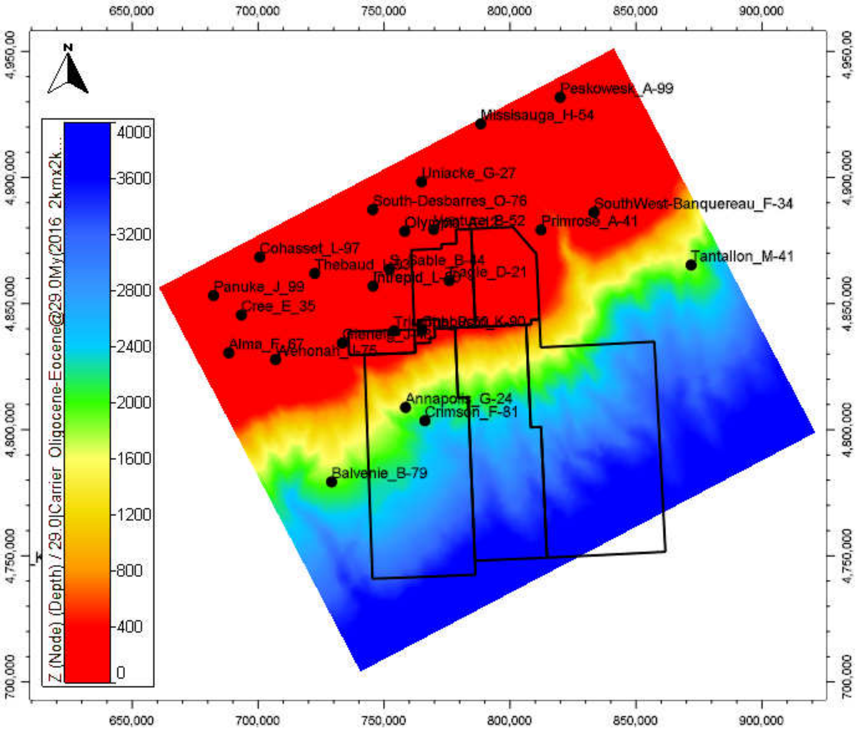

Figures 15 : Well locations plotted on the sea bottom depth map.

TEMPERATURE CALIBRATION

Figure 16: Example of temperature calibration for Tantallon, South Desbarres and Crimson wells.

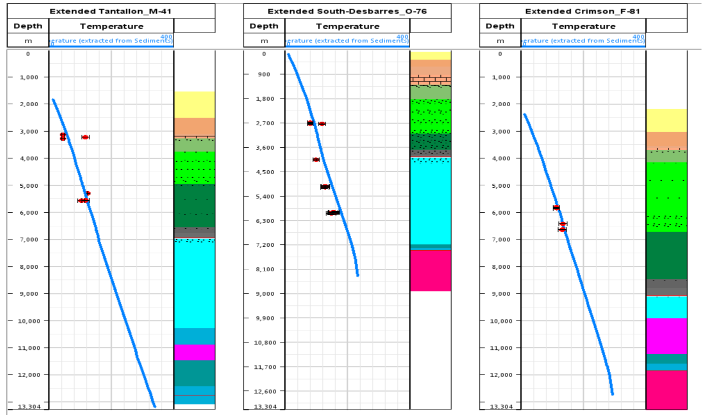

MATURITY CALIBRATION

Figure 17: Example of maturity calibration for Tantallon, South Desbarres and Crimson wells.

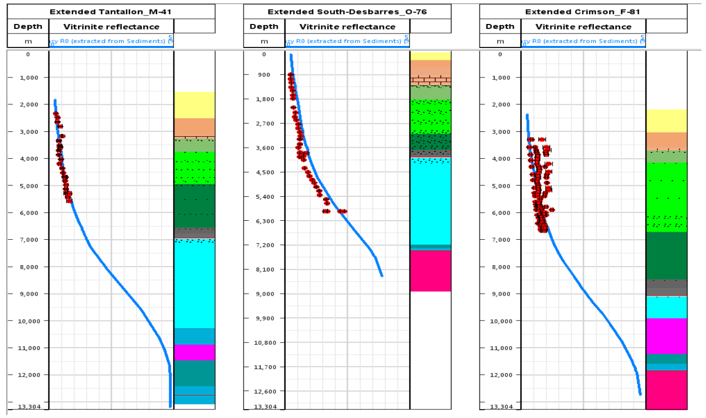

PRESSURE CALIBRATION

Figure 18: Example of pressure calibration for Tantallon, South Desbarres and Crimson wells.

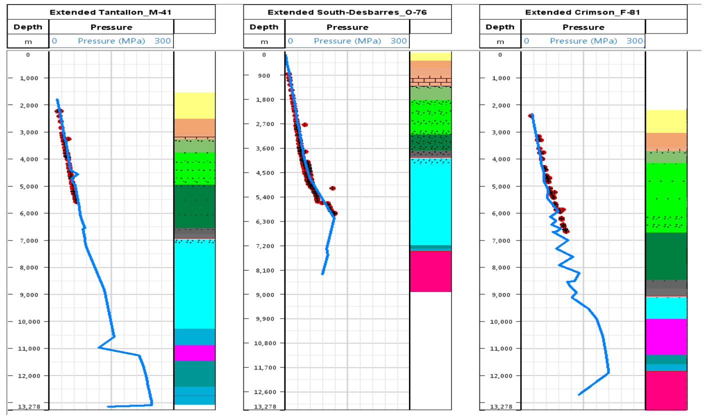

1) BURIAL CURVE ON THE SHELF

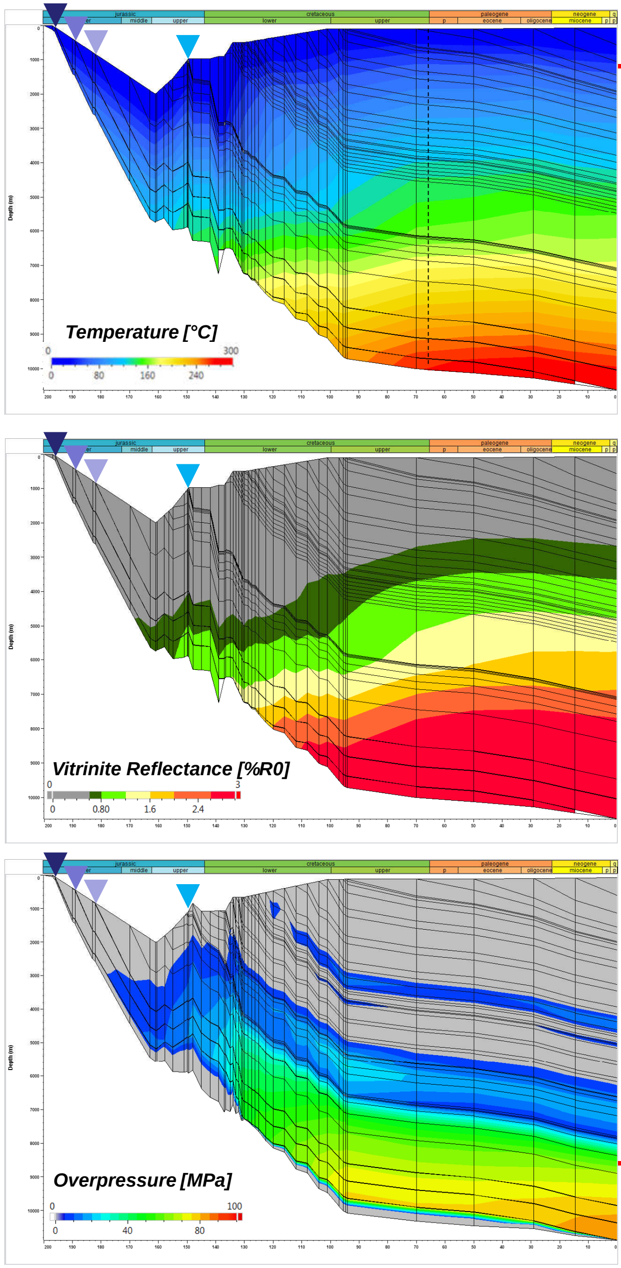

Figure 19: Example of burial history on the shelf overprinted with temperature, maturity and overpressure

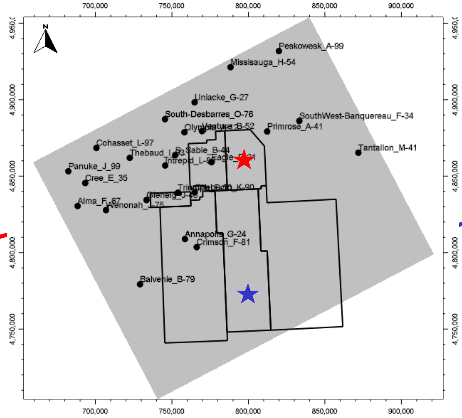

Burial Curves show the evolution of the burial indices through time at precise locations within the study area: (1) on the shelf, east of Eagle (Figure 19), (2) in the distal part of the salt basin (Figure 20). Temperature, vitrinite, and overpressure evolution are indicated through time. Parameters are calculated at the cell center. Timing of source rock deposition is indicated by colored triangles.

Temperature

Temperatures are relatively high in this part of the basin. The temperature has exceeded 200°C in the L. M. Jurassic since the Mid Cretaceous (more than 10 km of burial at present day). A slight decrease of the thermal gradient has occurred since the Lower Jurassic.

Vitrinite

Vitrinite reflectance has exceeded 2% below the Tithonian SR since the Neogene. On average, kerogens are over mature.

Overpressure

Strong overpressure appeared very early in the basin and is related to rapid burial during the Lower Cretaceous. It is mainly related to an excessive overburden (and under compaction). Hydrocarbon generation is a secondary cause. Overpressure tended to decrease above Tithonian SR since Late Cretaceous times.

Temperature

Temperatures are relatively low in this part of the basin. The temperature reached a maximum 200°C since the Oligocene (at 9 km of burial).

Vitrinite

Vitrinite reflectance increased early in the Lower Jurassic strata. The maturity level increased progressively since the Upper Cretaceous to reach 2% in the Tithonian at present-day.

Overpressure

Moderate overpressure appeared progressively after the Late Jurassic. Lower Cretaceous increase of the burial rate led to significant overpressure. Halokinesis maintained high levels of overpressure in this shale-dominated environment.

SR DEPOSITION

Tithonian SR	Pliensbachian SR
Toarcian SR	Sinemurian SR

2) BURIAL CURVE IN THE BASIN

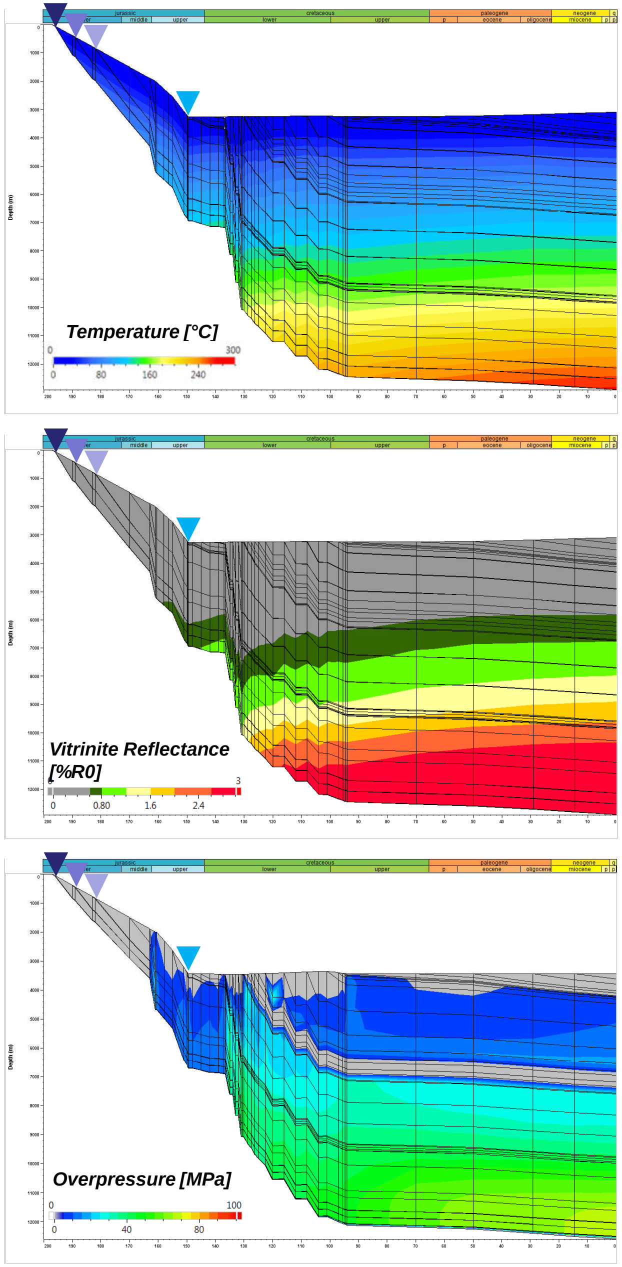

Figure 20: Example of burial history in the basin overprinted with temperature, maturity and overpressure

TITHONIAN SOURCE ROCK

TITHONIAN SR (≈ 150 Ma)
TOARCIAN SR
PLIENSBACHIAN SR
SINEMURIAN SR

Transformation Ratio Map

Relationship TR / Vitrinite	TR = 5% Maturity (oil window)	TR = 50 %	TR = 95 % Over-maturity
Kerogen Type II	$VR_0 = 0.7$	$VR_0 = 0.9$	$VR_0 = 2$

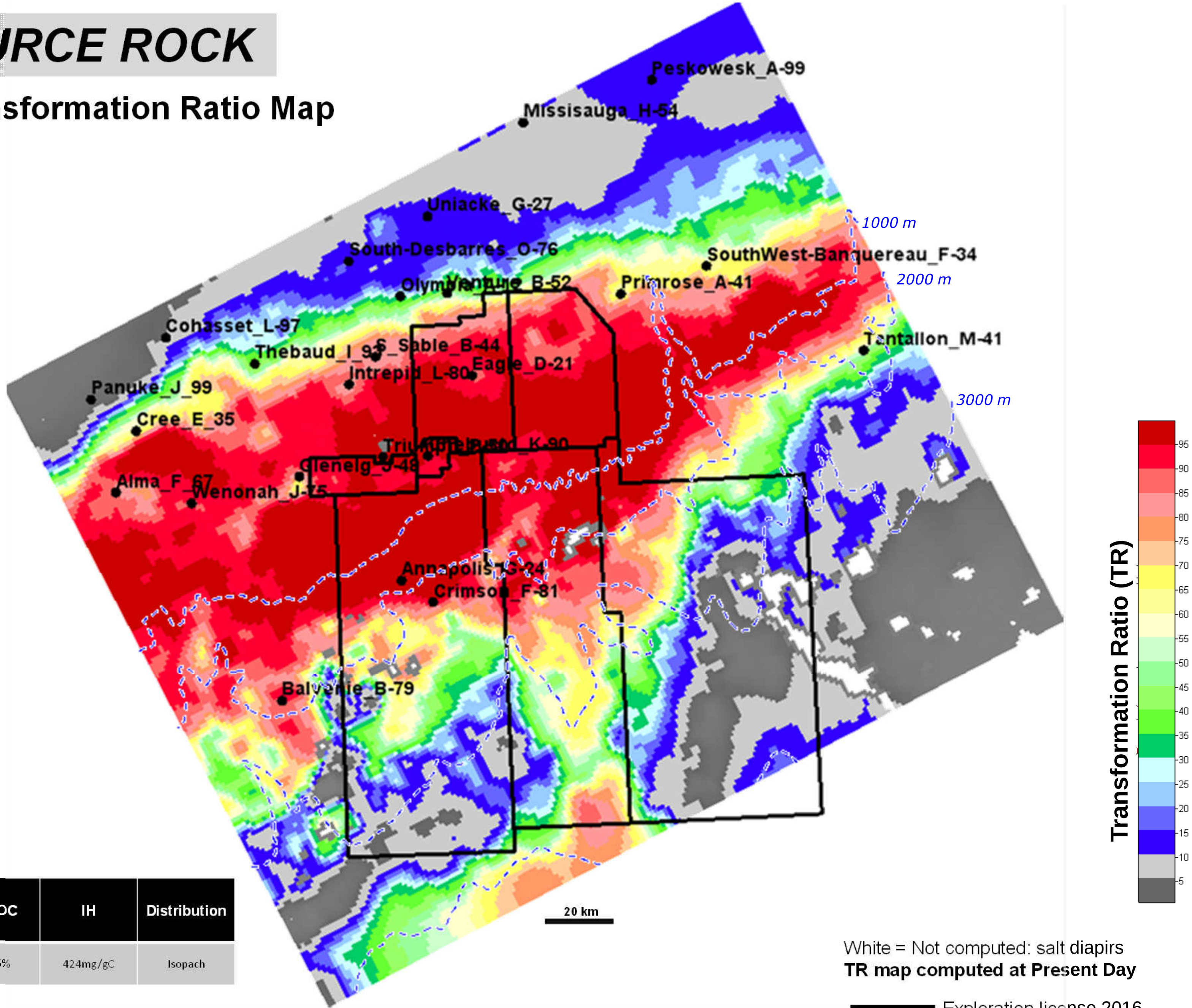

Figure 21: Transformation Ratio of Tithonian Source Rock at Present Day.

Source Rock	Age	Type	Thickness	TOC	IH	Distribution
Tithonian	150Ma	TYII-III	20 meters	5%	424mg/gC	Isopach

TITHONIAN SOURCE ROCK

TITHONIAN SR (≈ 150 Ma)
TOARCIAN SR
PLIENSBACHIAN SR
SINEMURIAN SR

Vitrinite Reflectance Map

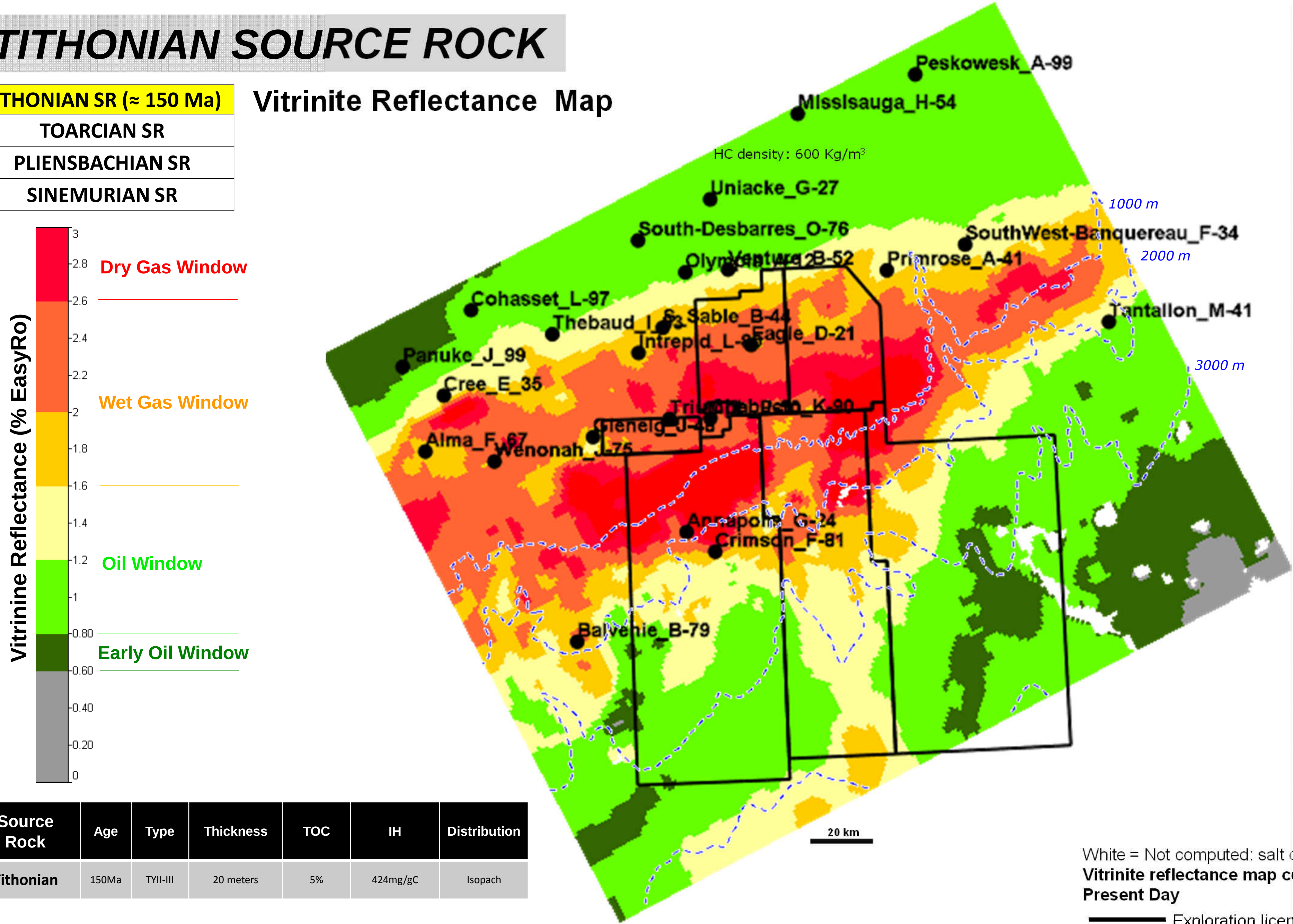

Figure 22: Vitrinite Reflectance (%Ro) map of Tithonian Source Rock at Present Day.

Source Rock	Age	Type	Thickness	TOC	IH	Distribution
Tithonian	150Ma	TYII-III	20 meters	5%	424mg/gC	Isopach

TITHONIAN SOURCE ROCK

TITHONIAN SR (≈ 150 Ma)
TOARCIAN SR
PLIENSBACHIAN SR
SINEMURIAN SR

HC Mass Expelled

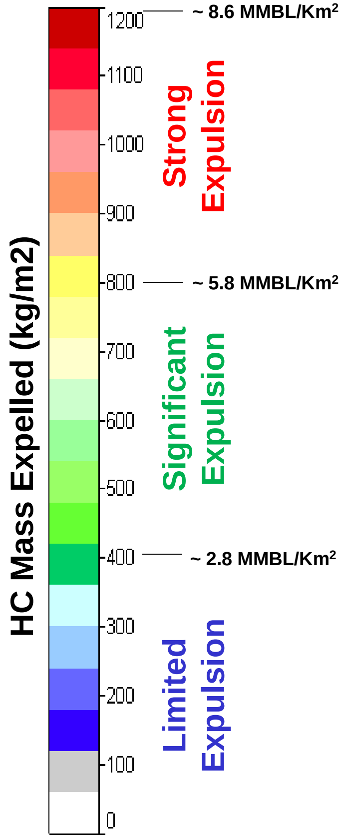

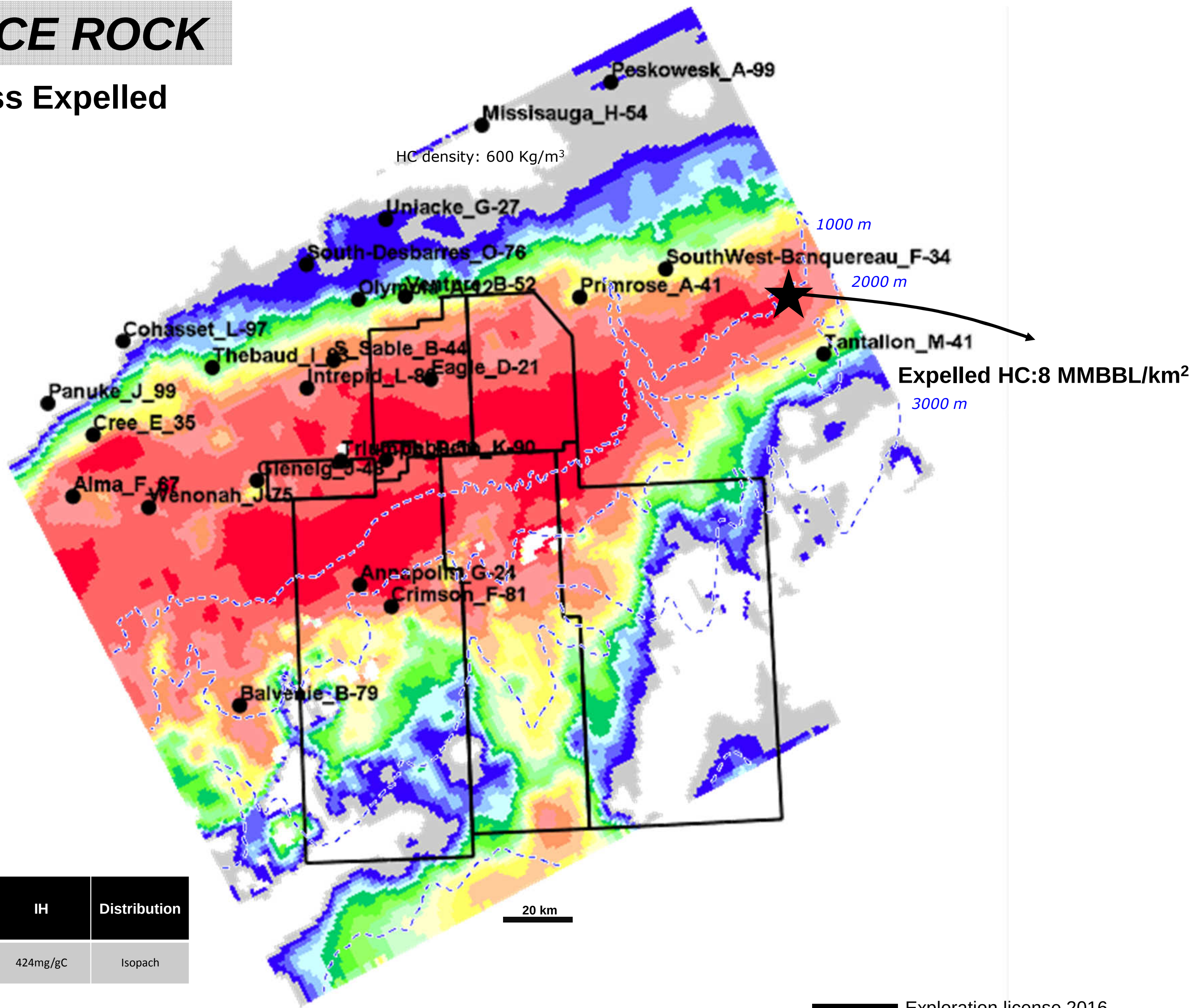

Source Rock	Age	Type	Thickness	TOC	IH	Distribution
Tithonian	150Ma	TYII-III	20 meters	5%	424mg/gC	Isopach

Figure 23: HC Mass Expelled from Tithonian Source Rock at Present Day.

TITHONIAN (SR)

TITHONIAN SR (≈ 150 Ma)
TOARCIAN SR
PLIENSBACHIAN SR
SINEMURIAN SR

Age of Maturity TR > 5 % = Beginning of the Oil Window

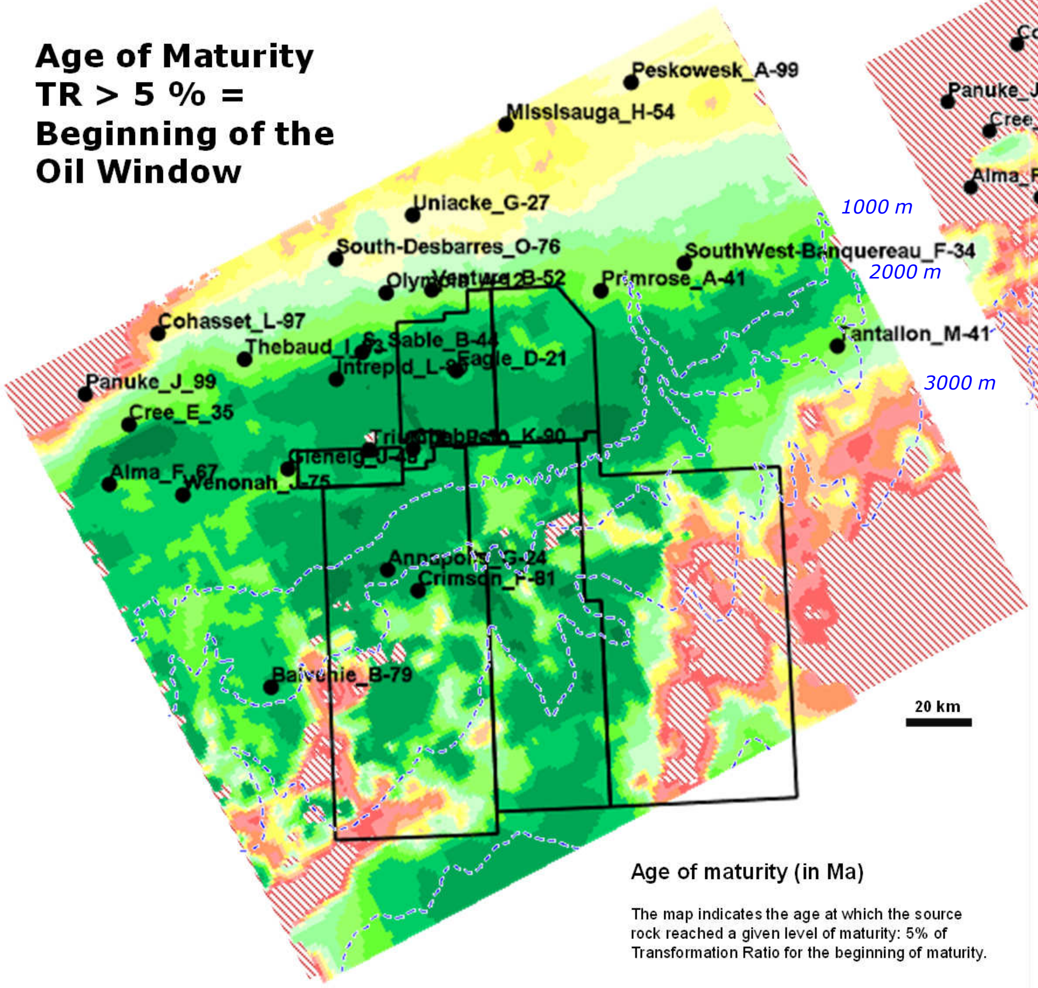

Age of maturity (in Ma)

The map indicates the age at which the source rock reached a given level of maturity: 5% of Transformation Ratio for the beginning of maturity.

Figure 24: Map of Age of Maturity for Tithonian SR.

Age of Over-Maturity TR > 95 %

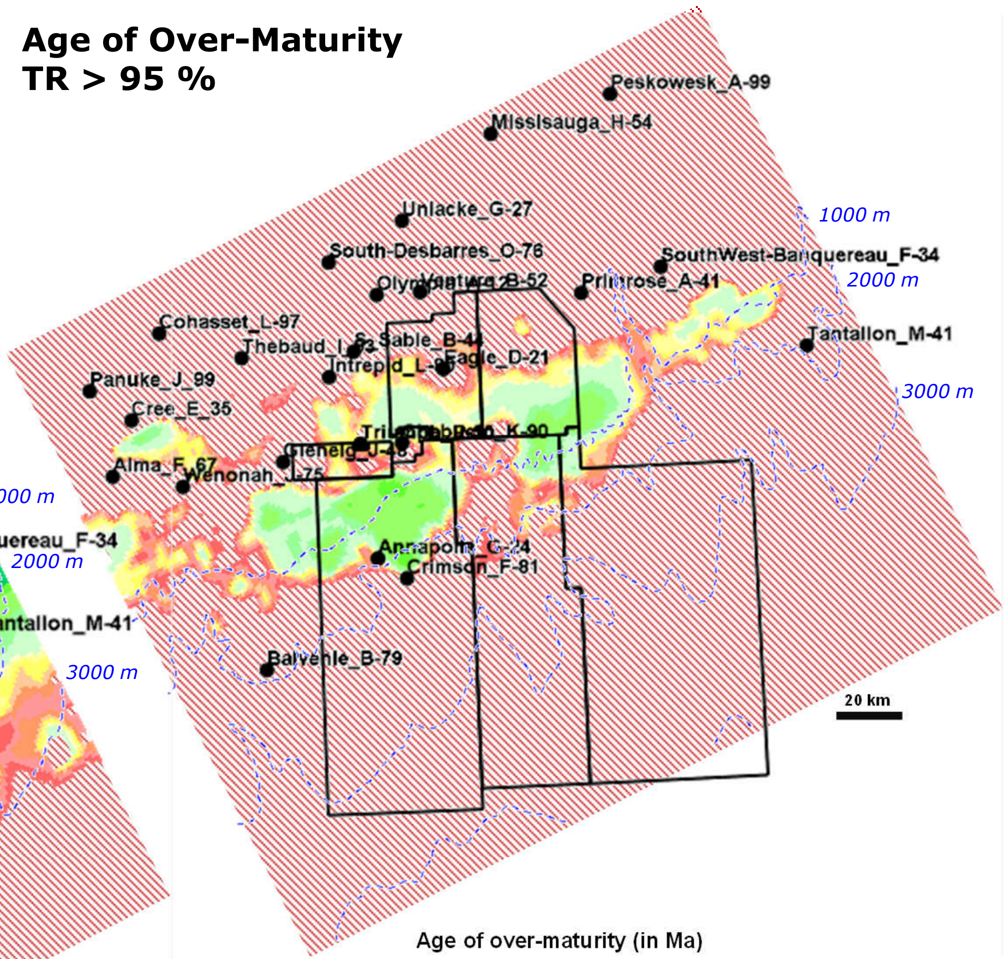

Age of over-maturity (in Ma)

The map indicates the age at which the source rock reached a given level of maturity: 95% of Transformation Ratio for over-maturity.

Figure 25: Map of Age of Over-Maturity for Tithonian SR

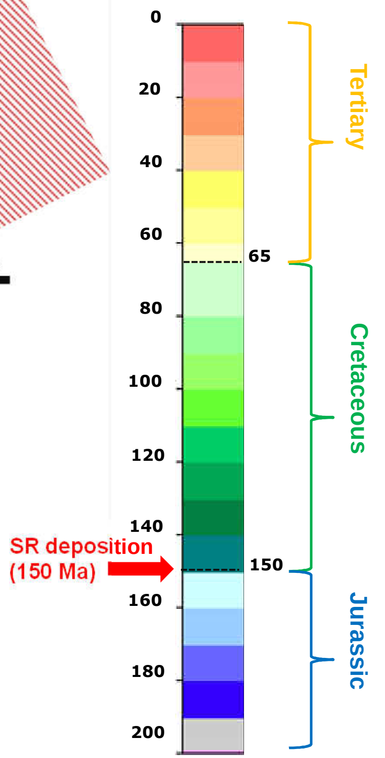

% of maturity not yet reached or computed

Exploration license 2016

TOARCIAN SOURCE ROCK

TITHONIAN SR
TOARCIAN SR (≈ 182 Ma)
PLIENSBACHIAN SR
SINEMURIAN SR

Transformation Ratio Map

Relationship TR / Vitrinite	TR = 5% Maturity (oil window)	TR = 50 %	TR = 95 % Over-maturity
Kerogen Type II	$VR_0 = 0.7$	$VR_0 = 0.9$	$VR_0 = 2$

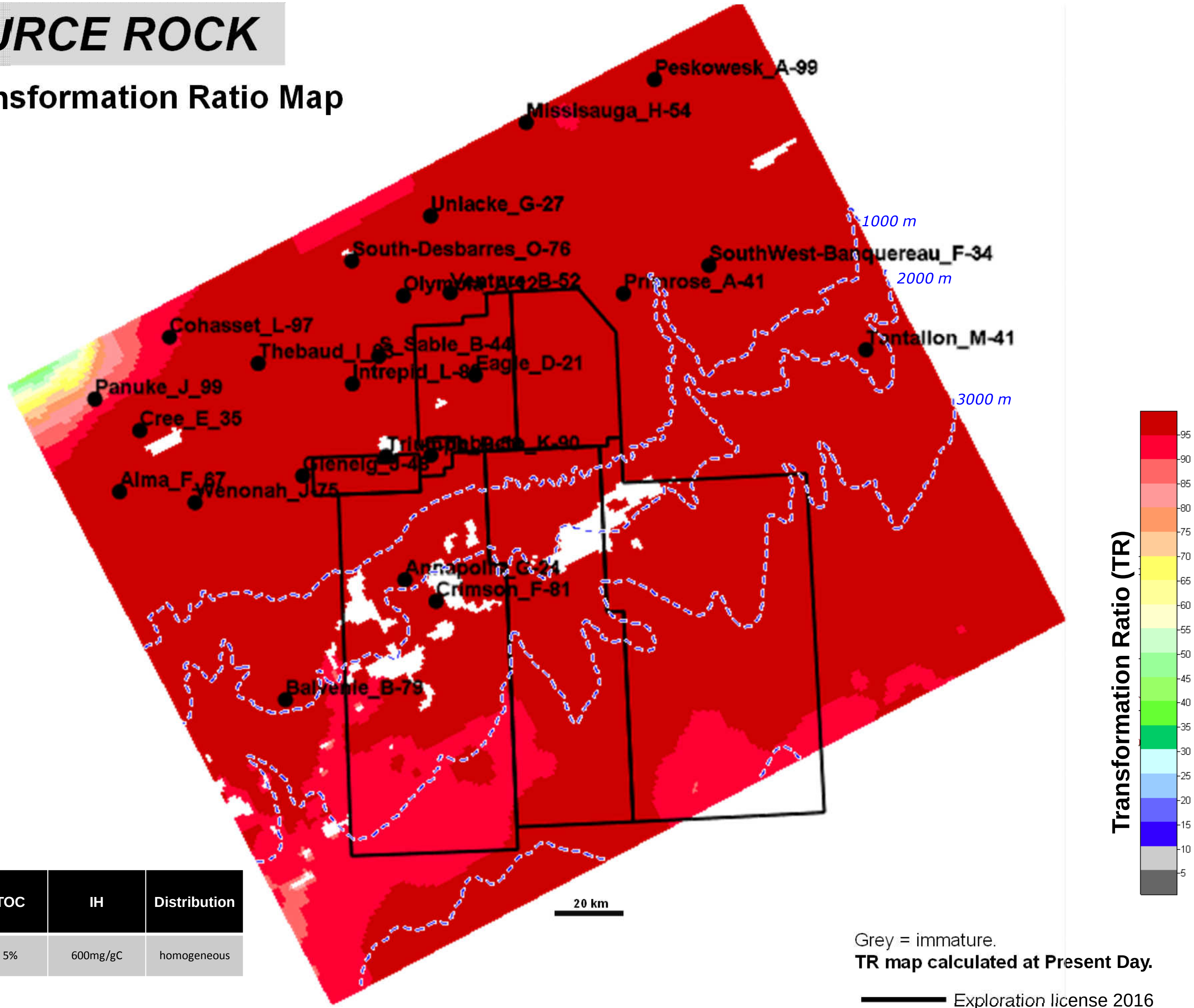

Figure 26: Transformation Ratio of Toarcian Source Rock at Present Day.

Source Rock	Age	Type	Thickness	TOC	IH	Distribution
Toarcian	182Ma	TYII	10 meters	5%	600mg/gC	homogeneous

TOARCIAN SOURCE ROCK

TITHONIAN SR
TOARCIAN SR (≈ 182 Ma)
PLIENSBACHIAN SR
SINEMURIAN SR

Vitrinite Reflectance Map

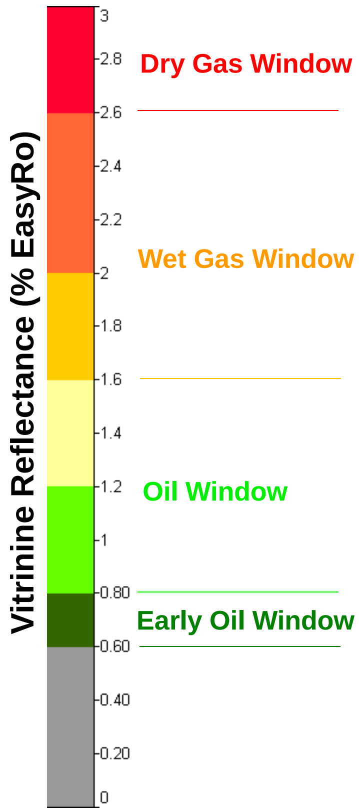

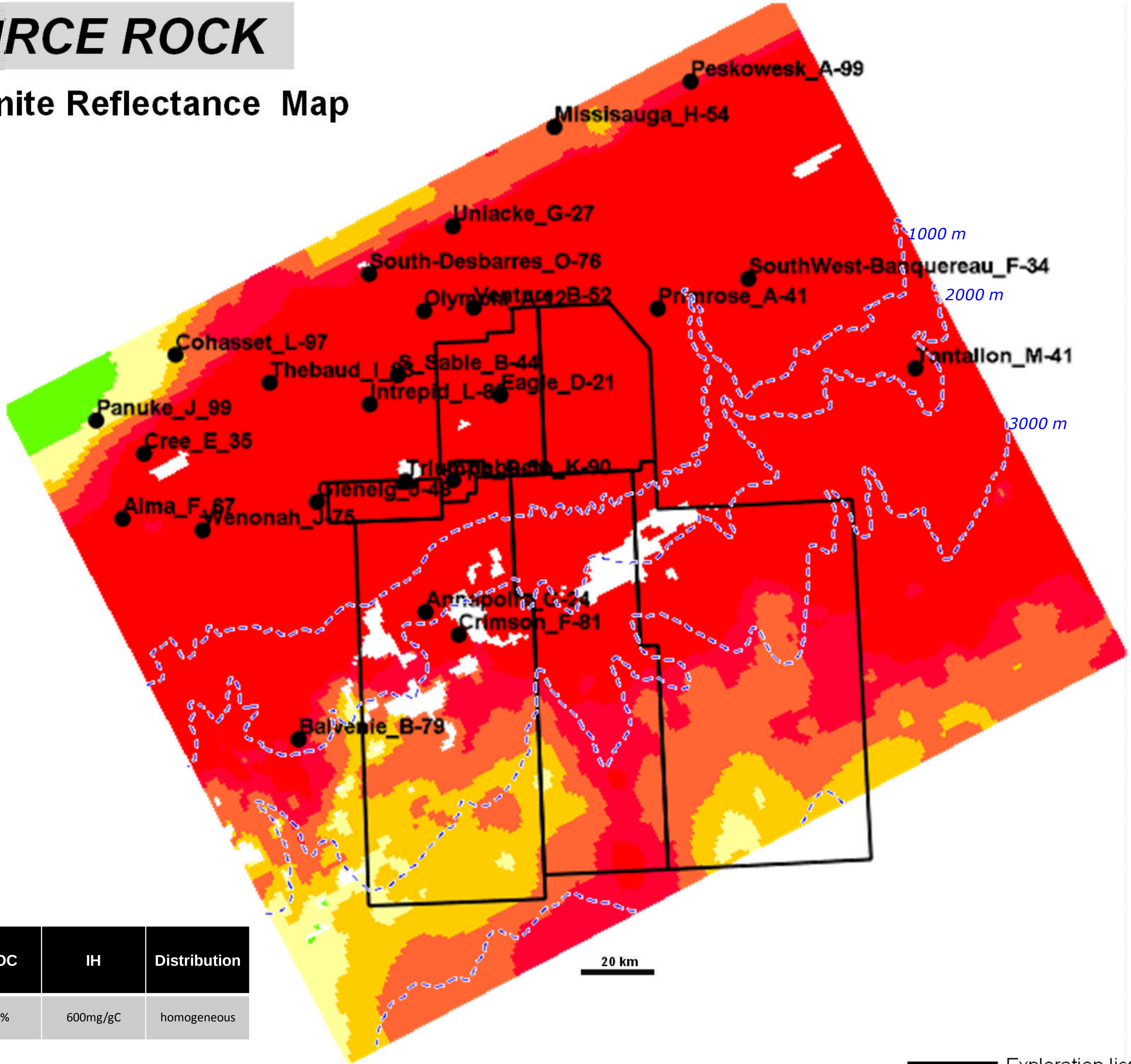

Source Rock	Age	Type	Thickness	TOC	IH	Distribution
Toarcian	182Ma	TYII	10 meters	5%	600mg/gC	homogeneous

Figure 27: Vitrinite Reflectance (%Ro) map of Toarcian Source Rock at Present Day.

Exploration license 2016

TOARCIAN SOURCE ROCK

TITHONIAN SR
TOARCIAN SR (≈ 182 Ma)
PLIENSBACHIAN SR
SINEMURIAN SR

HC Mass Expelled

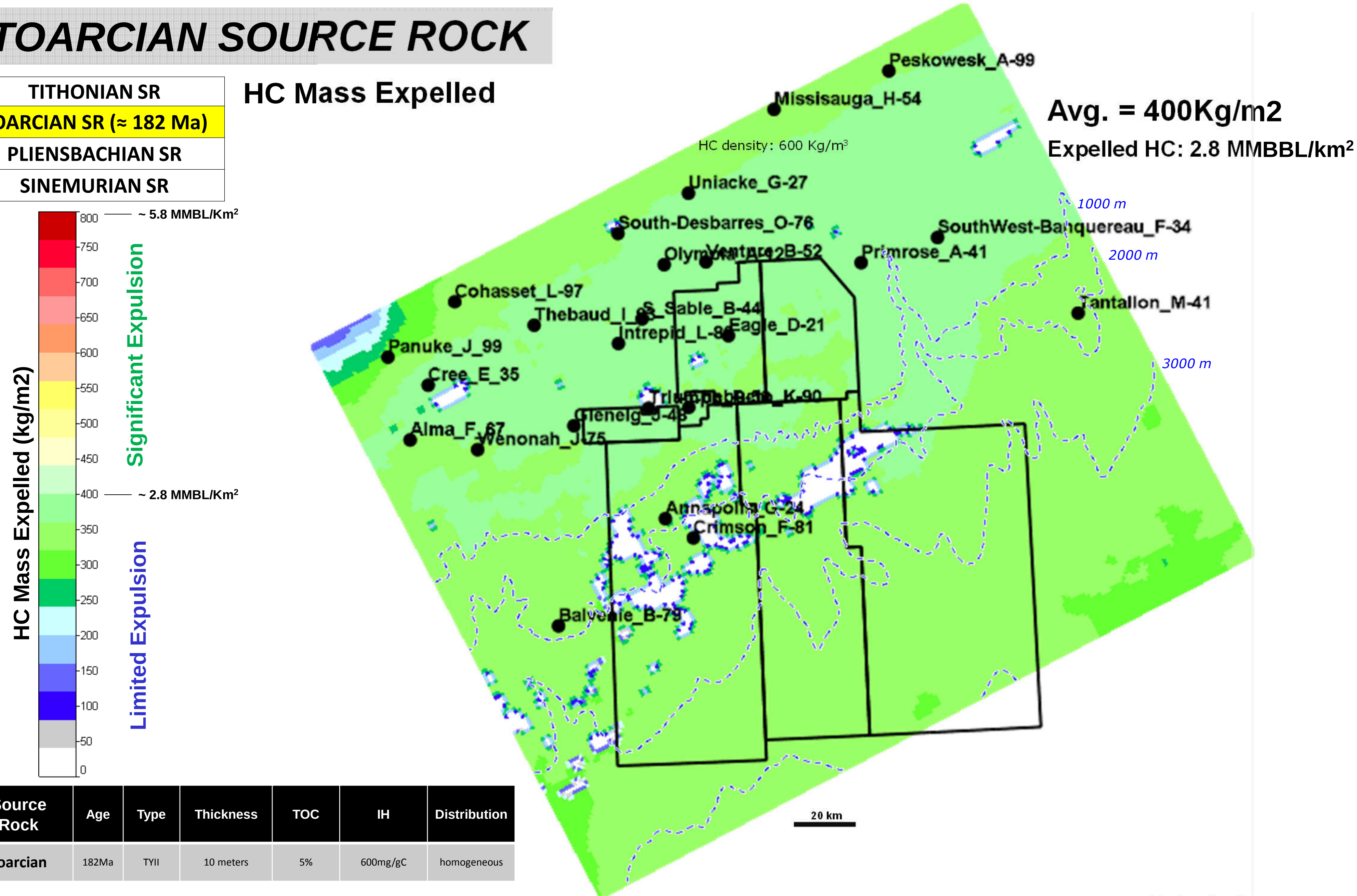

Source Rock	Age	Type	Thickness	TOC	IH	Distribution
Toarcian	182Ma	TYII	10 meters	5%	600mg/gC	homogeneous

Figure 28: HC Mass Expelled from Toarcian Source Rock at Present Day.

TOARCIAN (SR)

TITHONIAN SR
TOARCIAN SR (≈ 182 Ma)
PLIENSBACHIAN SR
SINEMURIAN SR

Age of Maturity TR > 5 % = Beginning of the Oil Window

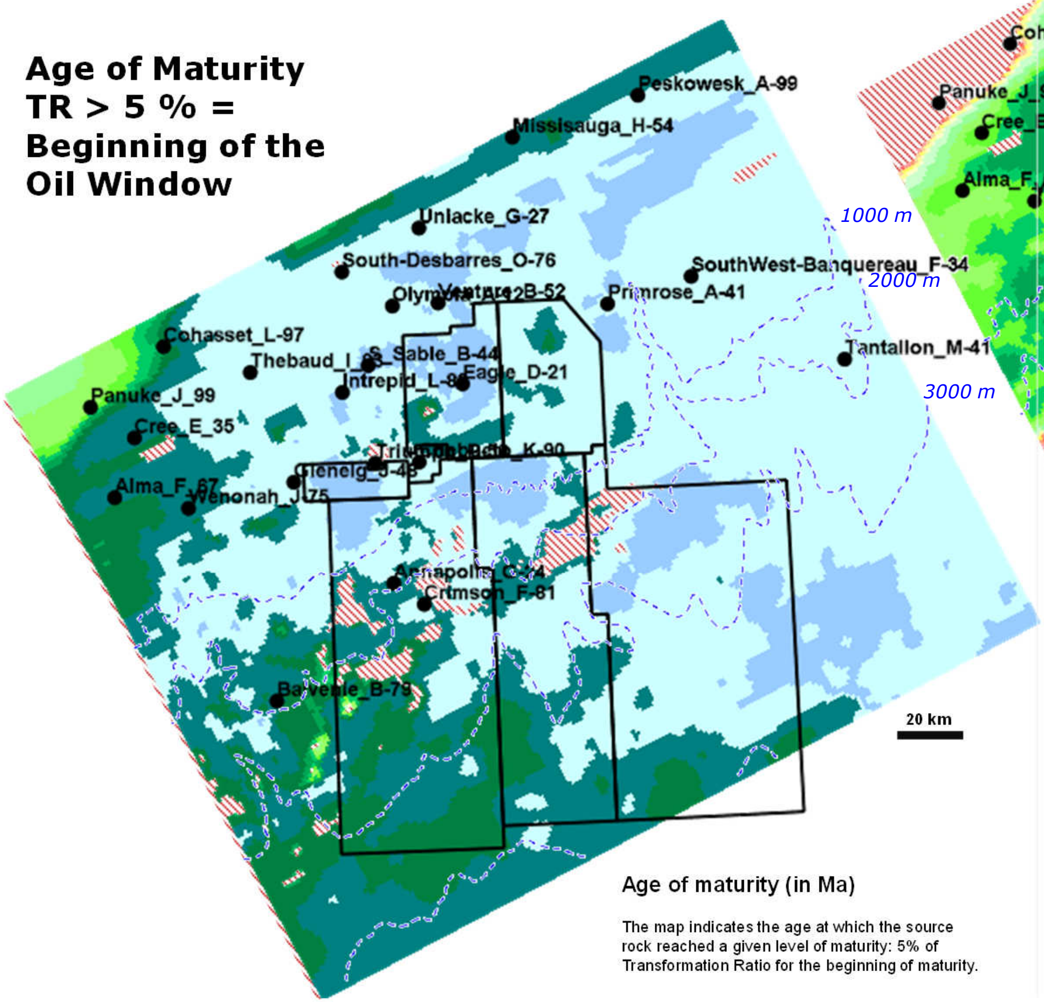

Age of maturity (in Ma)

The map indicates the age at which the source rock reached a given level of maturity: 5% of Transformation Ratio for the beginning of maturity.

Figure 29: Map of Age of Maturity for Toarcian SR

Age of Over-Maturity TR > 95 %

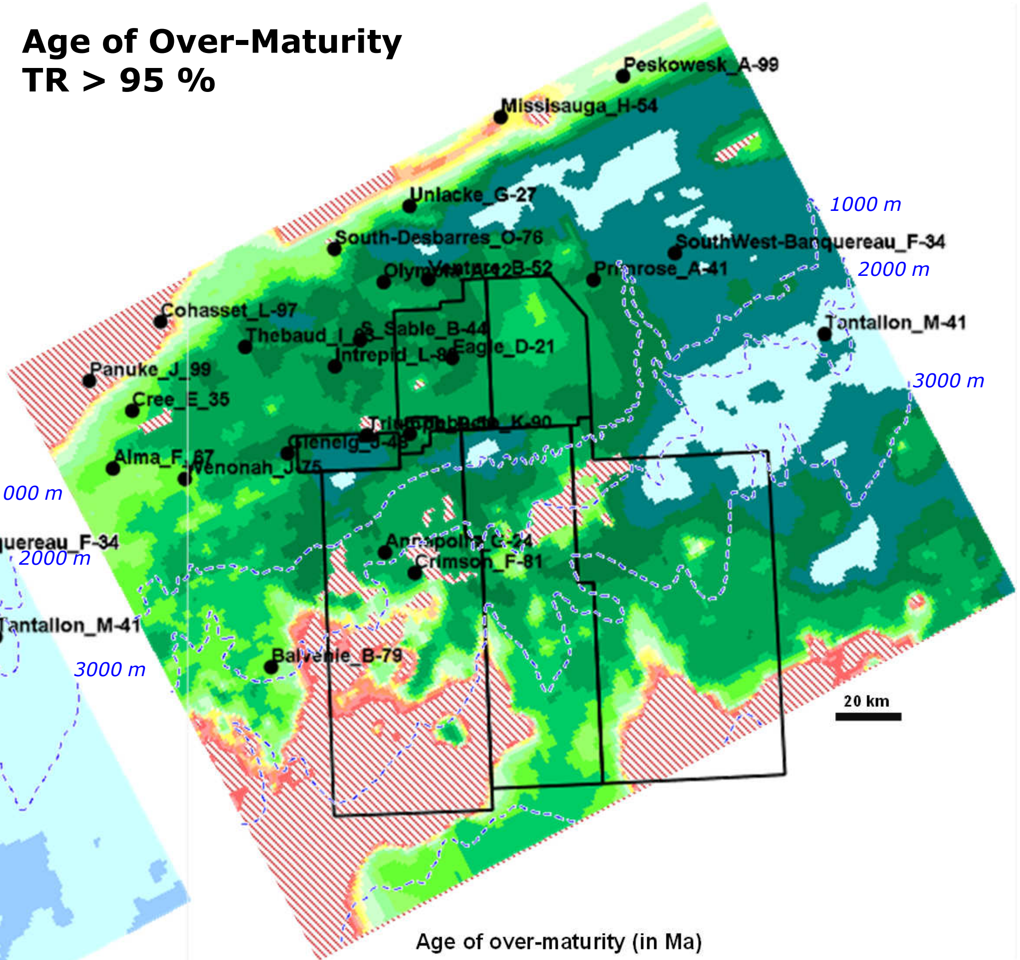

Age of over-maturity (in Ma)

The map indicates the age at which the source rock reached a given level of maturity: 95% of Transformation Ratio for over-maturity.

Figure 30: Map of Age of Over-Maturity for Toarcian SR

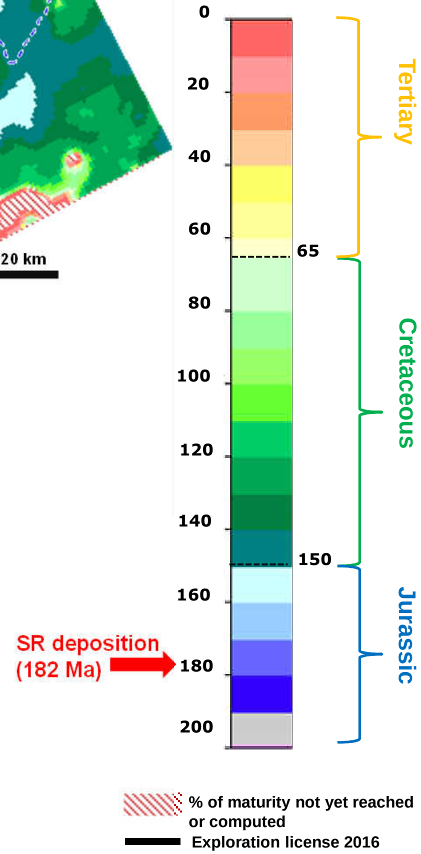

PLIENSBACHIAN SOURCE ROCK

TITHONIAN SR
TOARCIAN SR
PLIENSBACHIAN SR (≈ 189 Ma)
SINEMURIAN SR

Transformation Ratio Map

Relationship TR / Vitrinite	TR = 5% Maturity (oil window)	TR = 50 %	TR = 95 % Over-maturity
Kerogen Type II	VR_0 = 0.7	VR_0 = 0.9	VR_0 = 2

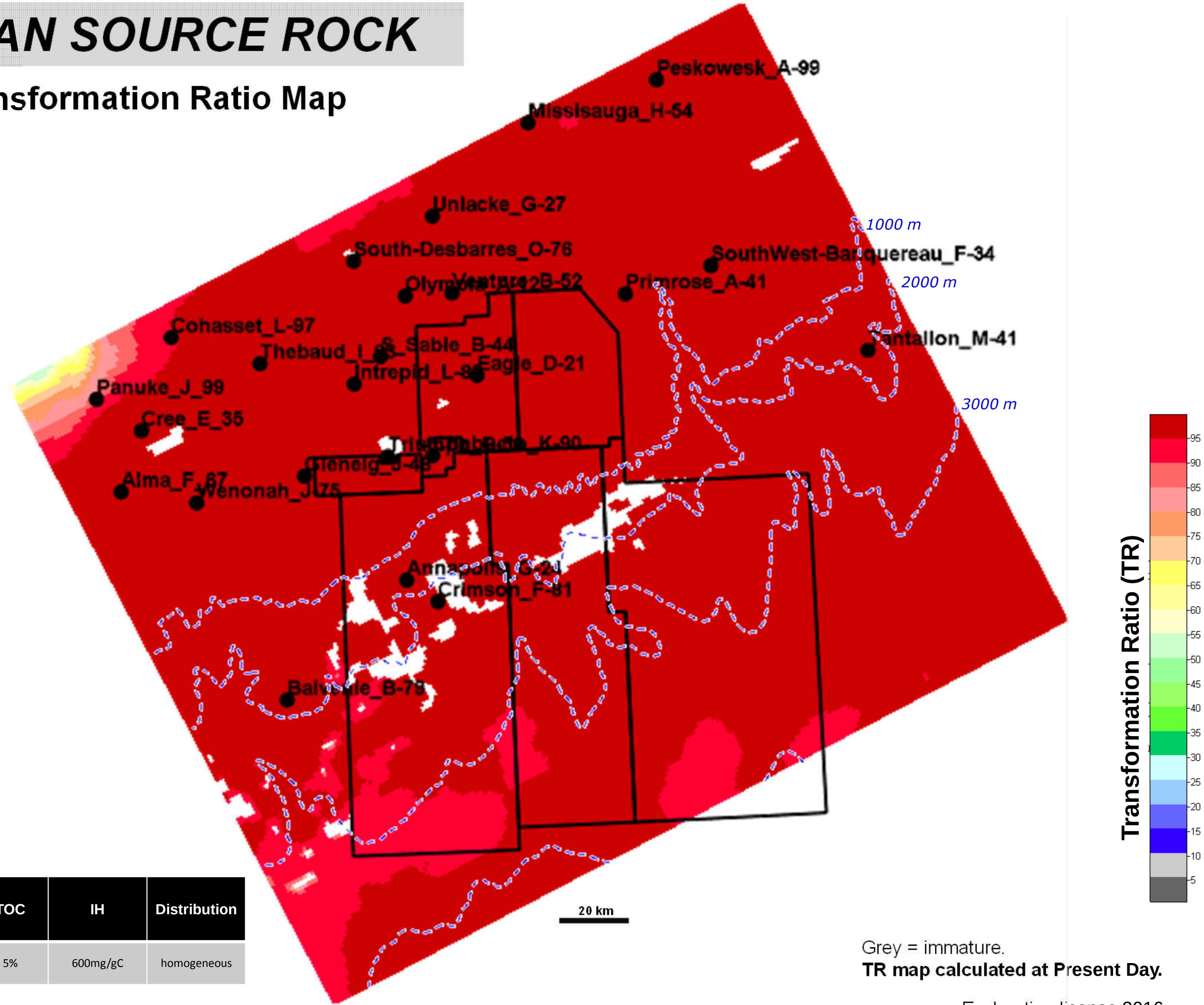

Source Rock	Age	Type	Thickness	TOC	IH	Distribution
Pliensbachian	189Ma	TYII	10 meters	5%	600mg/gC	homogeneous

Figure 31: Transformation Ratio of Pliensbachian Source Rock at Present Day.

PLIENSBACHIAN SOURCE ROCK

TITHONIAN SR
TOARCIAN SR
PLIENSBACHIAN SR (≈ 189 Ma)
SINEMURIAN SR

Vitrinite Reflectance Map

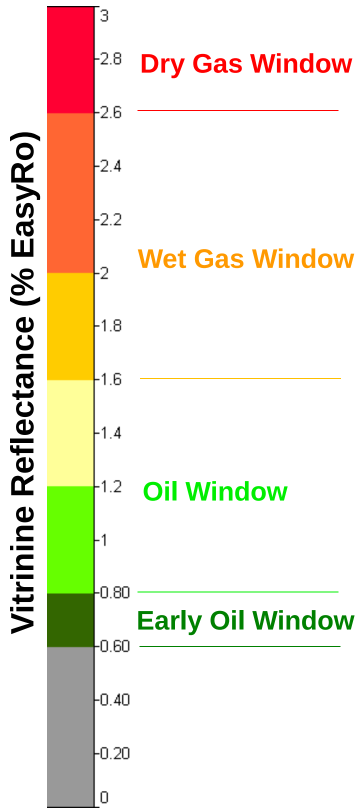

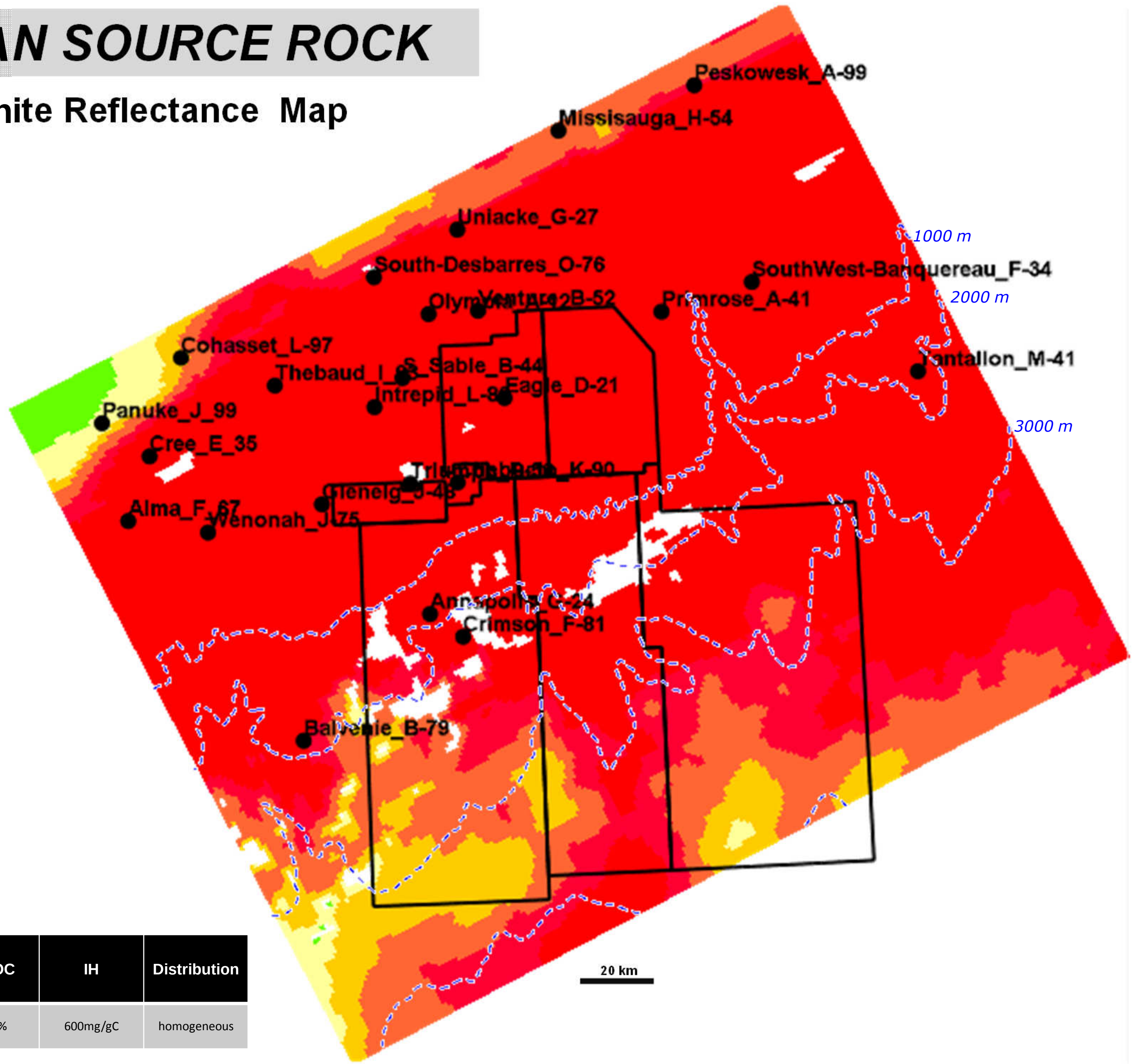

Source Rock	Age	Type	Thickness	TOC	IH	Distribution
Pliensbachian	189Ma	TYII	10 meters	5%	600mg/gC	homogeneous

Figure 32: Vitrinite Reflectance (%Ro) map of Pliensbachian Source Rock at Present Day.

Exploration license 2016

PLIENSBACHIAN SOURCE ROCK

TITHONIAN SR
TOARCIAN SR
PLIENSBACHIAN SR (≈ 189 Ma)
SINEMURIAN SR

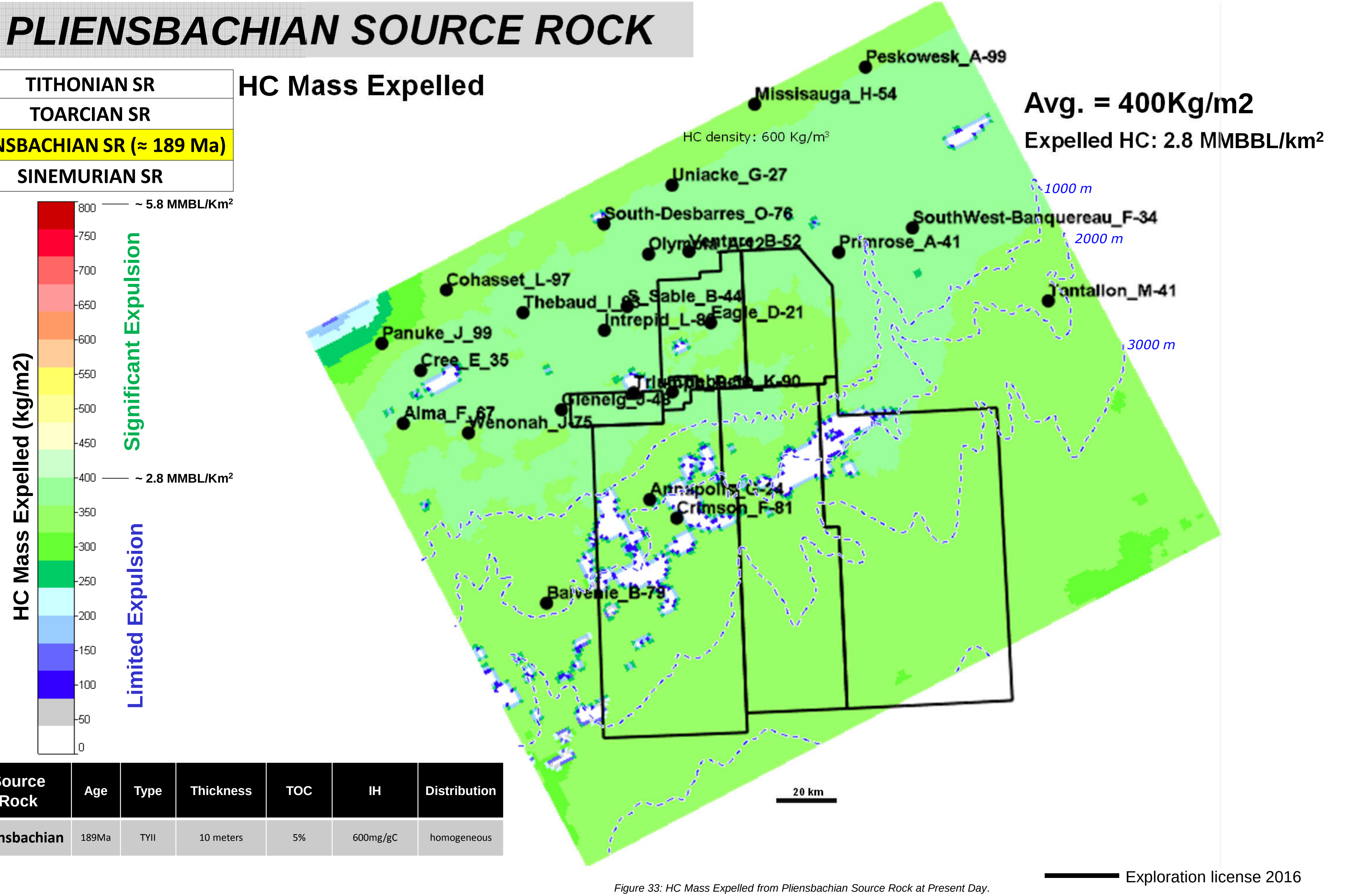

Figure 33: HC Mass Expelled from Pliensbachian Source Rock at Present Day.

Source Rock	Age	Type	Thickness	TOC	IH	Distribution
Pliensbachian	189Ma	TYII	10 meters	5%	600mg/gC	homogeneous

PLIENSBACHIAN (SR)

TITHONIAN SR
TOARCIAN SR
PLIENSBACHIAN SR (≈ 189 Ma)
SINEMURIAN SR

Age of Maturity TR > 5 % = Beginning of the Oil Window

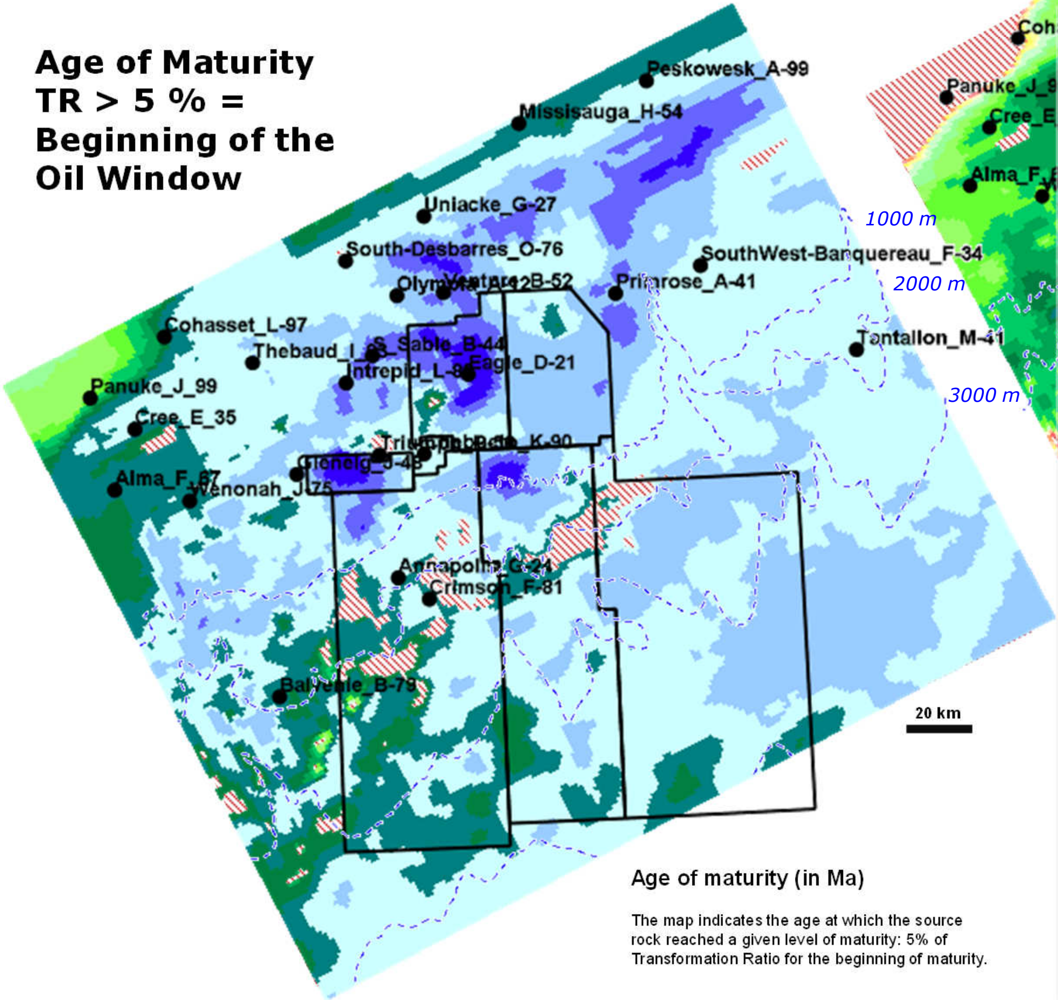

Age of maturity (in Ma)

The map indicates the age at which the source rock reached a given level of maturity: 5% of Transformation Ratio for the beginning of maturity.

Figure 34: Map of Age of Maturity for Pliensbachian SR

Age of Over-Maturity TR > 95 %

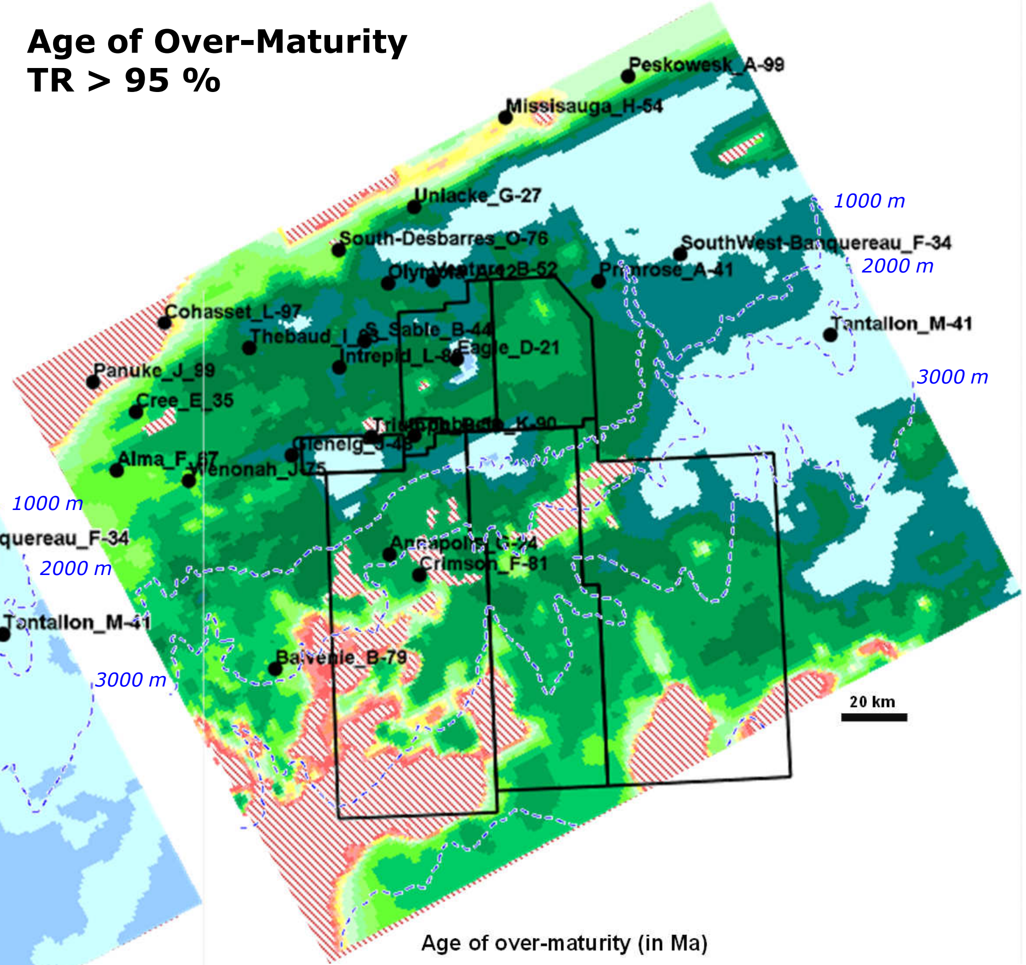

Age of over-maturity (in Ma)

The map indicates the age at which the source rock reached a given level of maturity: 95% of Transformation Ratio for over-maturity.

Figure 35: Map of Age of Over-Maturity for Pliensbachian SR

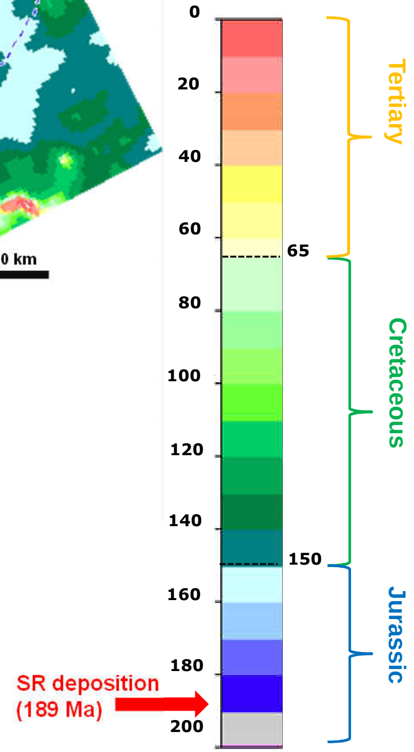

% of maturity not yet reached or computed

Exploration license 2016

SINEMURIAN SOURCE ROCK

TITHONIAN SR
TOARCIAN SR
PLIENSBACHIAN SR
SINEMURIAN SR (≈ 198 Ma)

Transformation Ratio Map

Relationship TR / Vitrinite	TR = 5% Maturity (oil window)	TR = 50 %	TR = 95 % Over-maturity
Kerogen Type II	$VR_0 = 0.7$	$VR_0 = 0.9$	$VR_0 = 2$

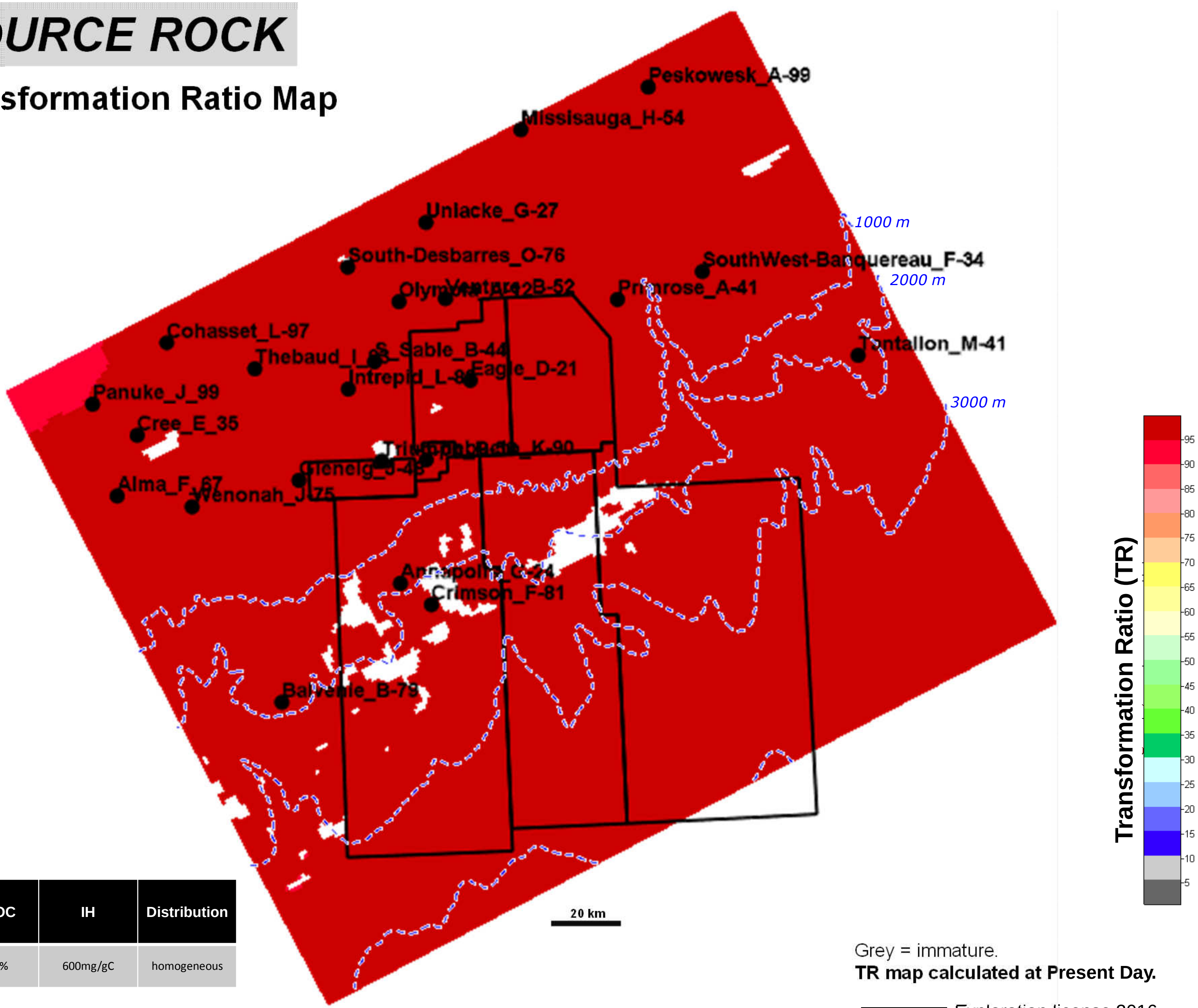

Figure 36: Transformation Ratio of Sinemurian Source Rock at Present Day.

Source Rock	Age	Type	Thickness	TOC	IH	Distribution
Sinemurian	198Ma	TYII-S	10 meters	5%	600mg/gC	homogeneous

SINEMURIAN SOURCE ROCK

TITHONIAN SR
TOARCIAN SR
PLIENSBACHIAN SR
SINEMURIAN SR (≈ 198 Ma)

Vitrinite Reflectance Map

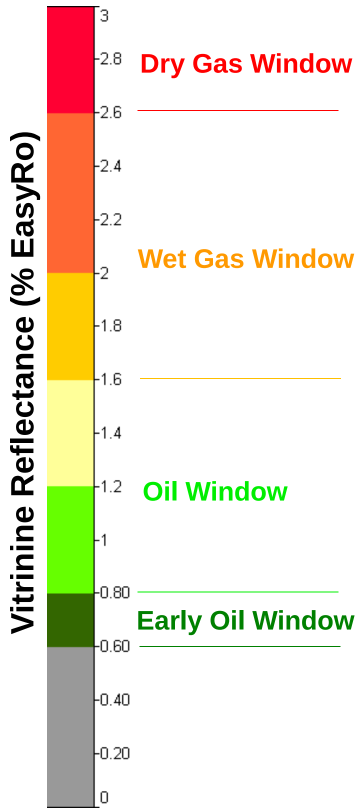

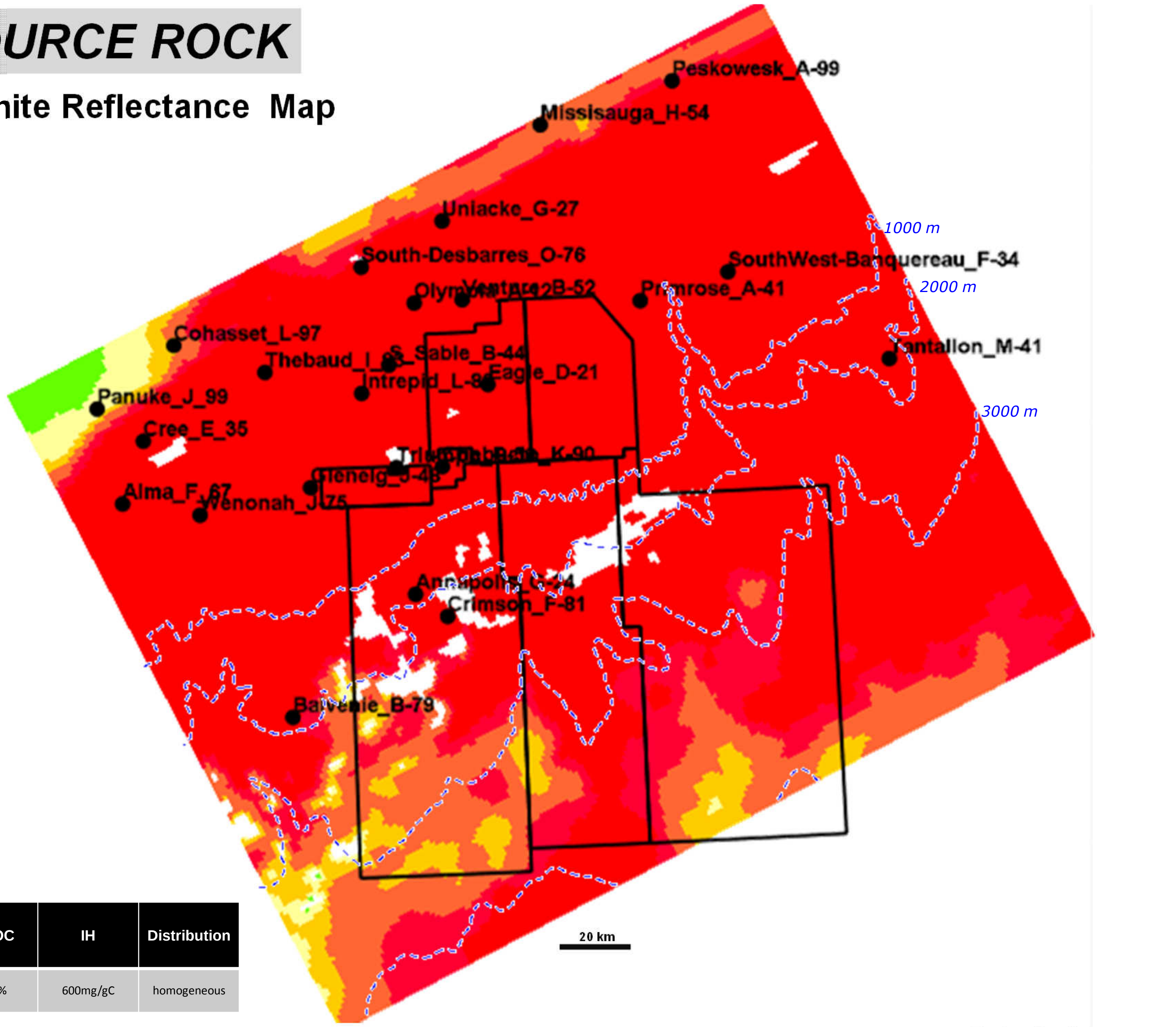

Source Rock	Age	Type	Thickness	TOC	IH	Distribution
Sinemurian	198Ma	TYII-S	10 meters	5%	600mg/gC	homogeneous

Figure 37: Vitrinite Reflectance (%Ro) map of Sinemurian Source Rock at Present Day.

SINEMURIAN SOURCE ROCK

TITHONIAN SR
TOARCIAN SR
PLIENSBACHIAN SR
SINEMURIAN SR (≈ 198 Ma)

HC Mass Expelled

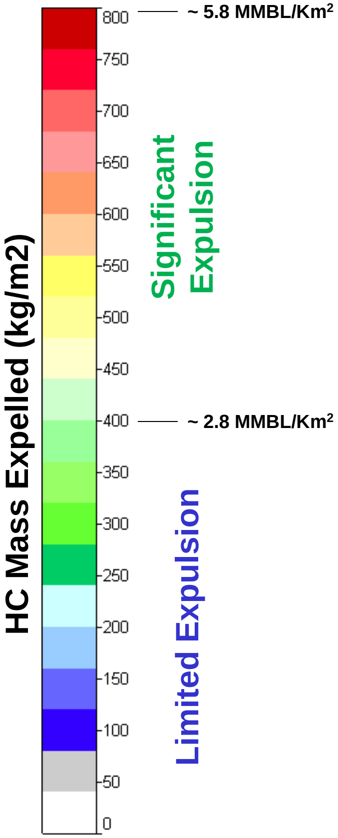

Avg. = 750Kg/m2

Expelled HC: 5.5 MMBBL/km²

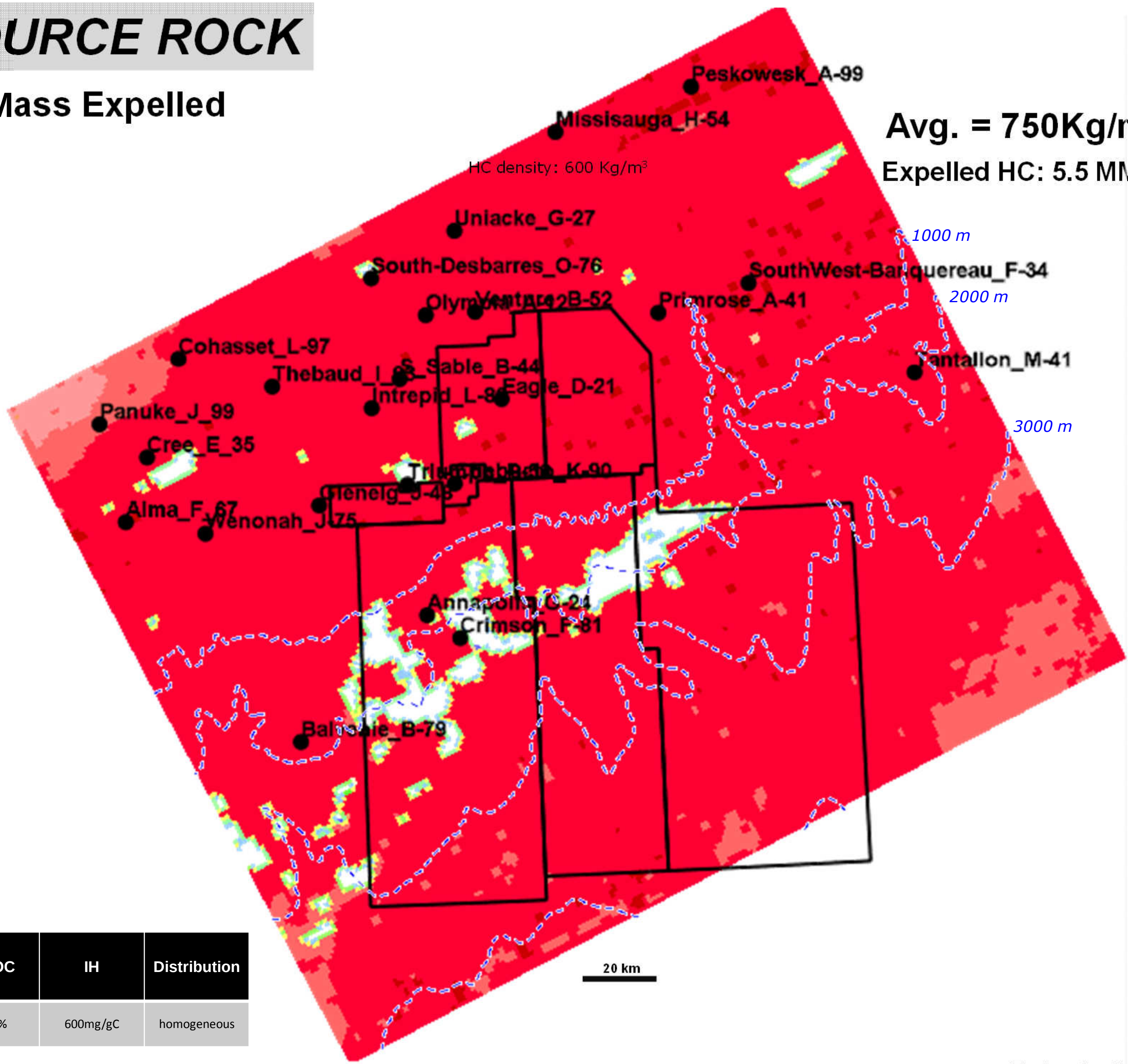

Source Rock	Age	Type	Thickness	TOC	IH	Distribution
Sinemurian	198Ma	TYII-S	10 meters	5%	600mg/gC	homogeneous

Exploration license 2016

Figure 38: HC Mass Expelled from Sinemurian Source Rock at Present Day.

SINEMURIAN (SR)

TITHONIAN SR
TOARCIAN SR
PLIENSBACHIAN SR
SINEMURIAN SR (≈ 198 Ma)

Age of Maturity TR > 5 % = Beginning of the Oil Window

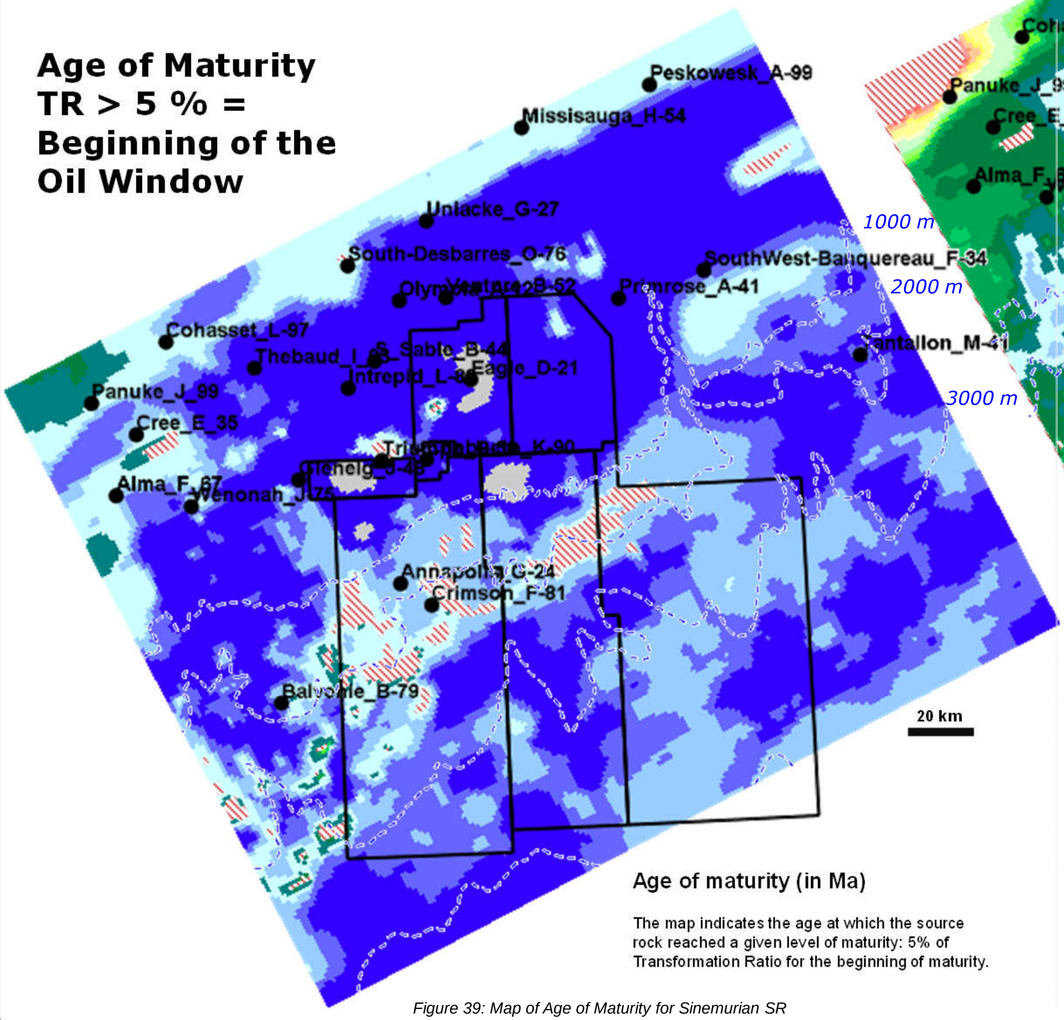

Age of maturity (in Ma)

The map indicates the age at which the source rock reached a given level of maturity: 5% of Transformation Ratio for the beginning of maturity.

Figure 39: Map of Age of Maturity for Sinemurian SR

Age of Over-Maturity TR > 95 %

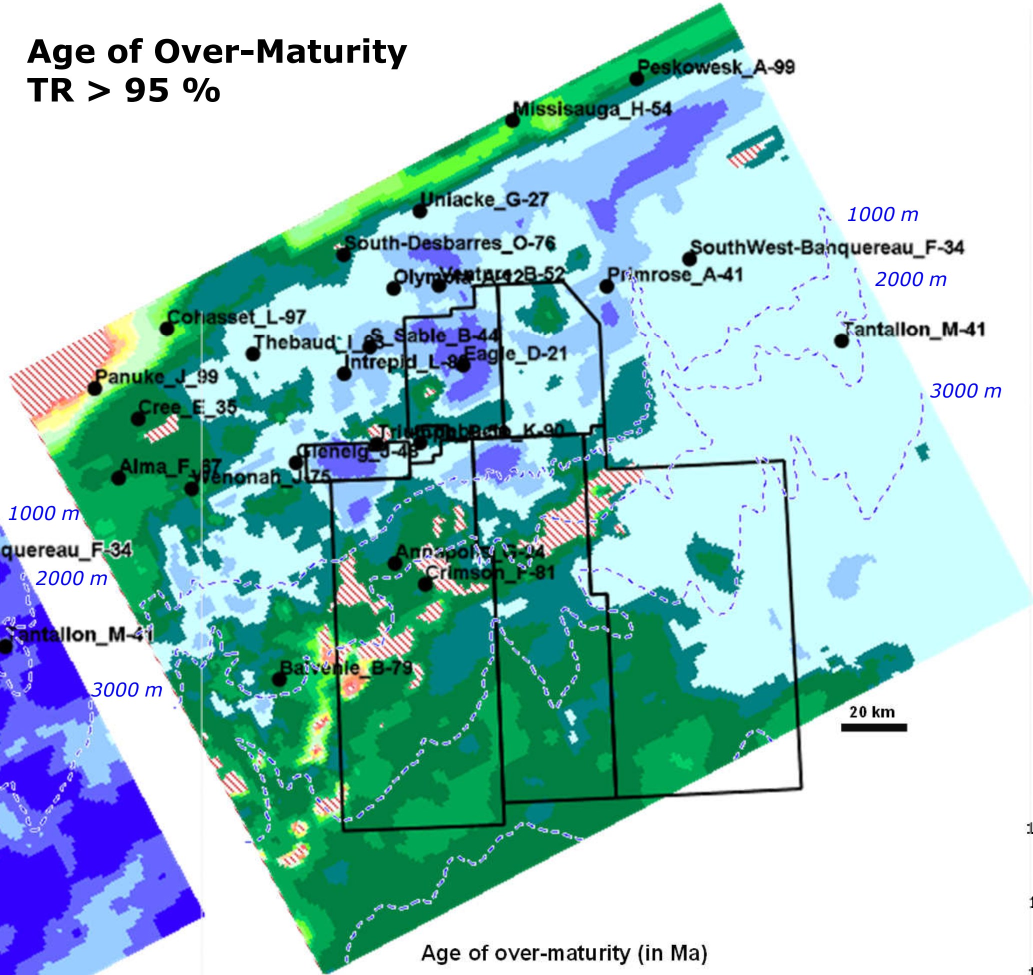

Age of over-maturity (in Ma)

The map indicates the age at which the source rock reached a given level of maturity: 95% of Transformation Ratio for over-maturity.

Figure 40: Map of Age of Over-Maturity for Sinemurian SR

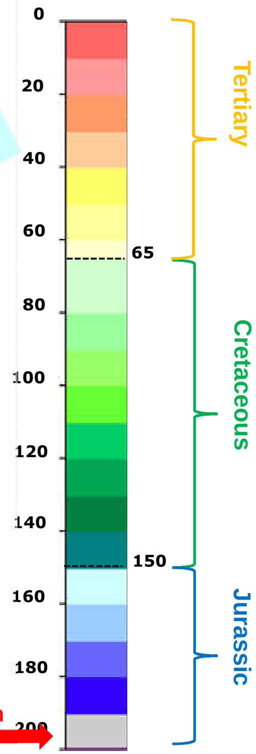

% of maturity not yet reached or computed

Exploration license 2016

	Total OIL-Heavy Expelled Mass Cell [Gkg]	Total OIL-Normal Expelled Mass Cell [Gkg]	Total OIL-Condensate Expelled Mass Cell [Gkg]	Total GAS-Thermogenic Expelled Mass Cell [Gkg]	Total Mass of HC Expelled [Gkg] in Oil Equivalent	Total Mass of Oil Expelled [BB bbl]	Total Volume of Gas Expelled [tcf]	Total Volume of HC Expelled [billion bbl] of Oil Equivalent
All SR	17225	23795	10609	15187	66816	**400.3**	**725.2**	**525.4**
Tithonian	1120	3229	4641	9029	18019	**74.4**	**431.1**	**148.7**
Toarcian	2682	5266	2023	1923	11894	**77.6**	**91.8**	**93.5**
Pliensbachian	2663	5270	2030	1968	11931	**77.6**	**94.0**	**93.8**
Sinemurian	10760	10030	1915	2267	24972	**170.8**	**108.3**	**189.4**

Table 7: Total of expelled components for each SR and equivalent HC volumes.

Expelled HC masses - By SOURCE ROCK (Table 7, Figures 41 and 42)

This ratio does not take into account secondary cracking of heavy HCs occurring within the source rock layer as this is considered to occur during migration (secondary cracking in the SR can be neglected due to the temperature and the limited quantities affected).

Expelled HC Mass by Fraction

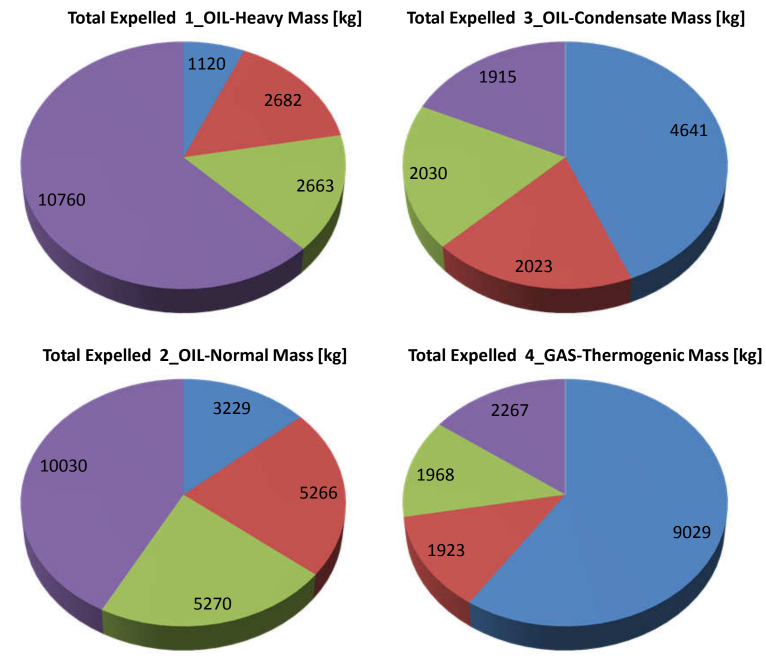

Figure 42: Hydrocarbon fractions generated by each source rock.

Expelled HC Volume and Mass by SR and Total

Figure 41 shows that the contribution of the Lower Jurassic Complex SR in the system is very significant, especially the highly reactive (but speculative) Type IIS Sinemurian SR. Mixed Type II-III Tithonian SRs contribute significantly to the primary generated gas in the system. Nonetheless, oil expelled from the Lower Jurassic SR is likely to have generated important amounts of gas by secondary cracking during its migration.

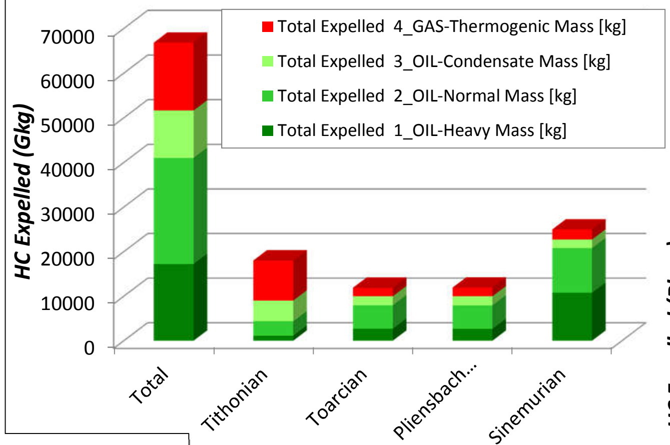

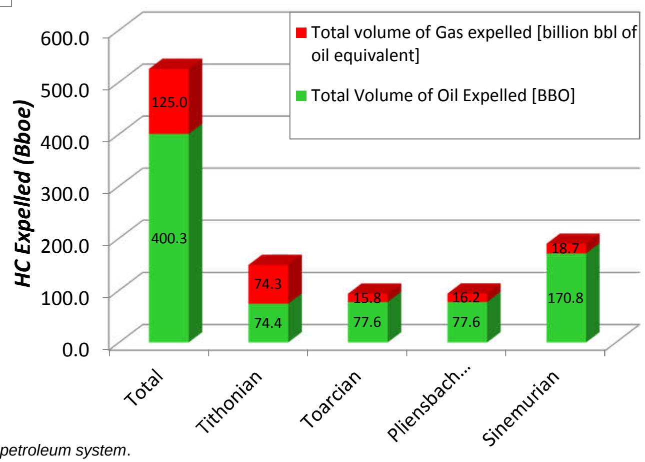

Figure 41: Contribution of each SR to the petroleum system.

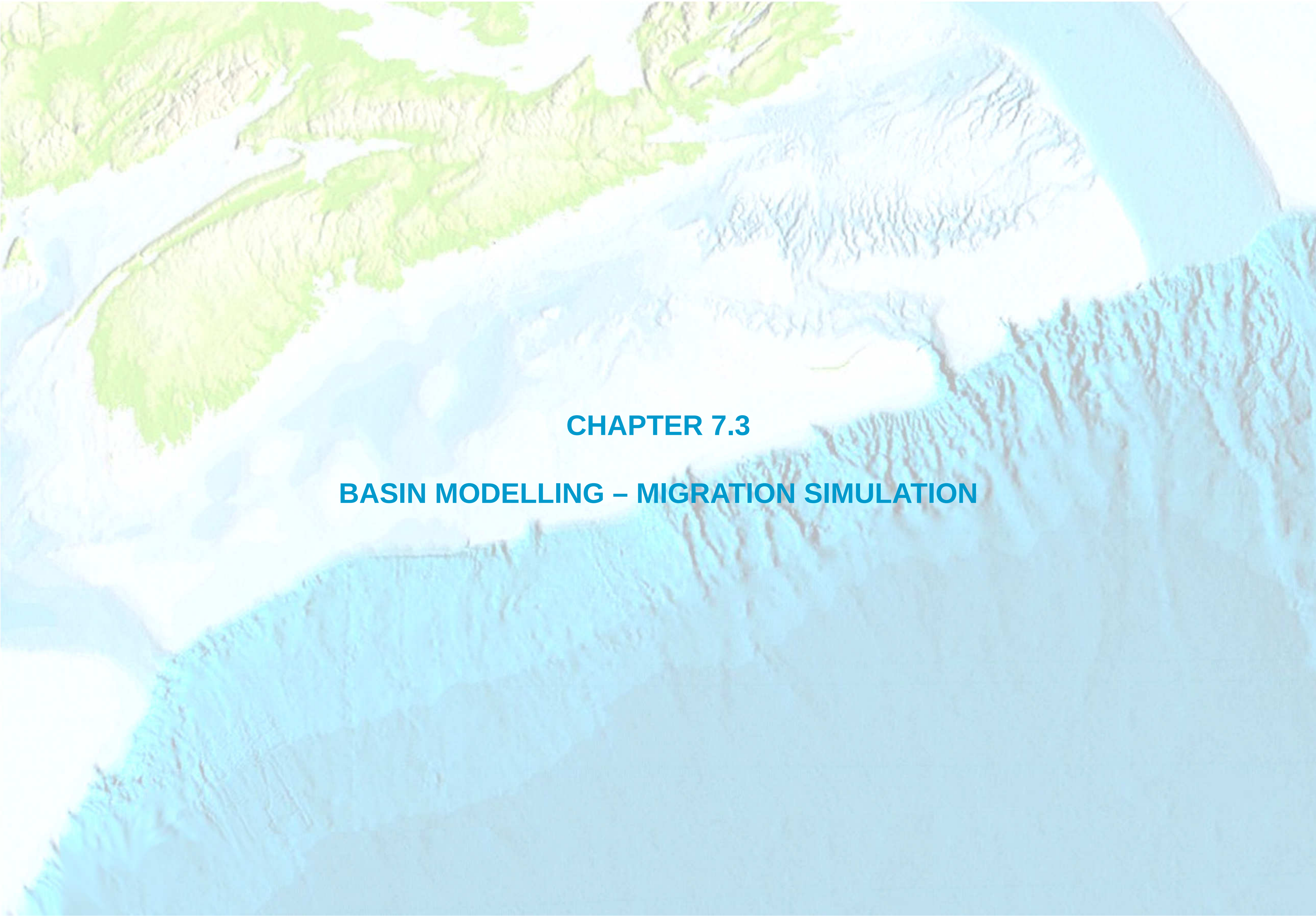

CHAPTER 7.3

BASIN MODELLING – MIGRATION SIMULATION

Horizon	Age (Ma)	Petroleum System Element	Comment
Sea Bed	0		
Miocene	14.5		
Oligocene Unc	29		
Top Paleocene	50		
Top Wyandot	70		
Top Cenomanian Unc	94		Upper Logan Canyon
Cenomanian U. Albian	94.75		
Cenomanian U. Albian	95.5		
U. Albian	97		
Top Unc U. Albian	101		Lower Logan Canyon
Albian	104		
Albian	108		
Aptian	112		
Aptian	116		
Aptian	120		
Top Naskapi	122.5		Upper Missisauga
Top Barremian	125		
Barremian	126.3		
Barremian	127.5		
Barremian	128.8		
Top Hauterivian	130		Middle Missisauga
Hauterivian Valanginian	130.5		
Hauterivian Valanginian	131		
Hauterivian Valanginian	132		
Hauterivian Valanginian	133		
Hauterivian Valanginian	134		
Hauterivian Valanginian	135		
Top Allochtonous Salt	136.5		
BCU	137		Lower Missisauga
Valanginian Berriasian	139		
Valanginian Berriasian	142		
Valanginian Berriasian	145		
Top Allochtonous Salt	148		
Top Tithonian SR	149.5		
Tithonian	149.8		
Top Baccaro Mic Mac	150		
Base Baccaro	151		
Ind Baccaro	155		
Ind Baccaro	156.5		
Banquereau	158		
Top Allochtonous Salt	160.5		
Base Allochtonous Salt	161		
Top Scatarie	163		
Mid Jurassic	170		
Top Toarcian SR	182		
Base Toarcian	183		
Top Pliensbachian SR	189		
Base Pliensbachian	190		
Top Sinemurian SR	196		
Top Salt Autochtonous	197		
Top Basement	200		

Table 8: Stratigraphic Chart of the TemisFlow™ 3D Model.

— Seismic horizon

Syn rift sediments are present below the autochthonous salt but they have been included in the advanced basement as they are not interpreted

Note: The play name corresponds to the stratigraphic sequence in which the reservoirs are distributed

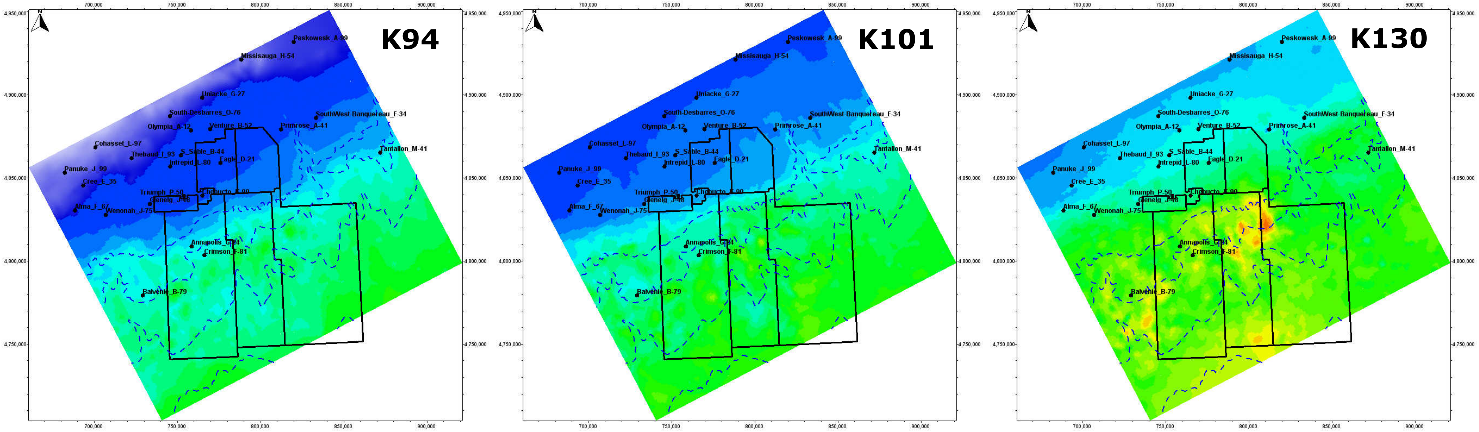

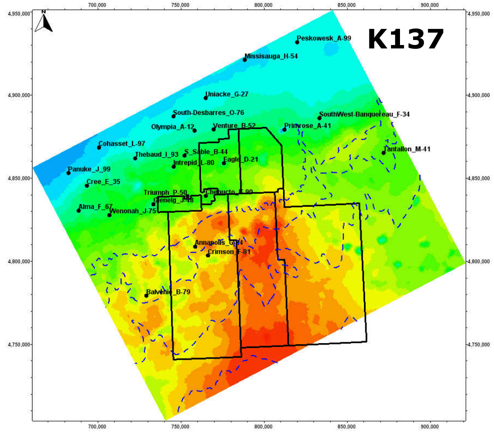

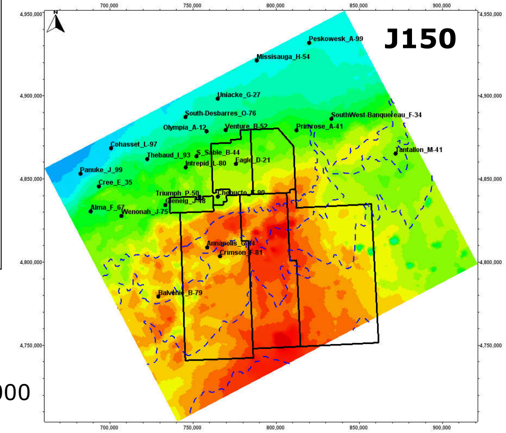

The workflow of the migration simulations is present in Figure 43.

The migration simulations are performed using Full Darcy capabilities of TemisFlow™ that relate the flow rate Ui of phase i to the different driving forces (calculation of HCs and water movements within the porous media) in the 2 km * 2 km grid with a high vertical resolution.

Intrinsic permeability K

Relative permeability phase i

$$U_i = -\frac{Kkr_i}{\mu_i}\left(\boxed{\mathrm{grad}(P-\rho_w gz)} + \boxed{\mathrm{grad}(P_c)} - \boxed{(\rho_w-\rho_i)g\,\mathrm{grad}(z)}\right)$$

Viscosity phase i | Hydrodynamism | Capillarity | Buoyancy

The volumetric calculations for the plays result from the redistribution of migrated HC in the 1 km * 1 km grid using the Trap Charge Assessment tool of TemisFlow™. The redistribution is based on topographical analysis (in terms of flow lines and drainage areas – Ray Tracing approach) of the top horizon of the analyzed layer/play (Figure 44). A definition of thresholds for hydrocarbon fluid concentration (in terms of masses) is defined, thresholds below which hydrocarbon quantities are discarded from the volumes computation as they are considered as non-pay.

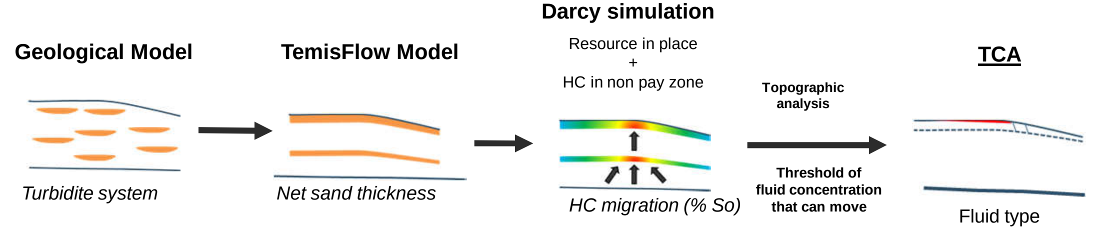

Figure 43: Workflow of migration modelling.

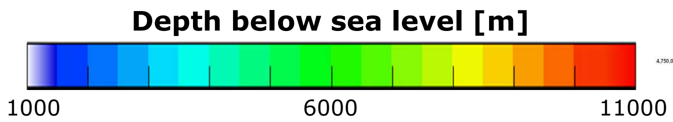

Figure 44: Structural maps of the plays assessed with TCA tool of TemisFlow™

K101/94

Figure 45: Hydrocarbon Saturation of the K101/94 Play

Hydrocarbon Liquid Saturation [%]

Hydrocarbon saturation is displayed with a condensed color scale that highlights areas with concentrated hydrocarbons.

Fault corridors are defined as migration pathways in the model. Consequently, highest concentrations are found on the shelf (on top of the fault block or against faults).

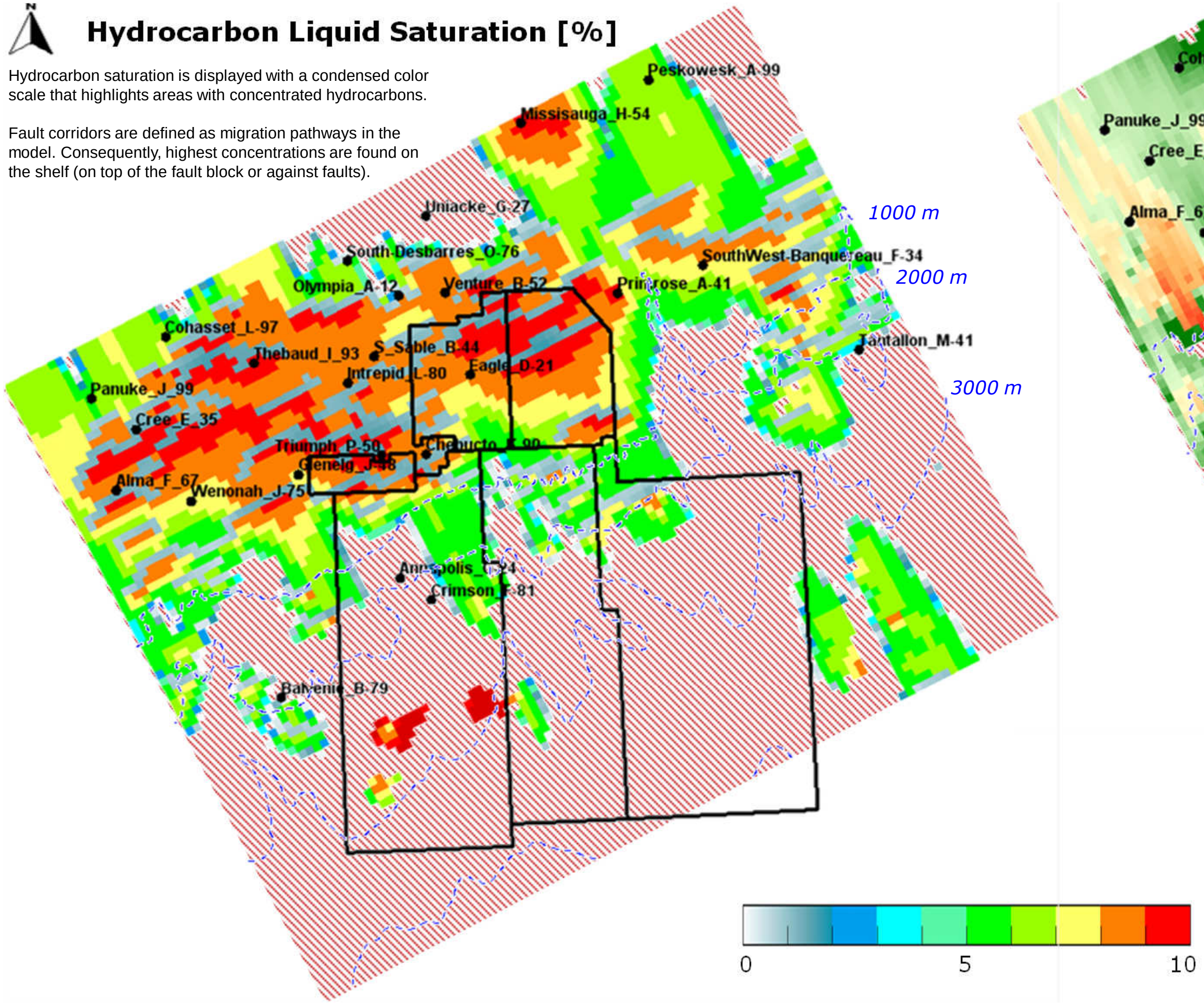

Figure 46: Oil content of the vapor phase in the K101/94 Play

Mass CGR [mg /g HC]

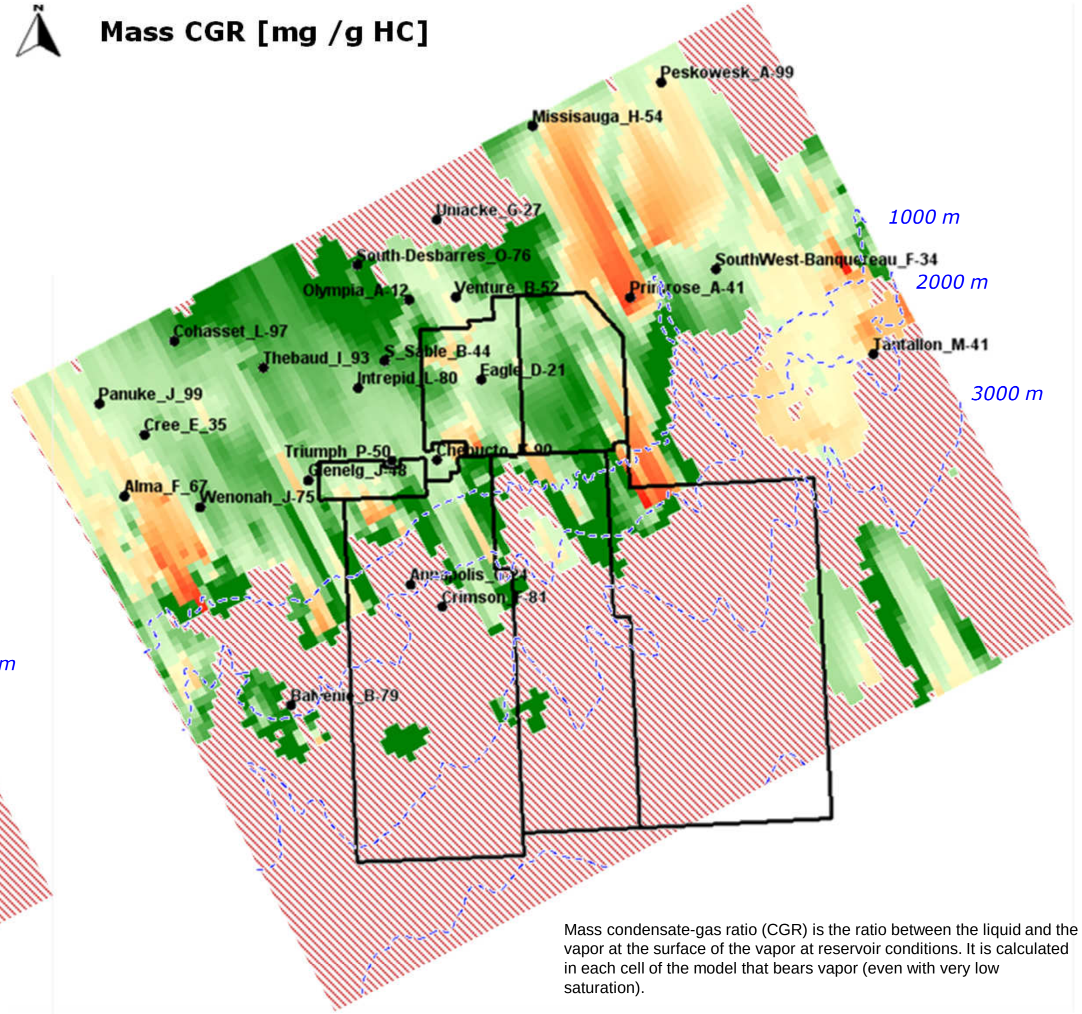

Mass condensate-gas ratio (CGR) is the ratio between the liquid and the vapor at the surface of the vapor at reservoir conditions. It is calculated in each cell of the model that bears vapor (even with very low saturation).

It demonstrates the wetness or dryness of the gas.

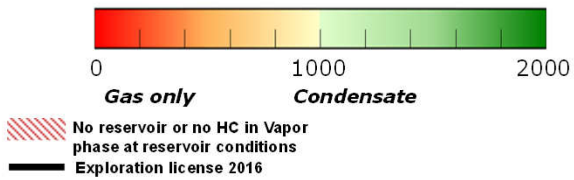

Migration Simulation – K101/94 - HC Saturation and Mass CGR

K101/94

Figure 47: Oil density of the K101/94 Play

API of Liquid from Liquid Phase

API density is calculated for the liquids in liquid phase at reservoir conditions in each cell of the model that bears liquid (even with very low saturation).

Light oil should be expected in some accumulations within the Parcels 4, 5 and 6

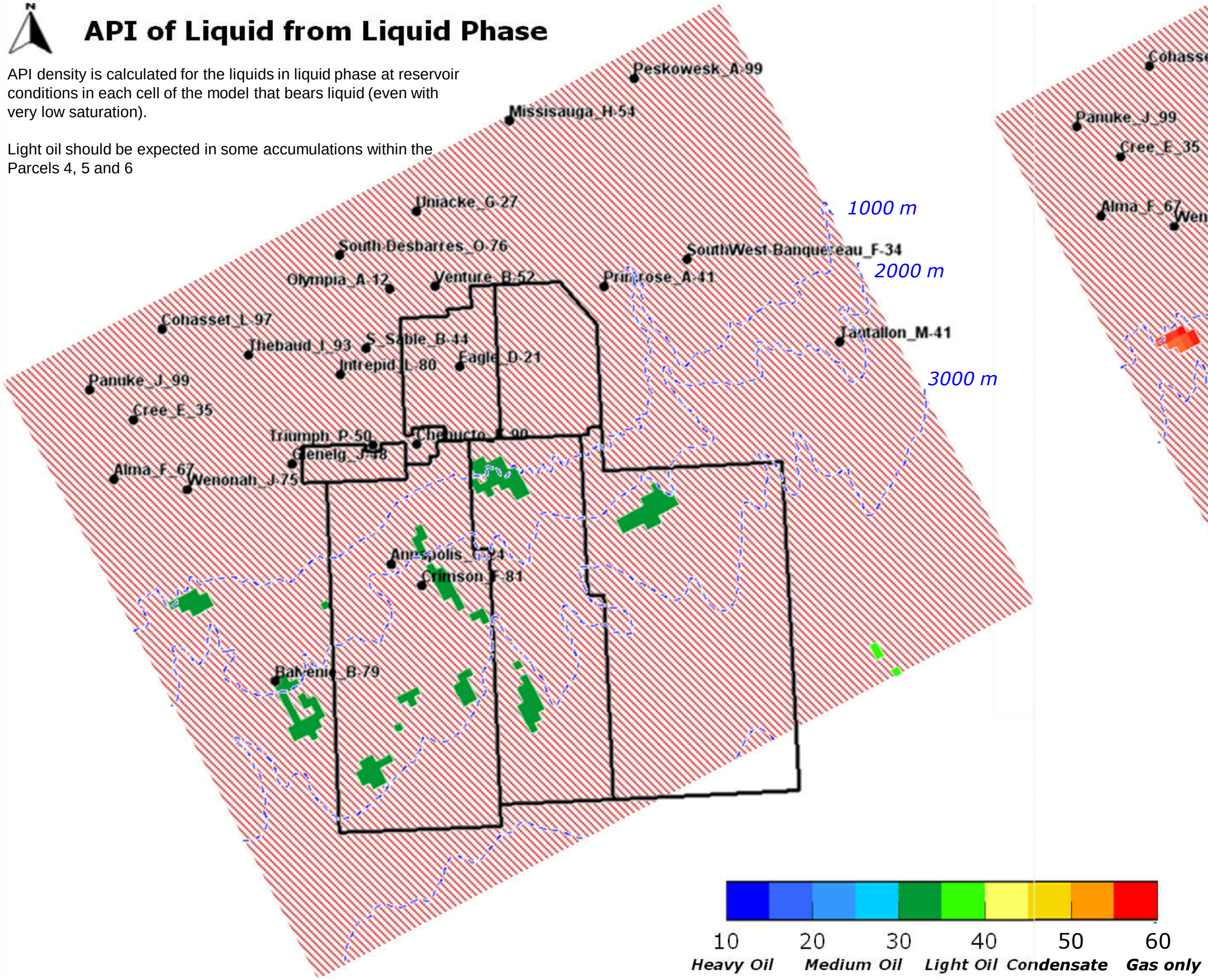

Figure 48: Gas content of the liquid phase in f the K101/94 Play

Solution GOR [ft³/stb]

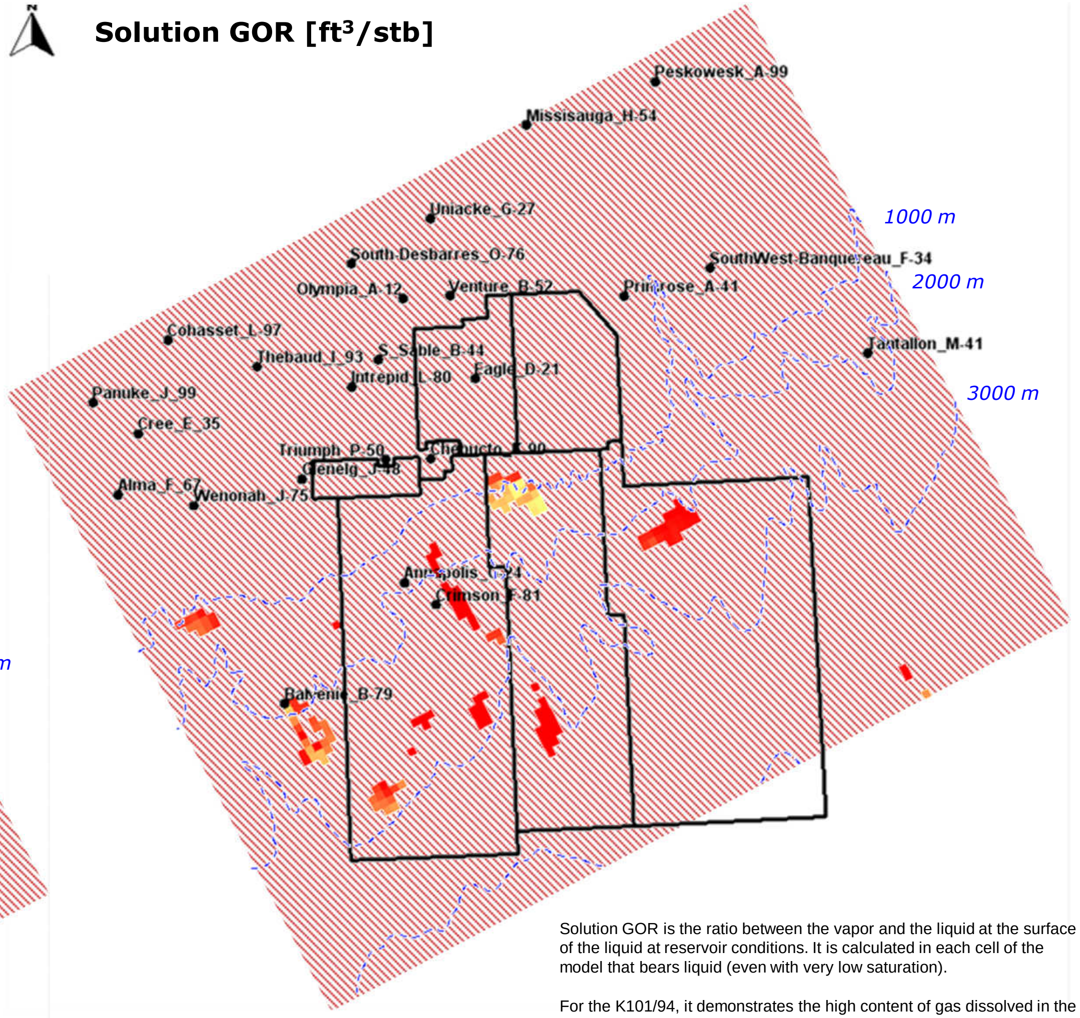

Solution GOR is the ratio between the vapor and the liquid at the surface of the liquid at reservoir conditions. It is calculated in each cell of the model that bears liquid (even with very low saturation).

For the K101/94, it demonstrates the high content of gas dissolved in the liquid fractions

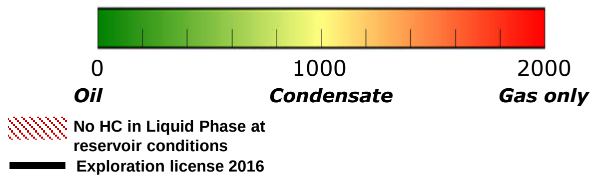

K101/94

Figure 49: Age of the first HC arrival in the K101/94 Play

Timing of first HC Saturation [Ma]

The timing of saturation is computed to display the age at which a cell reaches a fixed threshold for hydrocarbon saturation. Using a very low value allows visualizing the age at which hydrocarbons start to flow through a given layer.

For the K101/94, hydrocarbons started invading the reservoir during the Upper Cretaceous, with a continuous flow until present-day

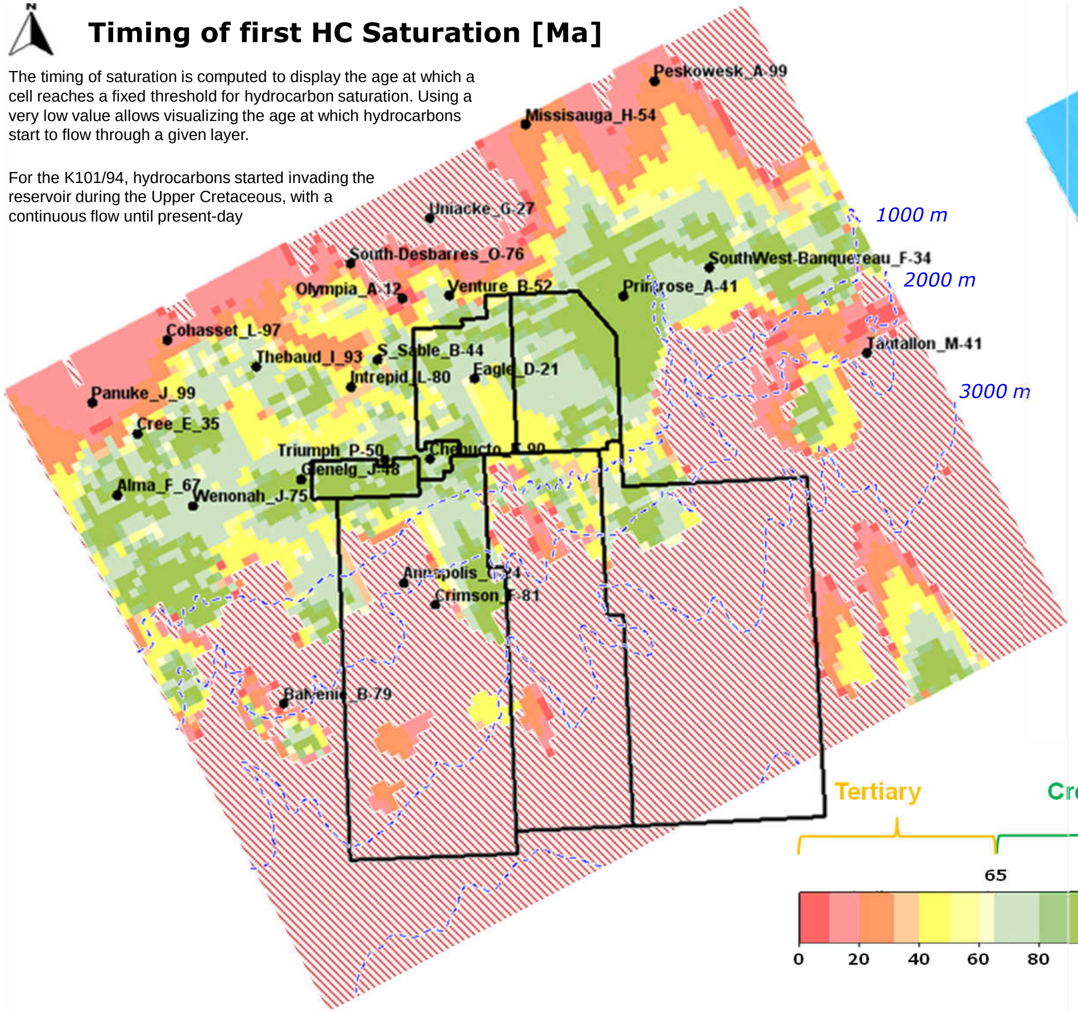

Figure 50: Percentage of gas generated in the Tithonian SR in the Play K101/94

SR Contribution for Gas Fraction [%]

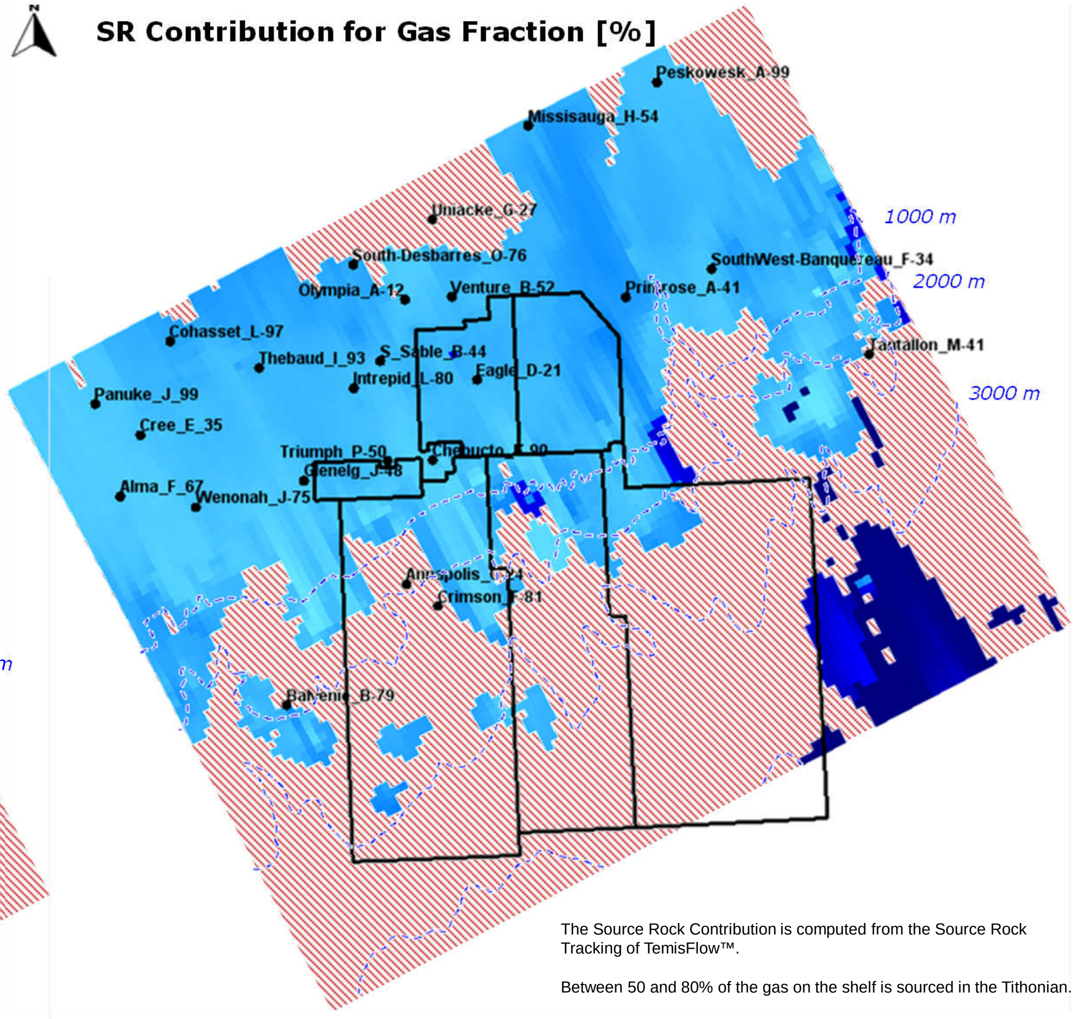

The Source Rock Contribution is computed from the Source Rock Tracking of TemisFlow™.

Between 50 and 80% of the gas on the shelf is sourced in the Tithonian.

In the distal part of the basin, between 60 and 100% of the gas was generated in the Lower Jurassic.

K130

Figure 51: Hydrocarbon Saturation of the K130 Play.

Hydrocarbon Liquid Saturation [%]

Hydrocarbon saturation is displayed with a condensed color scale that highlights areas with concentrated hydrocarbons.

Fault corridors are defined as migration pathways in the model. Consequently, highest concentrations on the shelf are found on top of fault blocks or against faults. Nonetheless, most hydrocarbon accumulations are found in the basin.

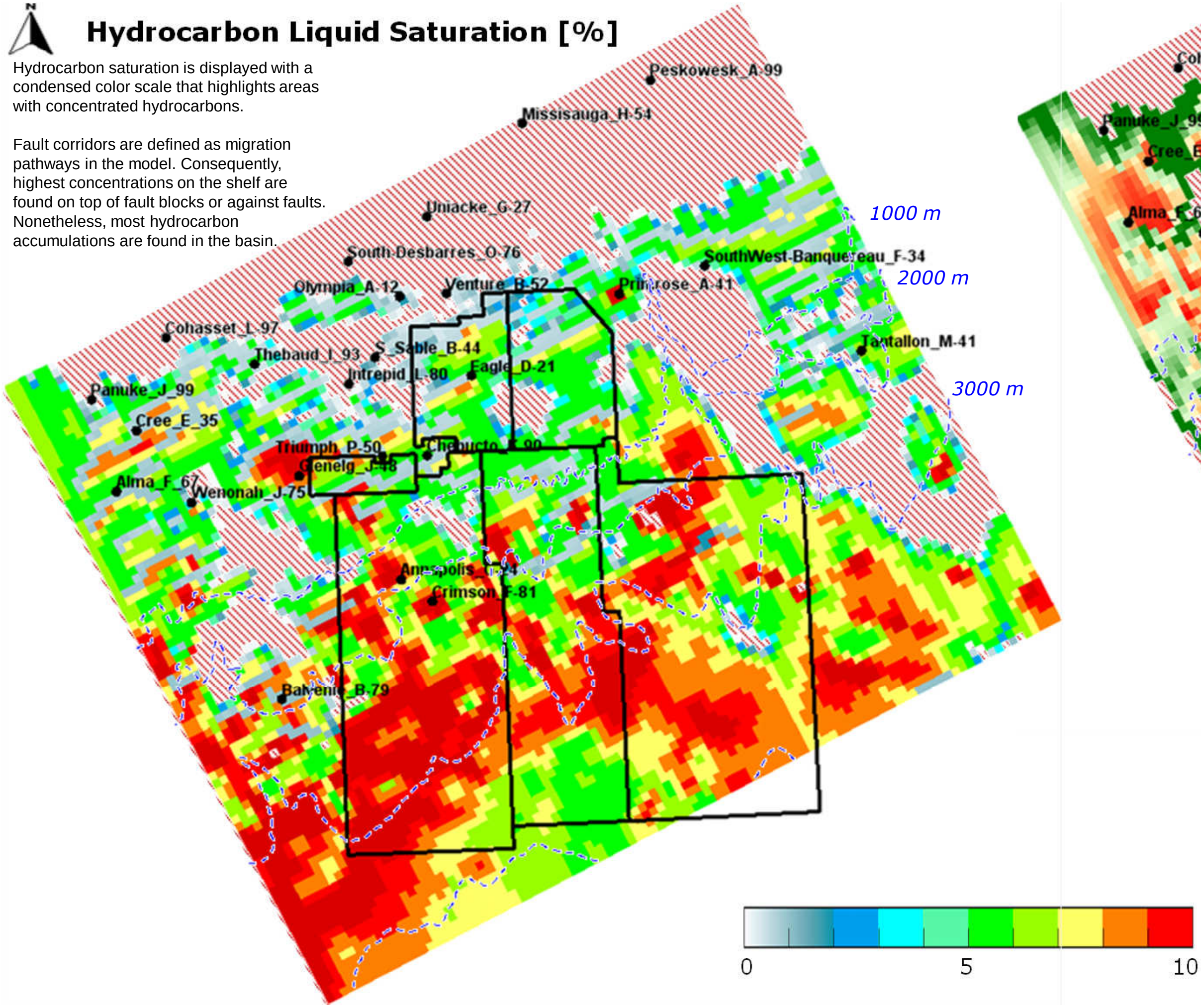

Figure 52: Oil content of the vapor phase in the K130 Play

Mass CGR [mg /g HC]

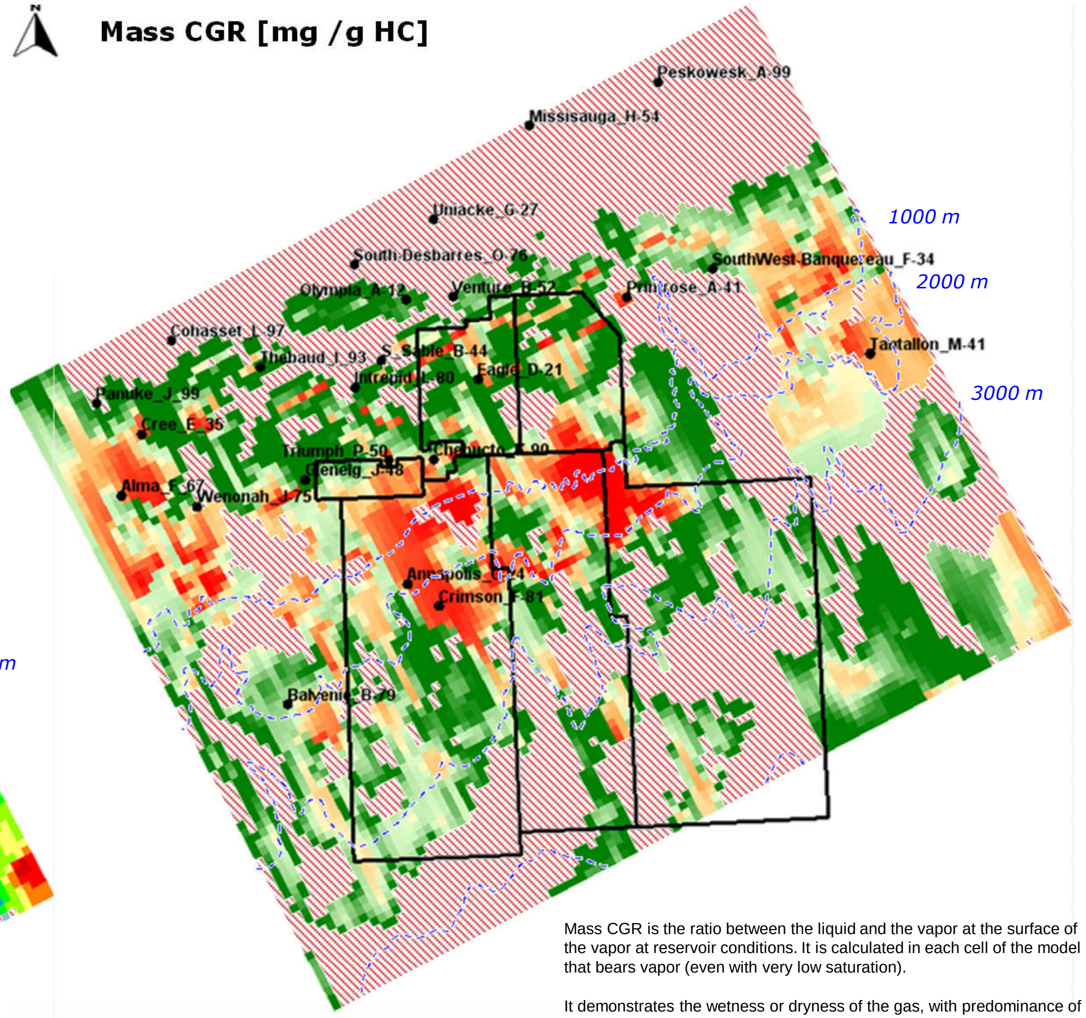

Mass CGR is the ratio between the liquid and the vapor at the surface of the vapor at reservoir conditions. It is calculated in each cell of the model that bears vapor (even with very low saturation).

It demonstrates the wetness or dryness of the gas, with predominance of dry gas in the Parcel 3, the northern part of Parcels 4, 5 and 6, and along faults on the shelf.

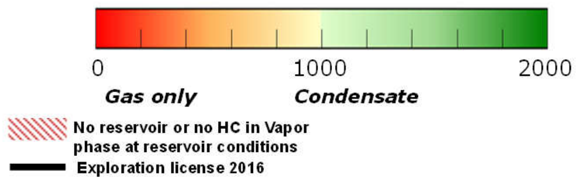

K130

Figure 53: Oil density of the K130 Play

API density is calculated for the liquids in liquid phase at reservoir conditions in each cell of the model that bears liquid (even with very low saturation).

Medium to light oil should be expected in distal part of the Parcels 4, 5 and 6

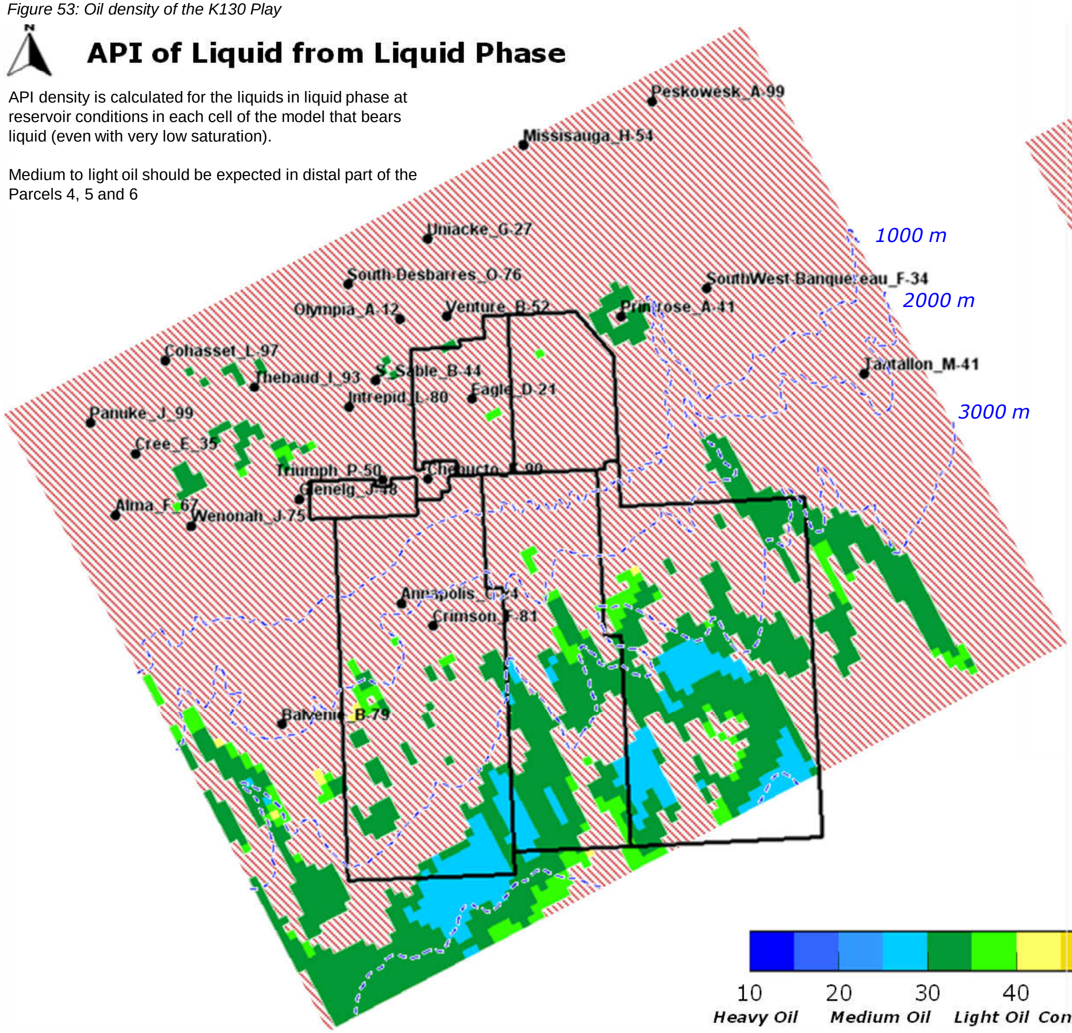

Figure 54: Gas content of the liquid phase in f the K130 Play

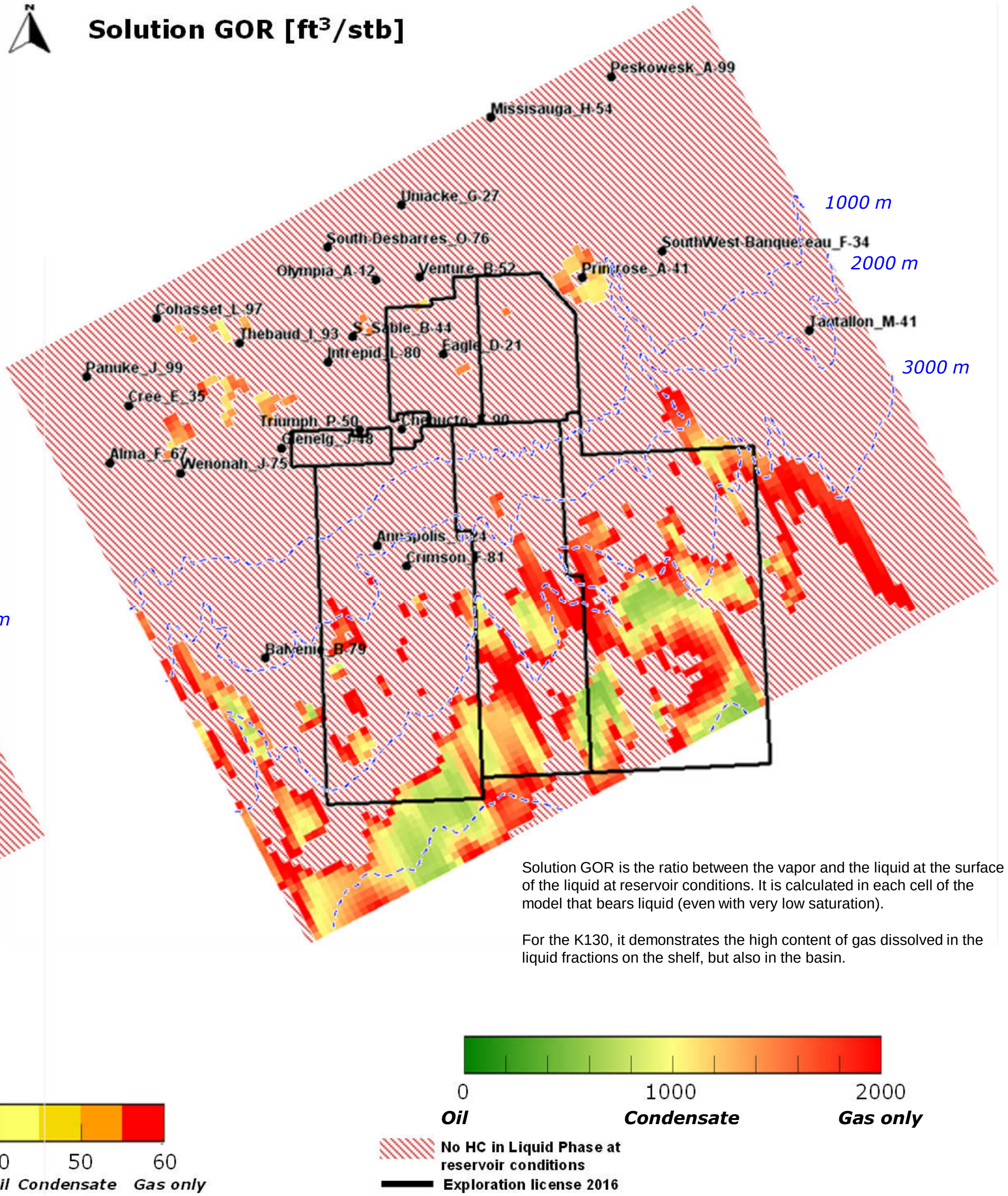

Solution GOR is the ratio between the vapor and the liquid at the surface of the liquid at reservoir conditions. It is calculated in each cell of the model that bears liquid (even with very low saturation).

For the K130, it demonstrates the high content of gas dissolved in the liquid fractions on the shelf, but also in the basin.

K130

Figure 56: Percentage of gas generated in the Tithonian SR in the Play K130

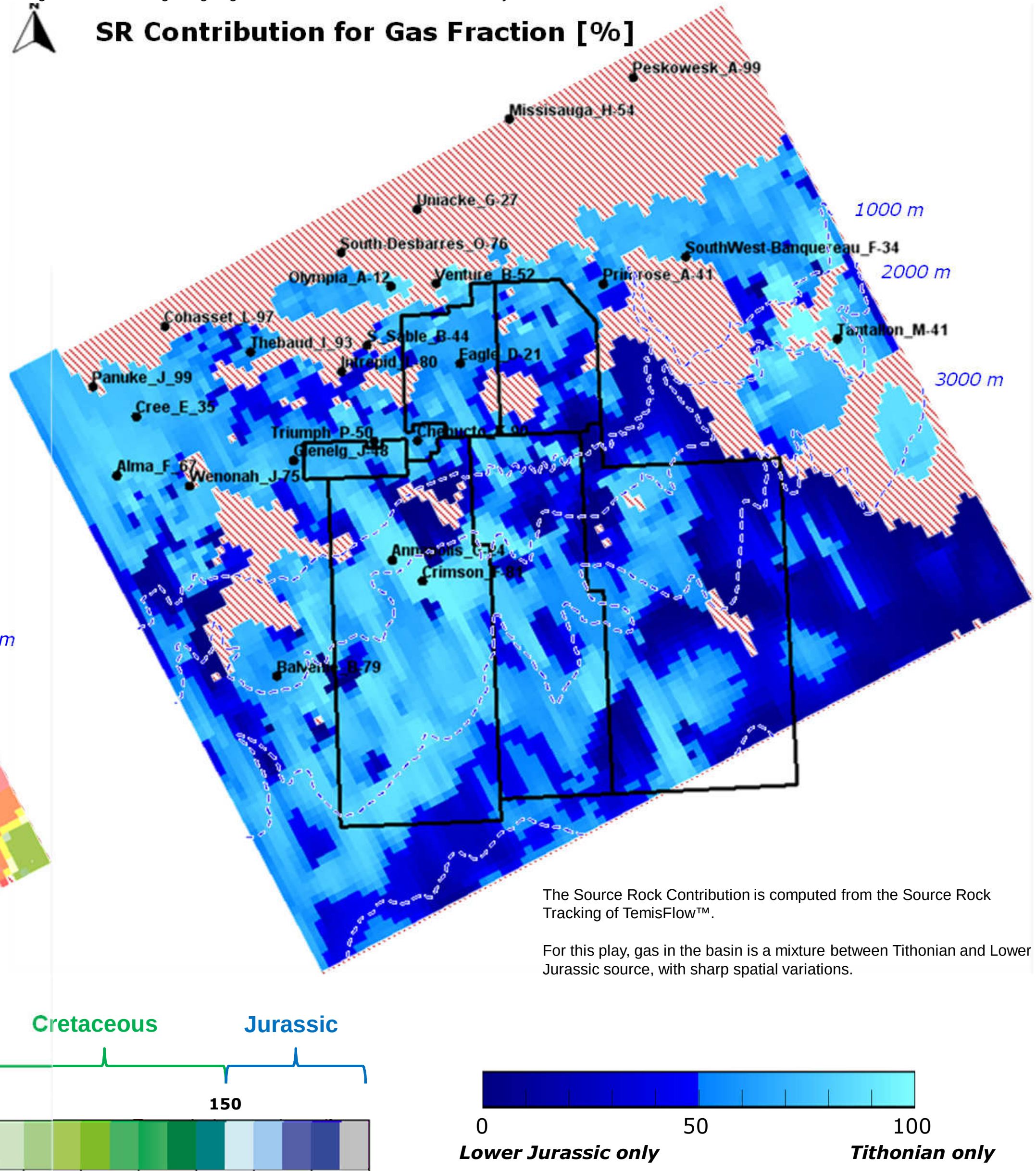

The Source Rock Contribution is computed from the Source Rock Tracking of TemisFlow™.

For this play, gas in the basin is a mixture between Tithonian and Lower Jurassic source, with sharp spatial variations.

Figure 55: Age of the first HC arrival in the K130 Play.

Timing of first HC Saturation [Ma]

The timing of saturation is computed to display the age at which a cell reaches a fixed threshold for hydrocarbon saturation. Using a very low value allows visualizing the age at which hydrocarbons start to flow through a given layer.

For the K130, hydrocarbons started invading the reservoir at the end of Lower Cretaceous, with a continuous flow until present-day.

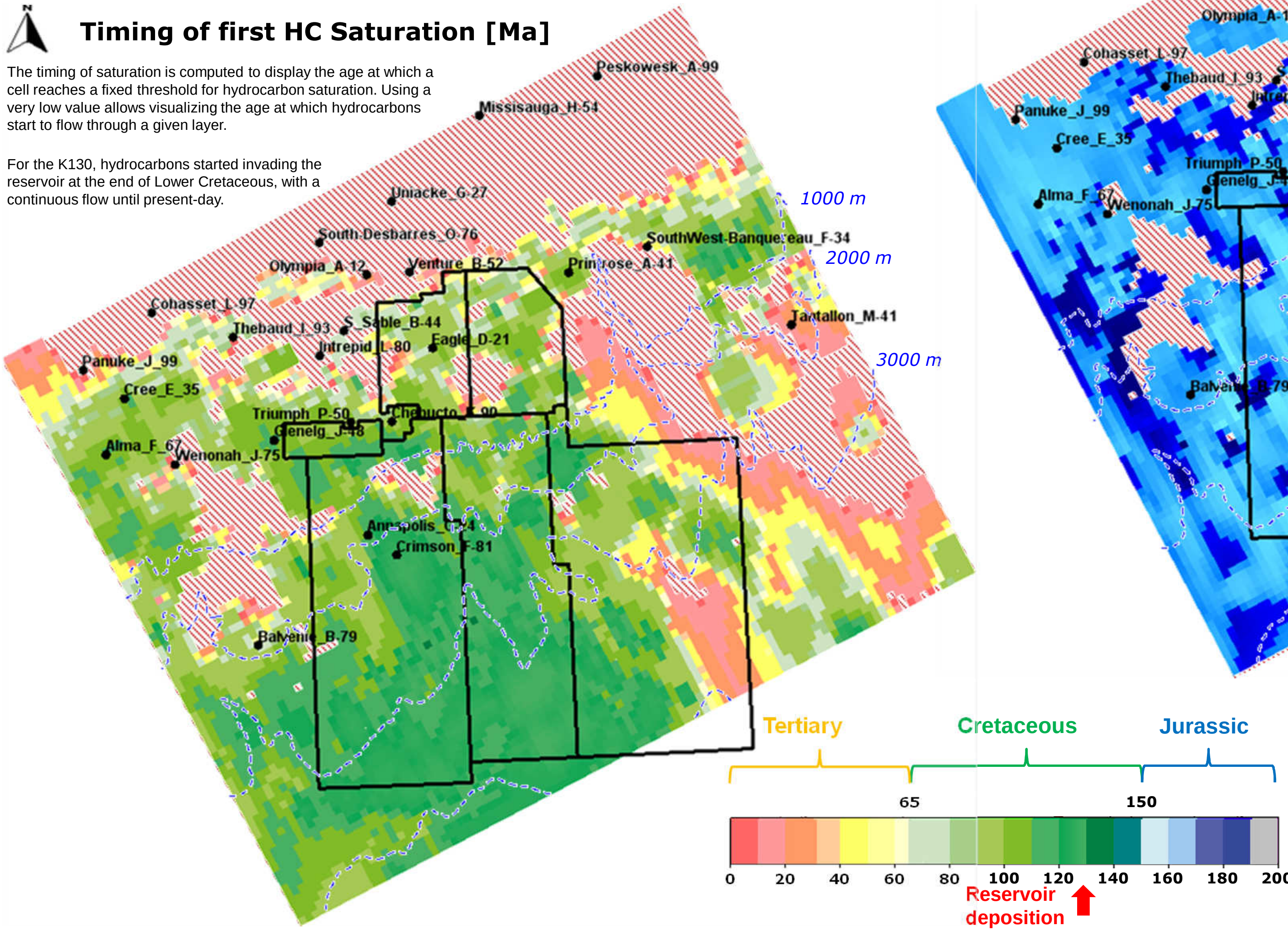

K137

Figure 57: Hydrocarbon Saturation of the K137 Play.

Hydrocarbon Liquid Saturation [%]

Hydrocarbon saturation is displayed with a condensed color scale that highlights areas with concentrated hydrocarbons.

Fault corridors are defined as migration pathways in the model. Consequently, highest concentrations on the shelf are found on top of fault blocks or against faults.
Nonetheless, most hydrocarbon accumulations are found in the basin.

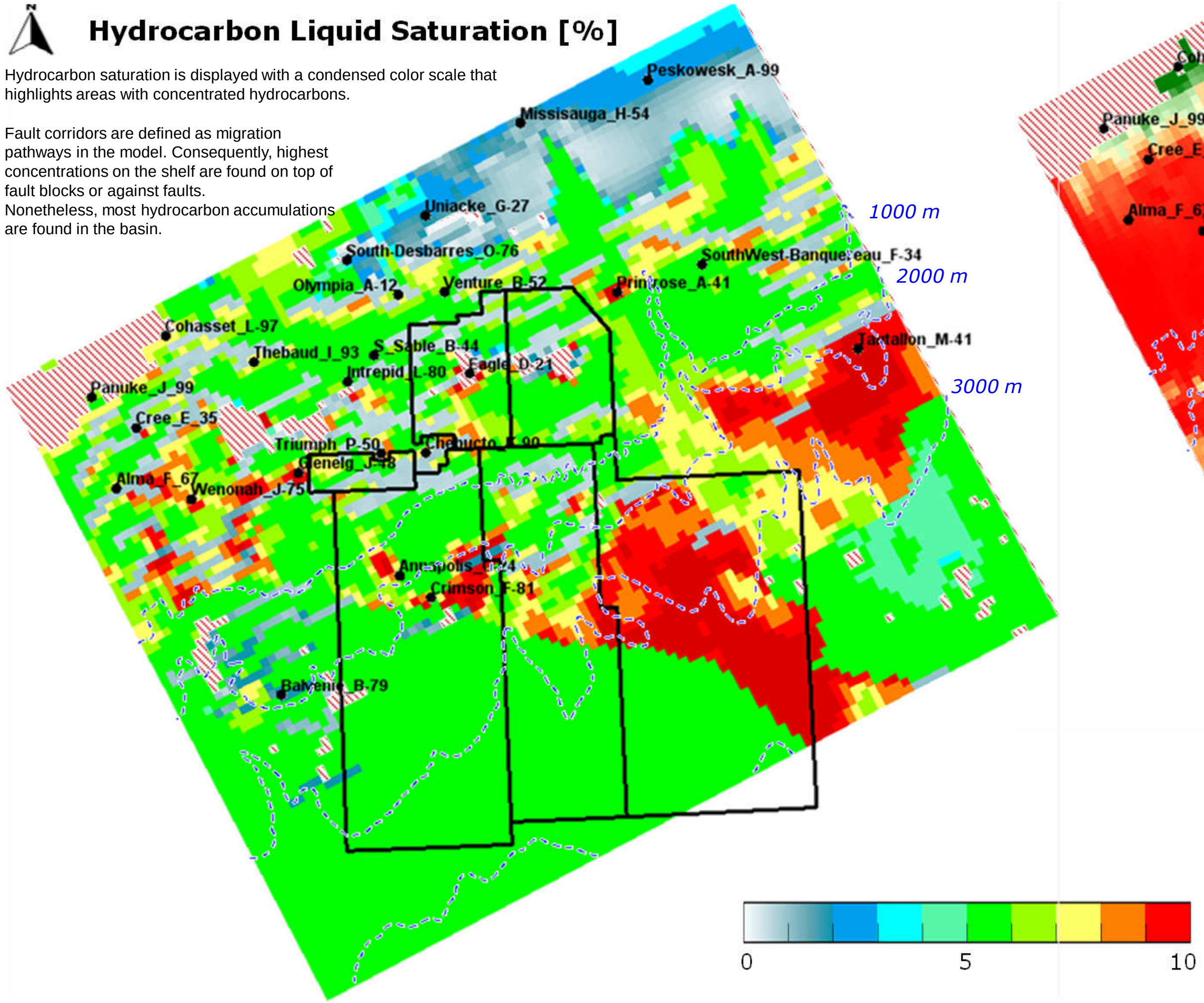

Figure 58: Oil content of the vapor phase in the K137 Play

Mass CGR [mg /g HC]

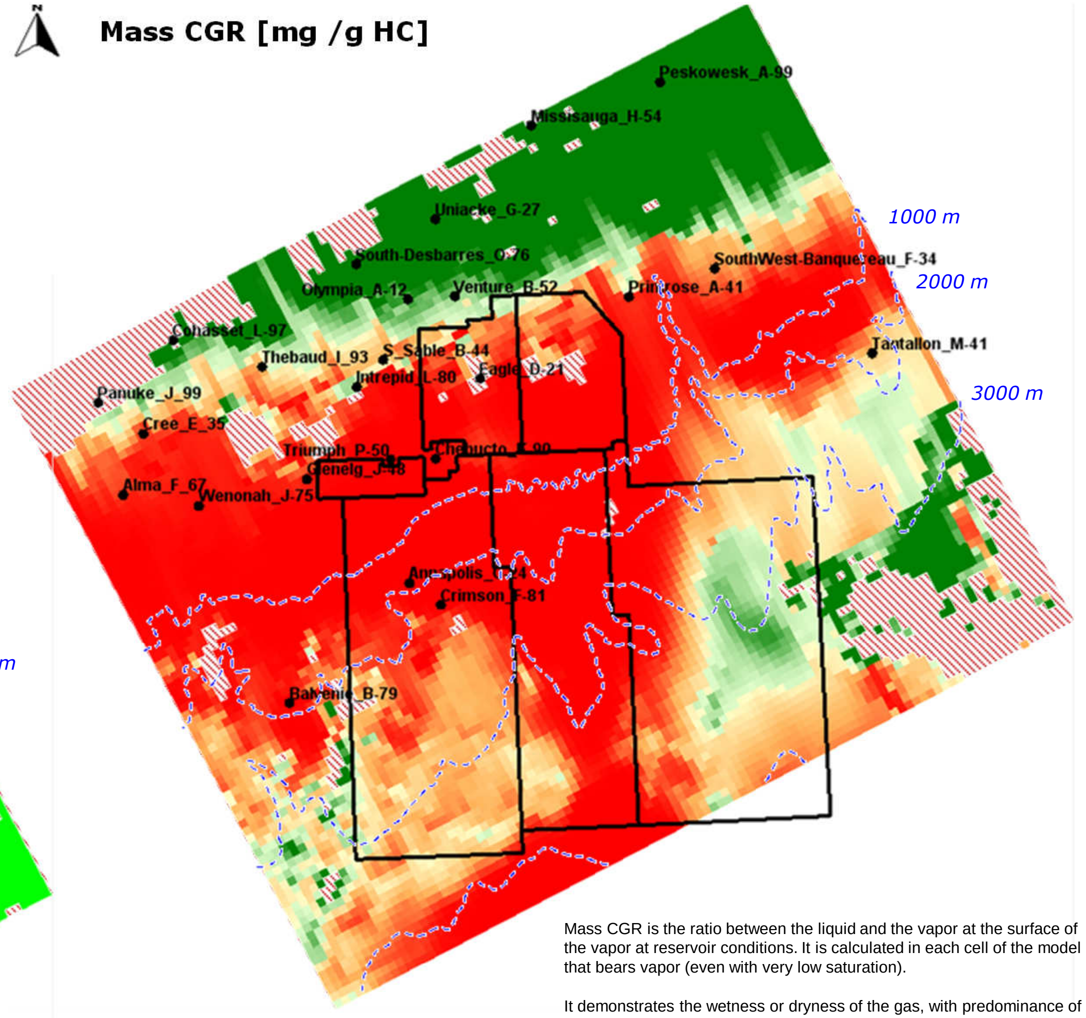

Mass CGR is the ratio between the liquid and the vapor at the surface of the vapor at reservoir conditions. It is calculated in each cell of the model that bears vapor (even with very low saturation).

It demonstrates the wetness or dryness of the gas, with predominance of dry gas in most of the study area, with a pattern corresponding to Tithonian SR maturity.

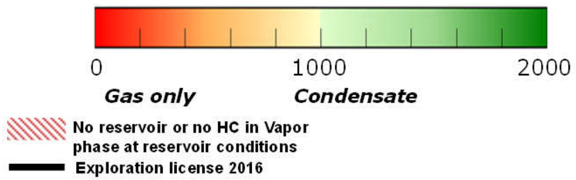

Migration Simulation – K137 - HC Saturation and Mass CGR

K137

Figure 59: Oil density of the K137 Play

API of Liquid from Liquid Phase

API density is calculated for the liquids in liquid phase at reservoir conditions in each cell of the model that bears liquid (even with very low saturation).

Medium to light oil should be expected in distal part of the Parcels 4, 5 and 6 and on the shelf.

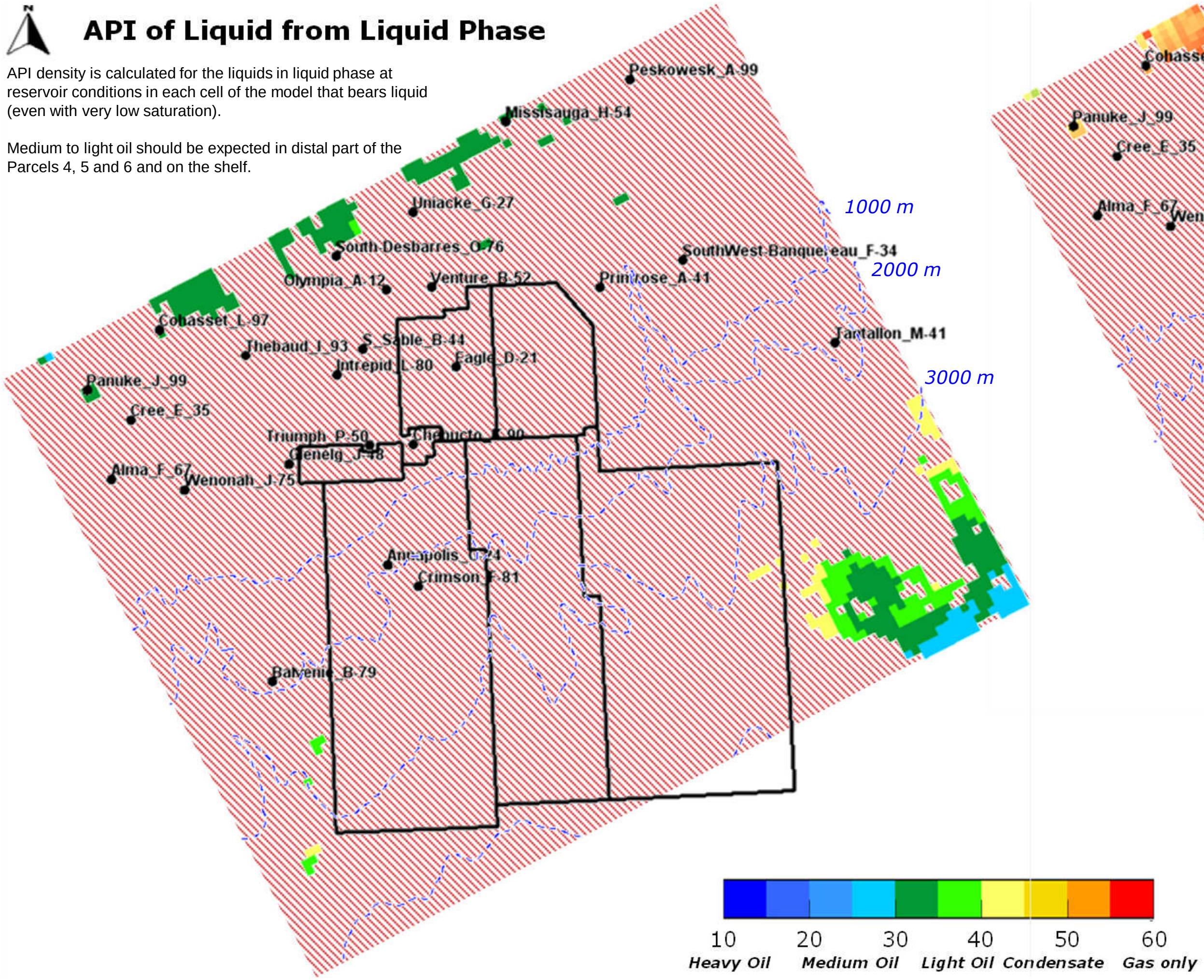

Figure 60: Gas content of the liquid phase in f the K137 Play

Solution GOR [ft³/stb]

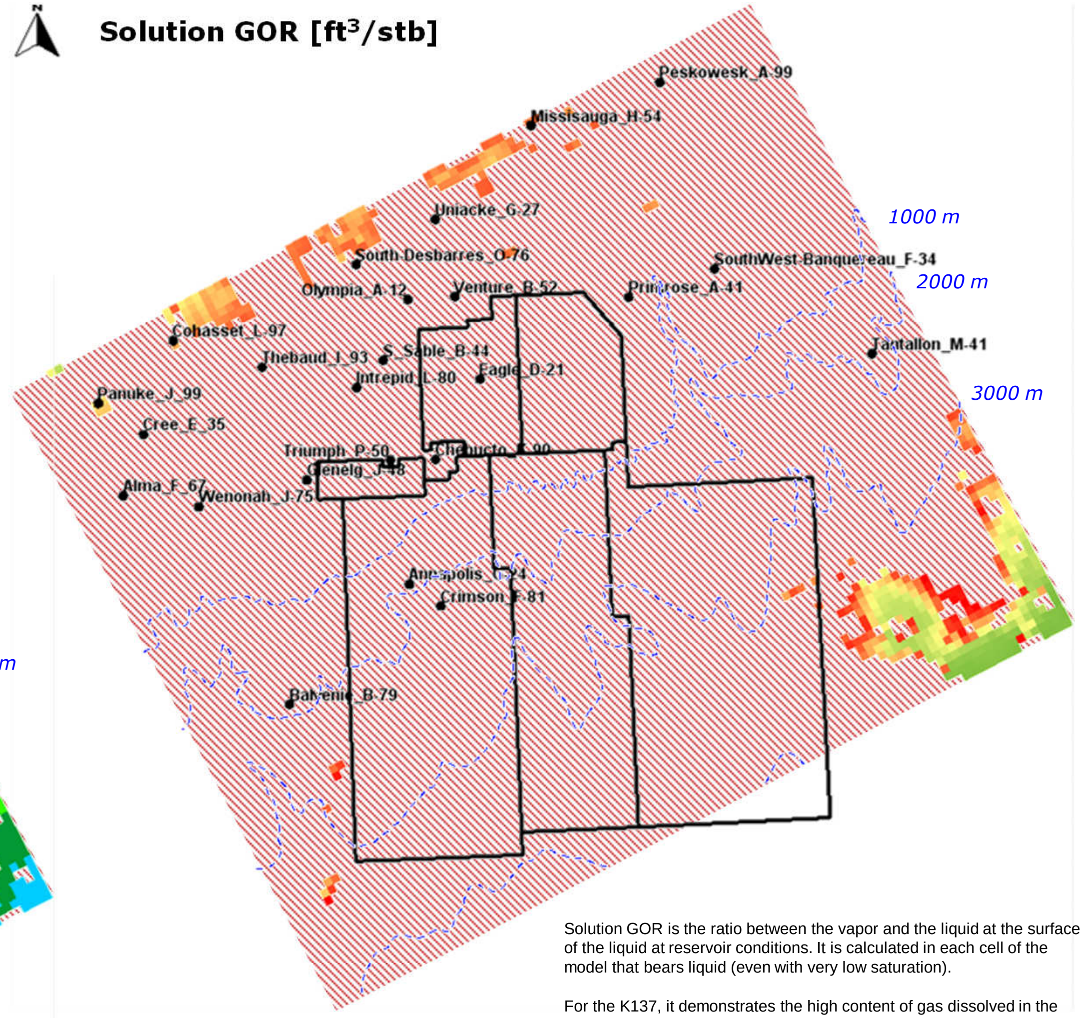

Solution GOR is the ratio between the vapor and the liquid at the surface of the liquid at reservoir conditions. It is calculated in each cell of the model that bears liquid (even with very low saturation).

For the K137, it demonstrates the high content of gas dissolved in the liquid fractions on the shelf, whereas gas content is low in the southern part of Banquereau Wedge.

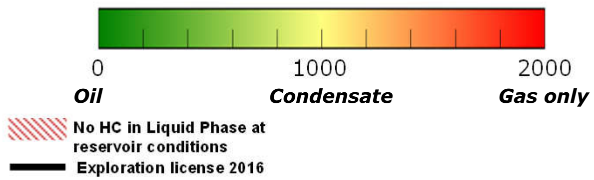

K137

Figure 61: Age of the first HC arrival in the K137 Play

Timing of first HC Saturation [Ma]

The timing of saturation is computed to display the age at which a cell reaches a fixed threshold for hydrocarbon saturation. Using a very low value allows visualizing the age at which hydrocarbons start to flow through a given layer.

For the K137, hydrocarbons started invading the reservoir during the early stages of Lower Cretaceous, with a continuous flow until present-day on the shelf and south of Tantallon.

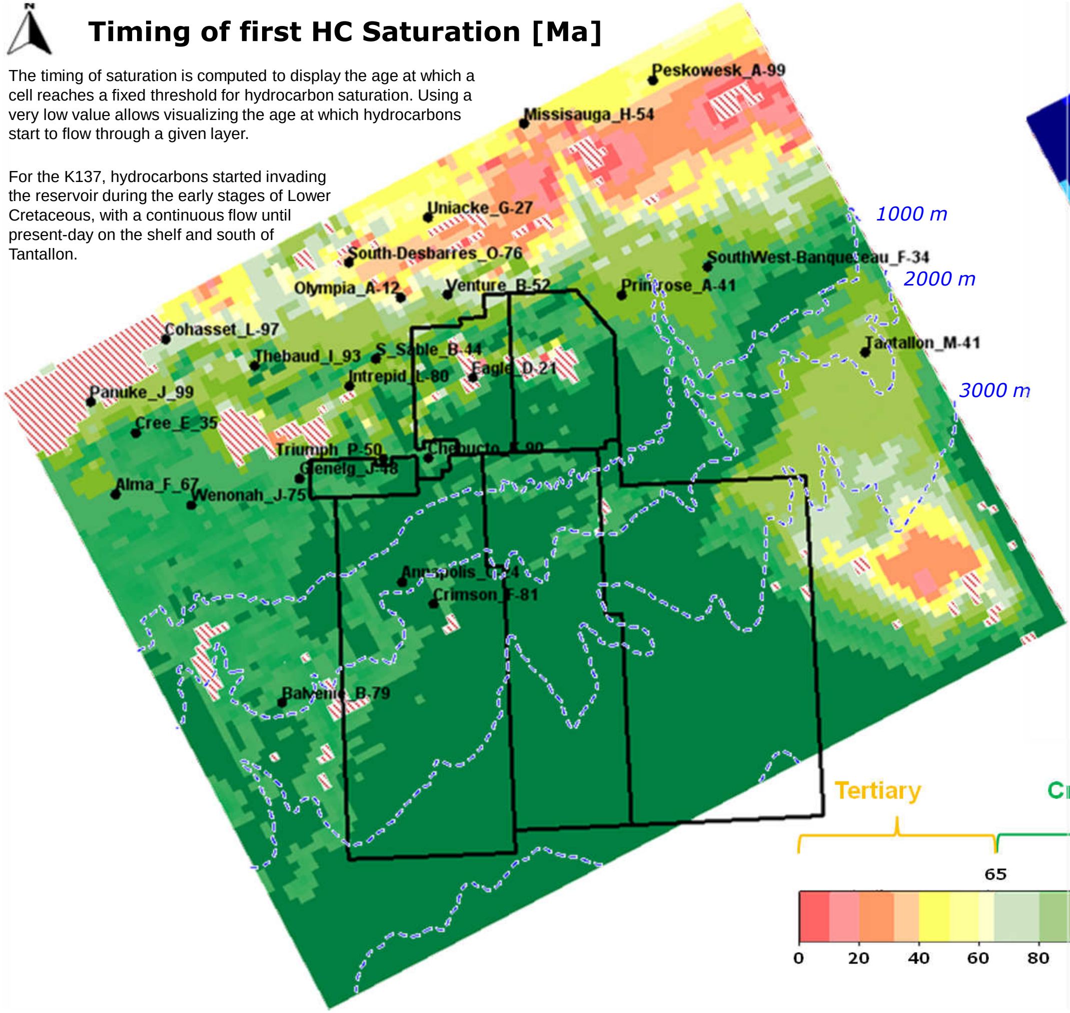

Figure 62: Percentage of gas generated in the Tithonian SR in the Play K137

SR Contribution for Gas Fraction [%]

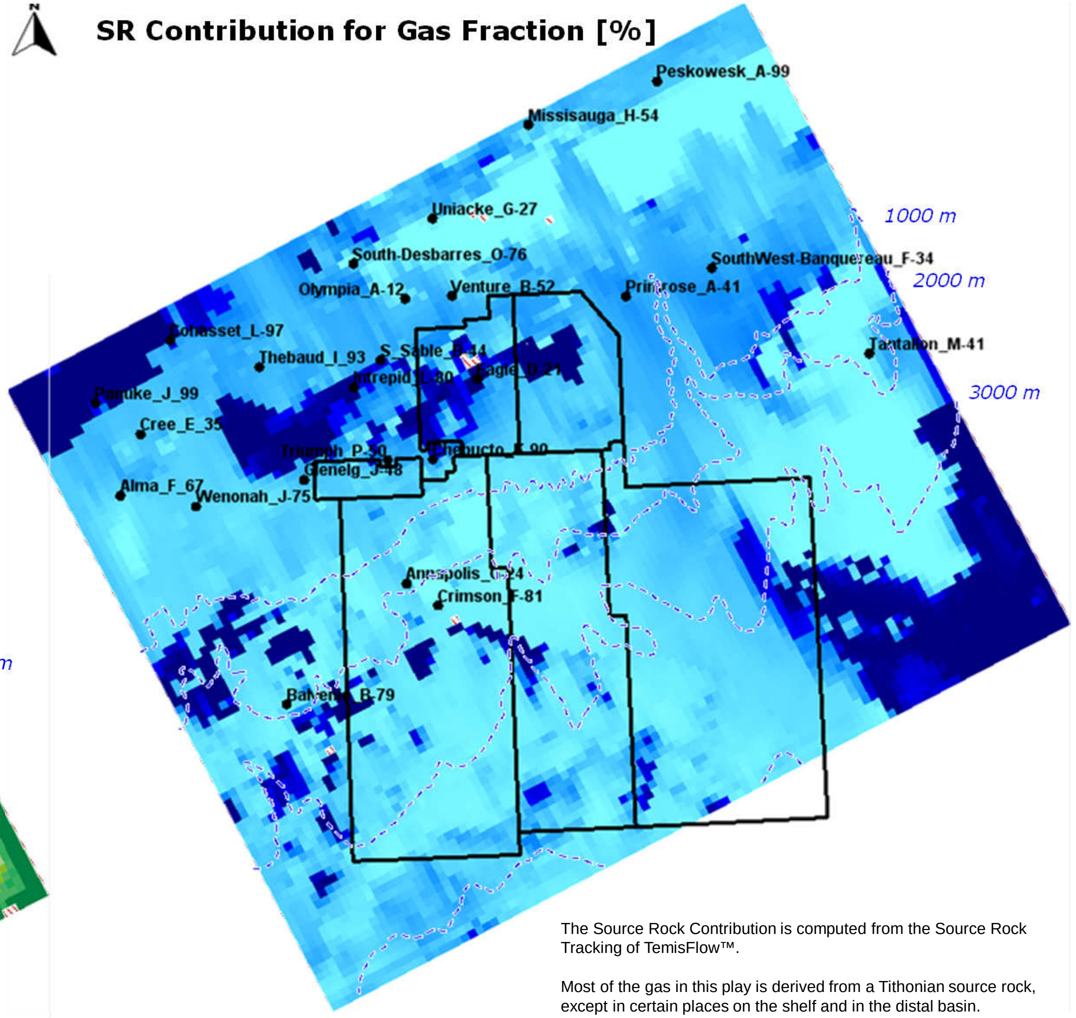

The Source Rock Contribution is computed from the Source Rock Tracking of TemisFlow™.

Most of the gas in this play is derived from a Tithonian source rock, except in certain places on the shelf and in the distal basin.
Rapid variations from 100% Tithonian source to 100% Lower Jurassic source reflect the distribution of salt bodies within the basin.

J150

Figure 63: Hydrocarbon Saturation of the J150 Play.

Hydrocarbon Liquid Saturation [%]

Hydrocarbon saturation is displayed with a condensed color scale that highlights areas with concentrated hydrocarbons.

Fault corridors are defined as migration pathways in the model, but their influence seems to be limited in this play. Most hydrocarbon accumulations are found in the basin.

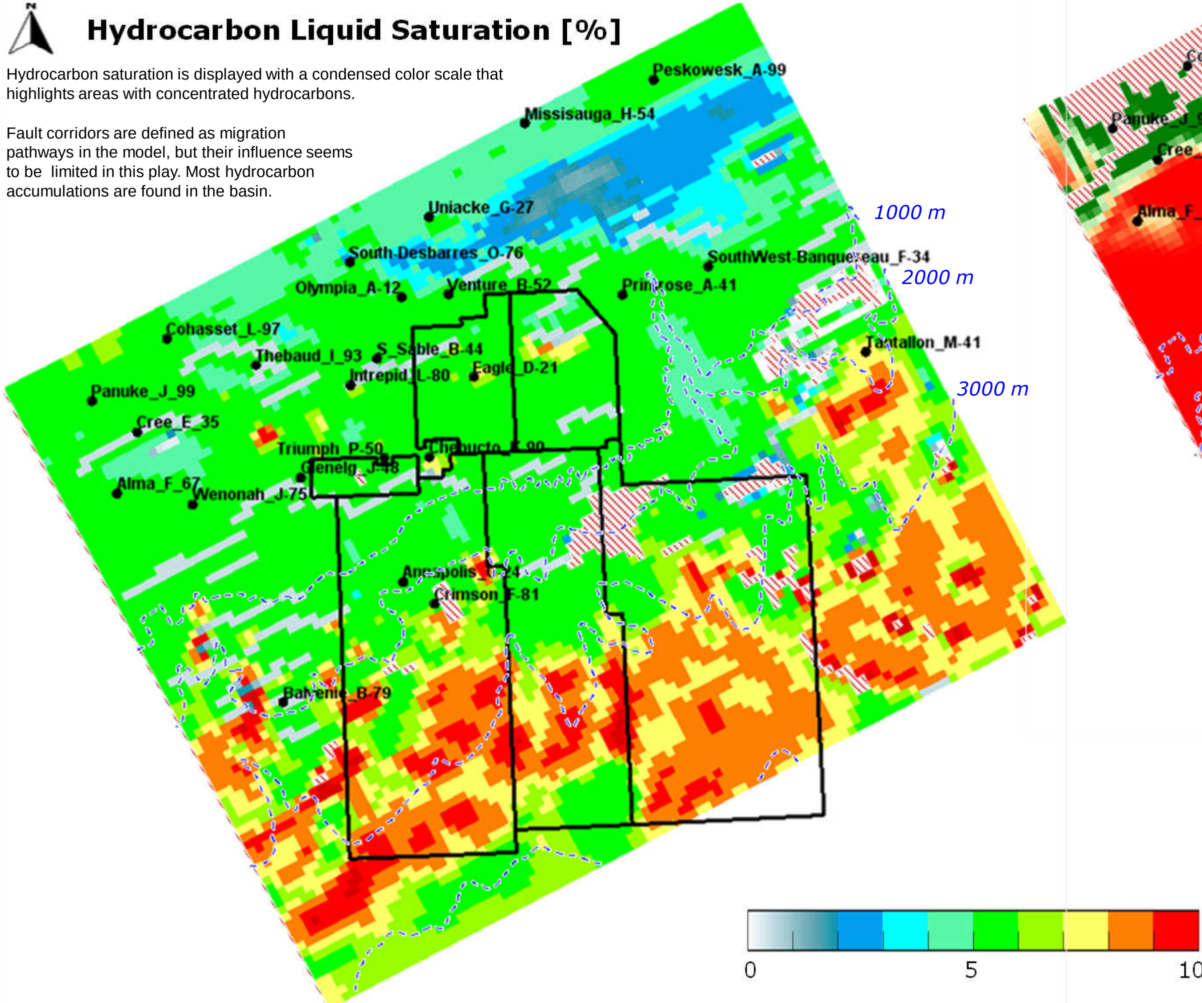

Figure 64: Oil content of the vapor phase in the J150 Play

Mass CGR [mg /g HC]

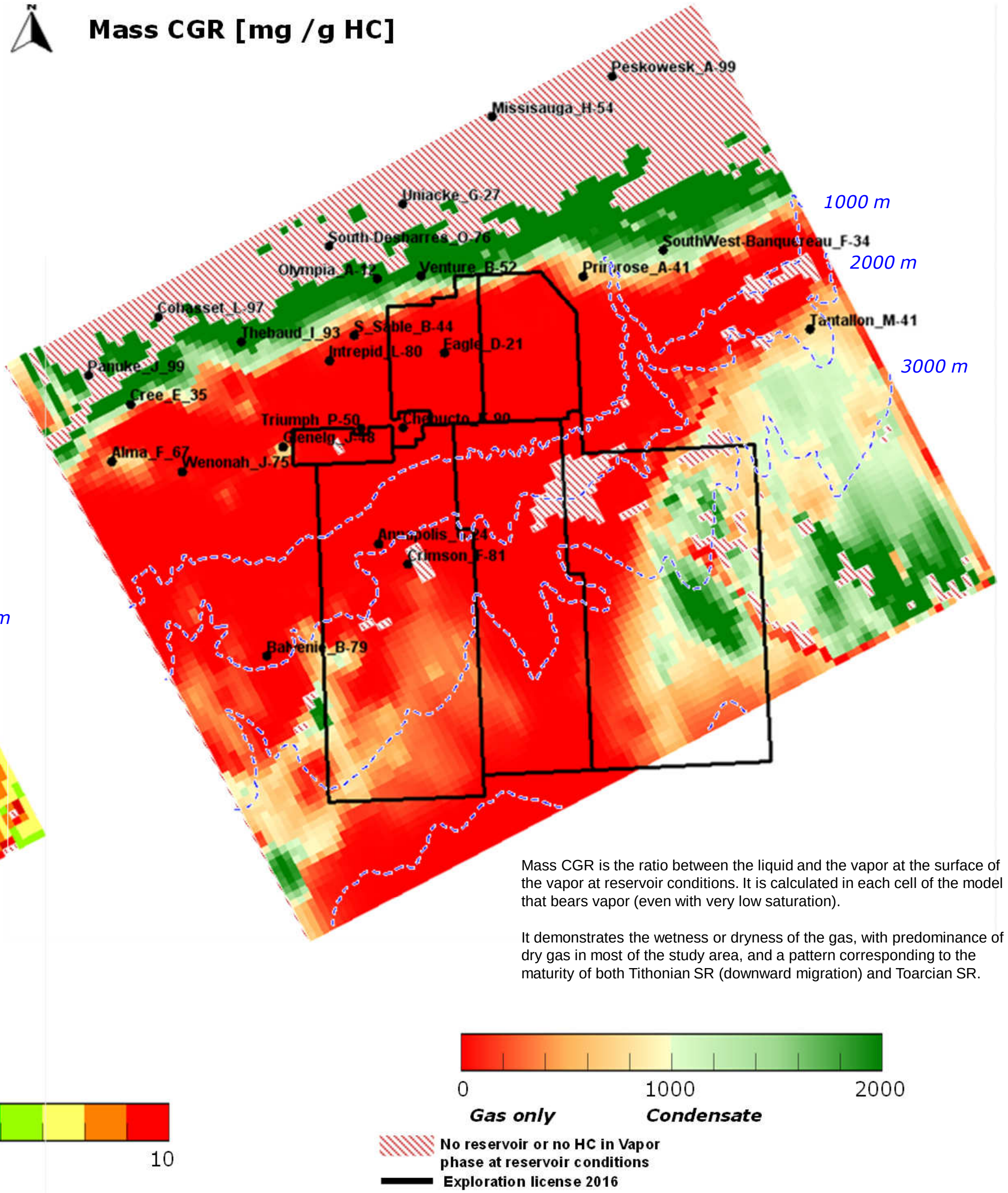

Mass CGR is the ratio between the liquid and the vapor at the surface of the vapor at reservoir conditions. It is calculated in each cell of the model that bears vapor (even with very low saturation).

It demonstrates the wetness or dryness of the gas, with predominance of dry gas in most of the study area, and a pattern corresponding to the maturity of both Tithonian SR (downward migration) and Toarcian SR.

J150

Figure 65: Oil density of the J150 Play

API of Liquid from Liquid Phase

API density is calculated for the liquids in liquid phase at reservoir conditions in each cell of the model that bears liquid (even with very low saturation).

Medium to light oil should be expected on the shelf.

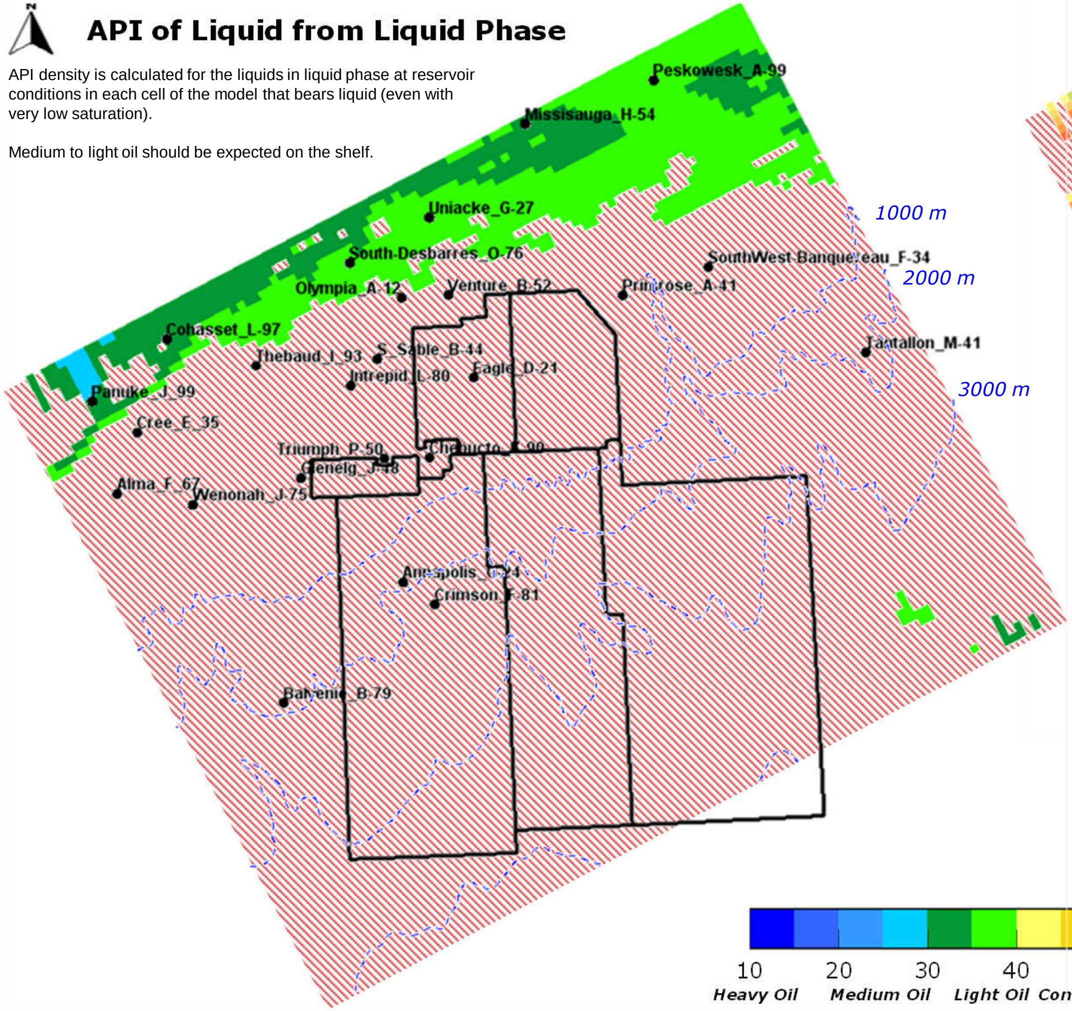

Figure 66: Gas content of the liquid phase in f the J150 Play

Solution GOR [ft³/stb]

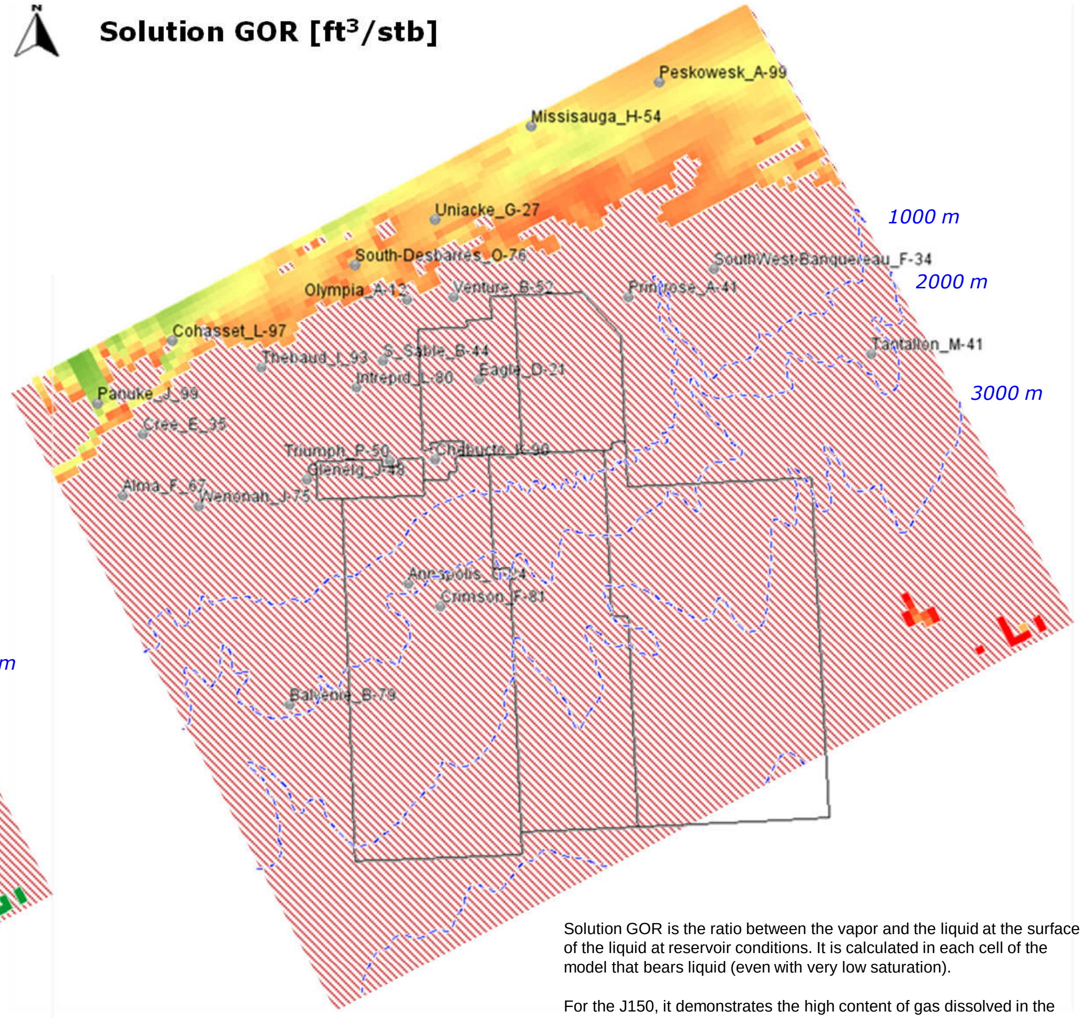

Solution GOR is the ratio between the vapor and the liquid at the surface of the liquid at reservoir conditions. It is calculated in each cell of the model that bears liquid (even with very low saturation).

For the J150, it demonstrates the high content of gas dissolved in the liquid fractions on the shelf.

J150

Figure 67: Age of the first HC arrival in the J150 Play

Timing of first HC Saturation [Ma]

The timing of saturation is computed to display the age at which a cell reaches a fixed threshold for hydrocarbon saturation. Using a very low value allows visualizing the age at which hydrocarbons start to flow through a given layer.

For the J150, hydrocarbons started invading the reservoir during the latest Upper Jurassic and Lower Cretaceous. Downward migration took place later (Early Tertiary) south of Tantallon.

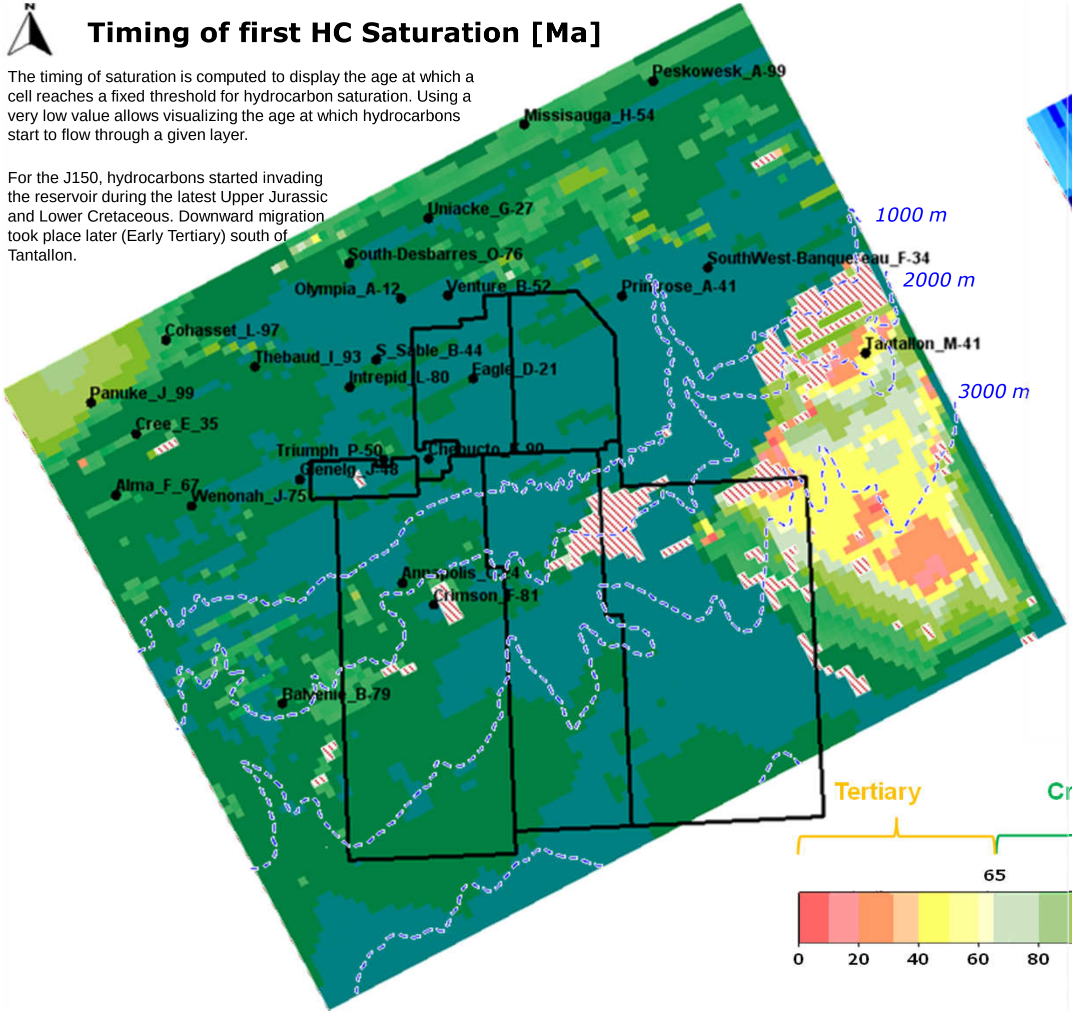

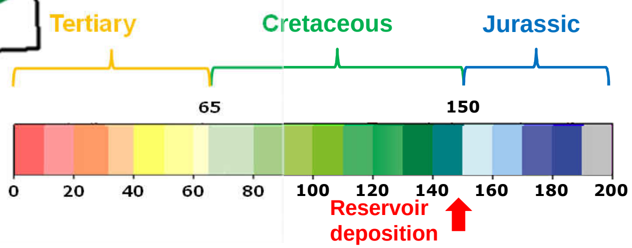

Figure 68: Percentage of gas generated in the Tithonian SR in the Play J150

SR Contribution for Gas Fraction [%]

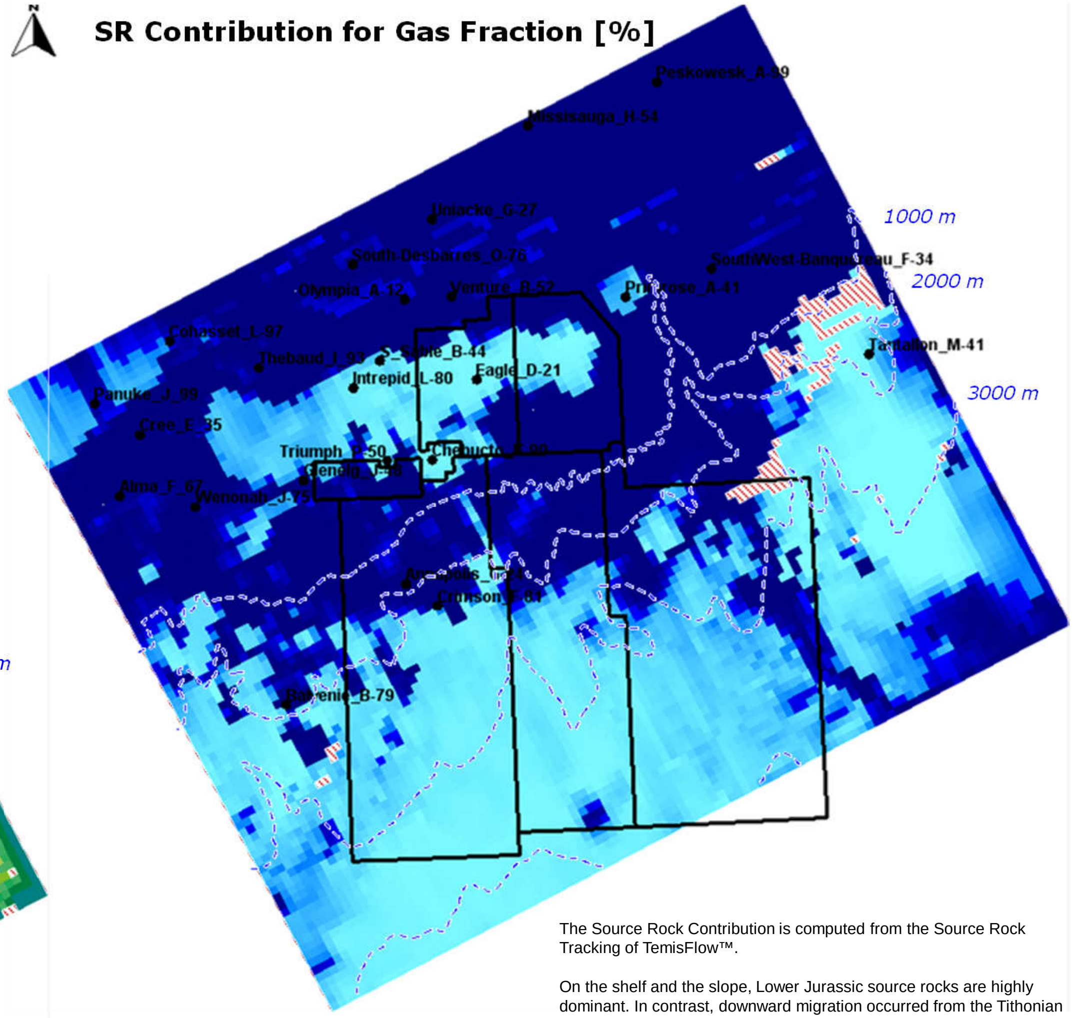

The Source Rock Contribution is computed from the Source Rock Tracking of TemisFlow™.

On the shelf and the slope, Lower Jurassic source rocks are highly dominant. In contrast, downward migration occurred from the Tithonian source rock to the south of Parcels 4, 5 and 6 and in the Banquereau Wedge.

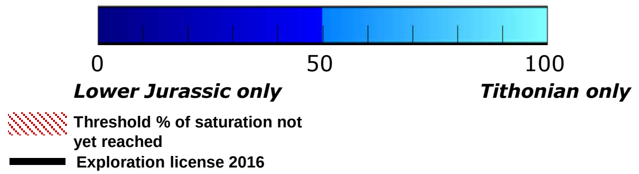

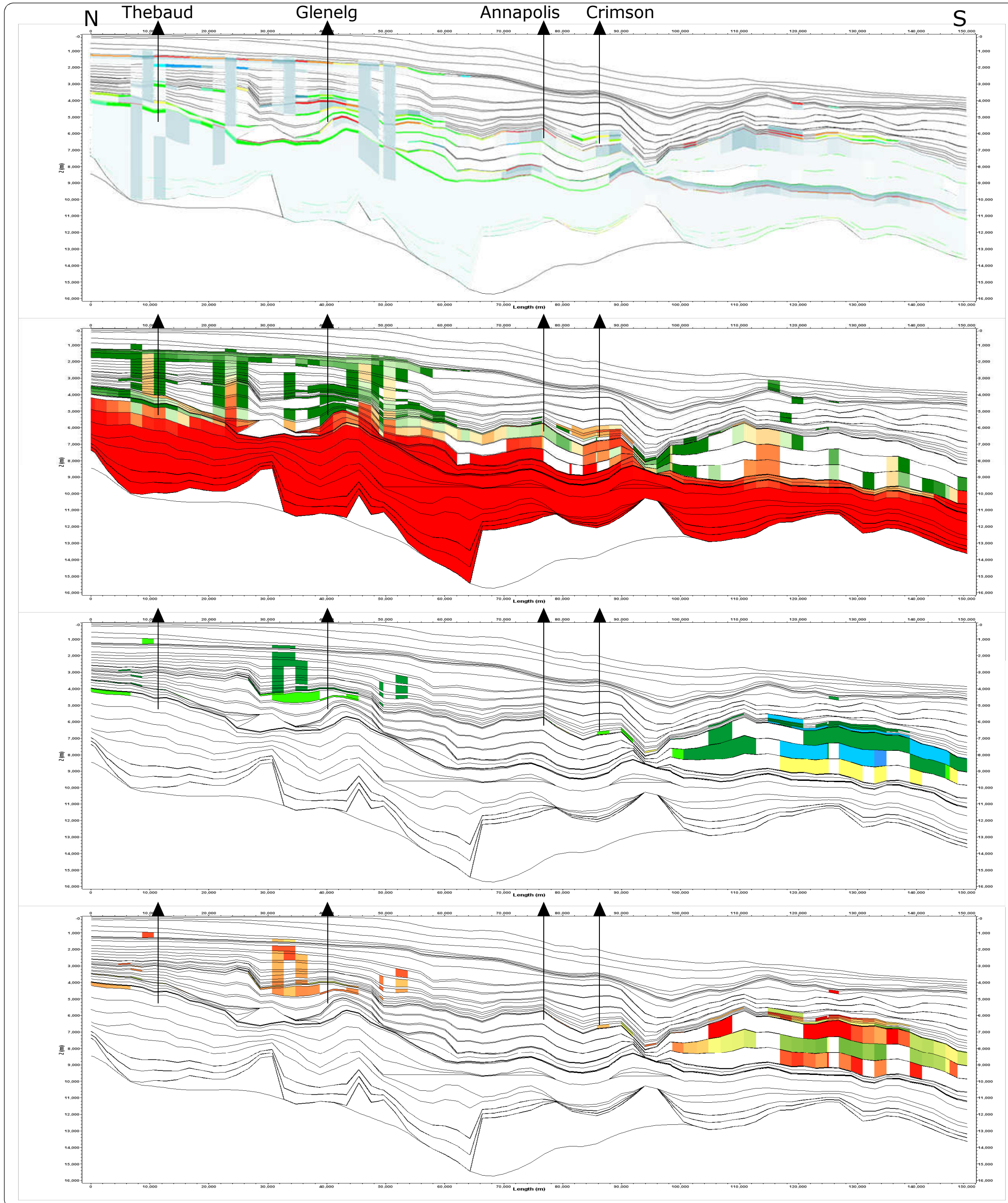

Hydrocarbon Liquid Saturation [%]

10

5

0

Hydrocarbon saturation is presented with a condensed color scale which displays both accumulations in thin reservoir layers and migration pathways in thick carrier beds.

On the shelf, hydrocarbon migration takes place in the fault corridors whereas migration pathways are more diffuse in the distal areas due to the shale-dominated infill.

On the shelf, significant accumulations are reproduced in Thebaud (Mic Mac and Lower Missisauga) and Glenelg (Lower and Middle Missisauga). Hydrocarbons can migrate up to the Upper Cretaceous.
In the basin, migration is active up to the Middle Missisauga

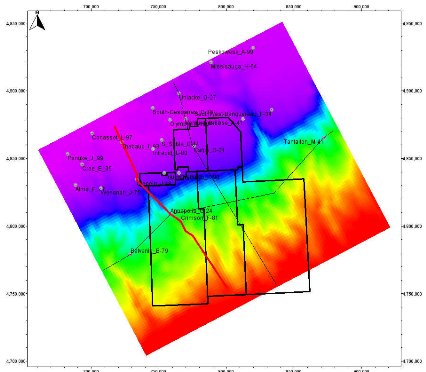

Mass CGR [mg /g HC]

2000

Condensate

1000

Gas only

0

Mass CGR compares the amount of condensate to the amount of gas for each cell that bears hydrocarbons in vapor phase (even for very small saturation).

This property demonstrates the likelihood of dry gas for nearly the whole Jurassic section.

In the distal part of the basin, the Tithonian SR marks the limit of possible condensate bearing beds. Going northwards between Crimson and Glenelg, gas can also be expected in the Lower Missisauga.

On the shelf, hydrocarbons should be encountered primarily as vapor but with significant amounts of condensate.

API of Liquid from Liquid Phase

60 ***Gas only***

50 ***Condensate***

40 ***Light Oil***

30 ***Medium Oil***

20 ***Heavy Oil***

10

API Gravity of the liquid in the liquid phase is calculated for the cells in which liquid hydrocarbon are expected at reservoir conditions. The calculation is done for every cell that bears hydrocarbons (even for very small saturation).

In the distal part of the basin, this property demonstrates the likelihood of finding liquid hydrocarbons. This domain corresponds to the low maturity area of the Tithonian SR.

Solution GOR [ft³/stb]

2000

1000

0

Solution GOR is the ratio between the vapor and the liquid at the surface of the liquid at reservoir conditions. It is calculated in each cell of the model that bears liquid (even with very low saturation).

Figure 69: Migration results of the 3D model on a NS section passing through Thebaud, Glenelg, Annapolis and Crimson

Migration Simulation – 2D Extraction – Saturation, HC Quality and GOR at Present-Day

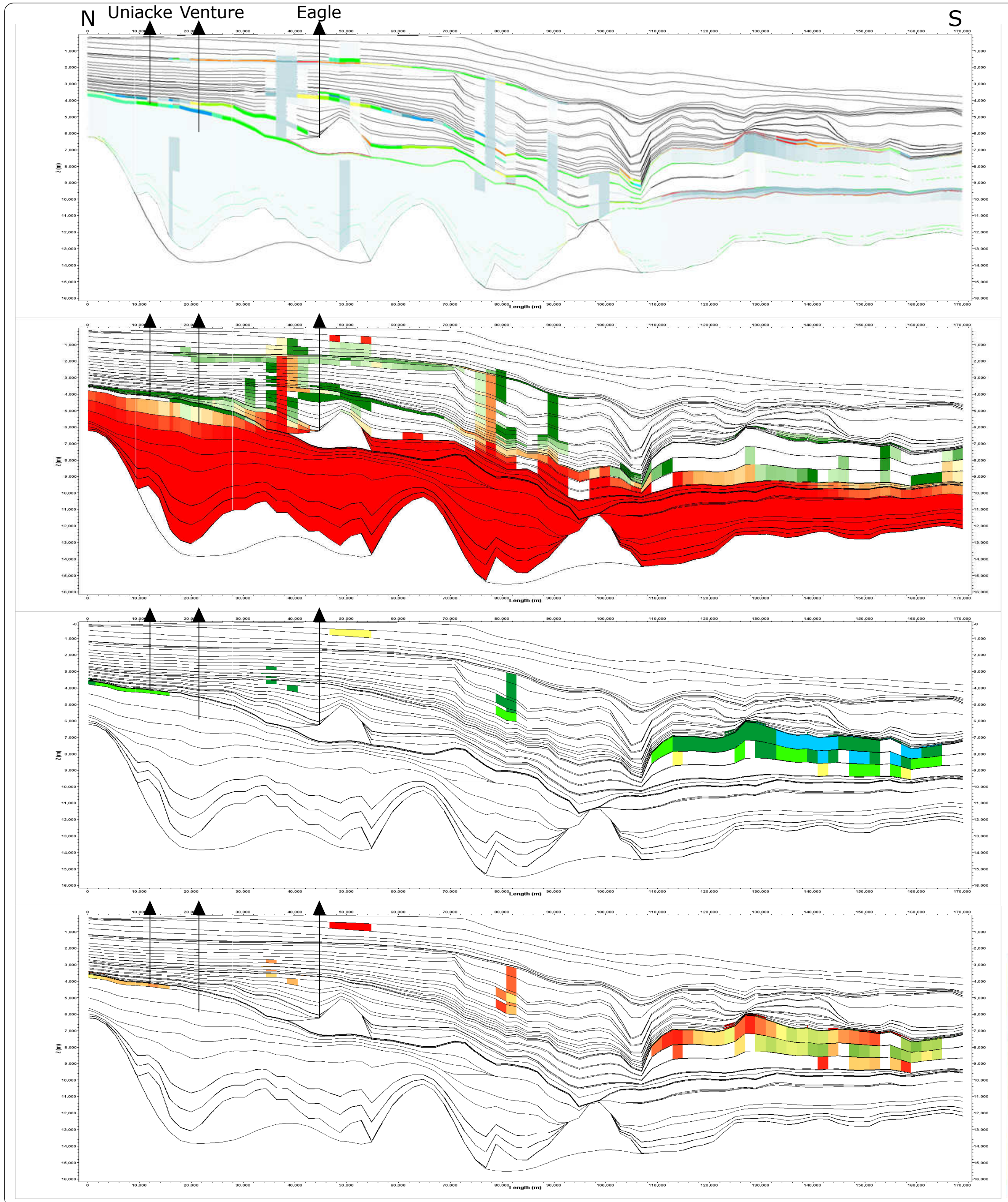

Hydrocarbon Liquid Saturation [%]

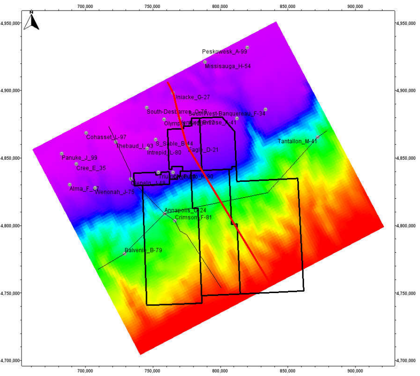

Hydrocarbon saturation is presented with a condensed color scale which displays both accumulations in thin reservoir layers and migration pathways in thick carrier beds.

On the shelf, hydrocarbon migration takes place in the fault corridors whereas migration pathways are more diffuse in the distal part due to the shale-dominated infill.

On the shelf, significant accumulations are reproduced in Uniacke (Mic Mac and Lower Missisauga), Venture (Mic Mac and Lower Missisauga) and Eagle (Wyandot). Hydrocarbons can migrate up to the surface.
In the basin, migration is active up to the Upper Missisauga.

Mass CGR [mg /g HC]

2000
Condensate
1000
Gas only
0

Mass CGR compares the amount of condensate to the amount of gas for each cell that bears hydrocarbons in vapor phase (even for very small saturation).

This property demonstrates the likelihood of dry gas for nearly the whole Jurassic section.

In the distal part of the basin, the Lower Missisauga marks the limit of possible condensate bearing beds. Going northwards on the slope, gas can also be expected in the Lower Missisauga.

On the shelf, hydrocarbons should be encountered primarily as vapor but with significant amounts of condensate.

API of Liquid from Liquid Phase

60 *Gas only*
50 *Condensate*
40 *Light Oil*
30 *Medium Oil*
20 *Heavy Oil*
10

API Gravity of the liquid in the liquid phase is calculated for the cells in which liquid hydrocarbon are expected at reservoir conditions. The calculation is done for every cell that bears hydrocarbons (even for very small saturation).

In the distal part of the basin, this property demonstrates the likelihood of finding liquid hydrocarbons. This domain corresponds to the low maturity area of the Tithonian SR.

Solution GOR [ft³/stb]

2000
1000
0

Solution GOR is the ratio between the vapor and the liquid at the surface of the liquid at reservoir conditions. It is calculated in each cell of the model that bears liquid (even with very low saturation).

Figure 70: Migration results of the 3D model on a NS section passing through Uniacke, Venture and Eagle

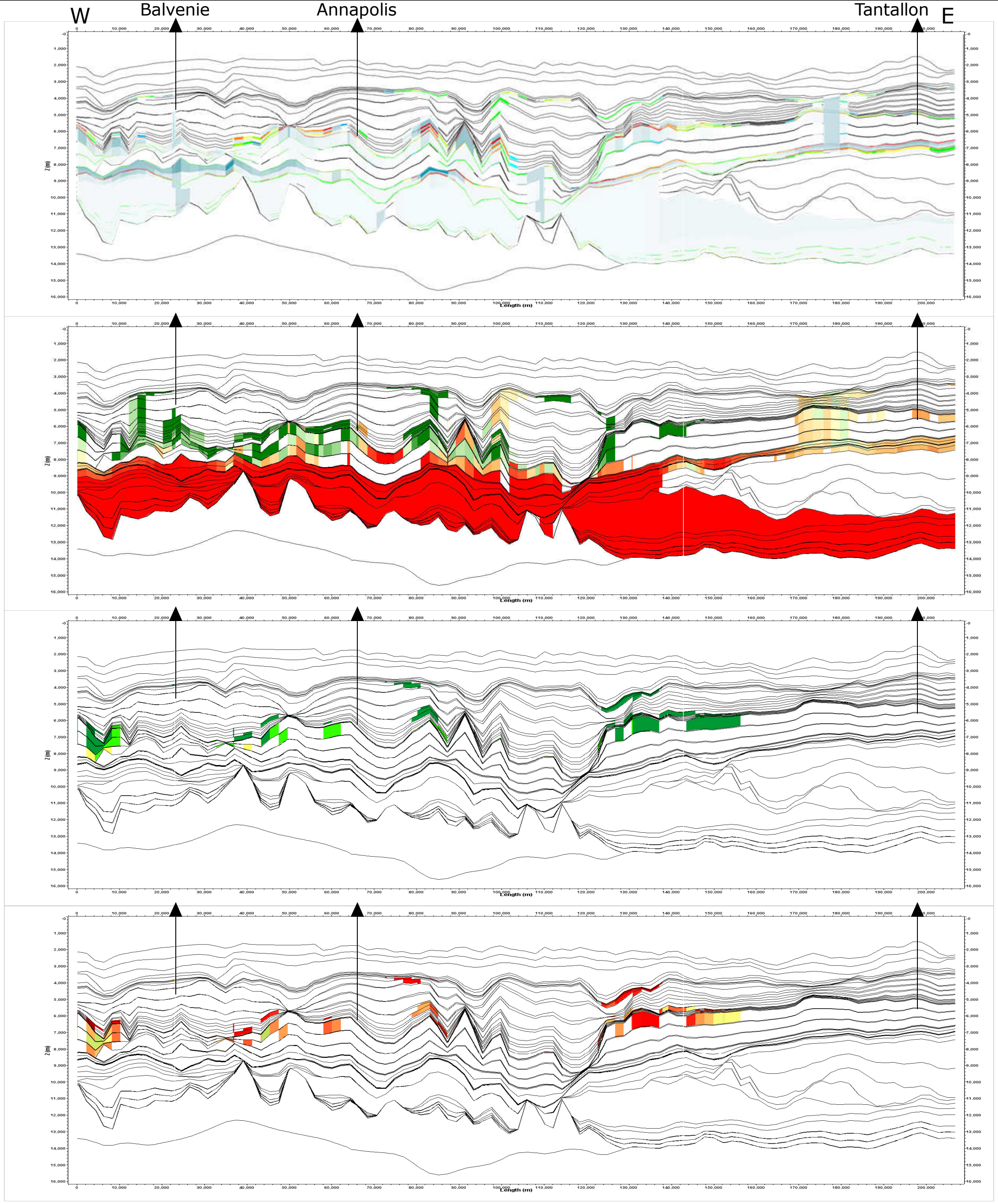

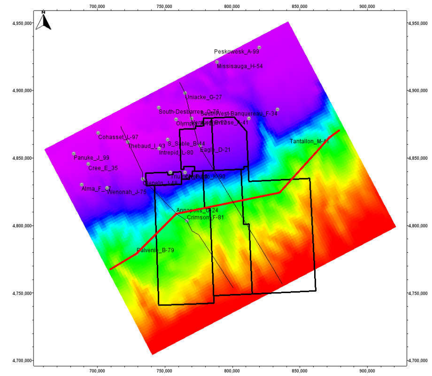

Hydrocarbon Liquid Saturation [%]

Hydrocarbon saturation is presented with a condensed color scale which displays both accumulations in thin reservoir layers and migration pathways in thick carrier beds.

Migration pathways are diffuse in this distal part of the basin due to the shale-dominated infill, except around Balvenie and Tantallon where seismic quality allowed the interpretation of faults.

In the basin, migration is highly efficient up to the Upper Missisauga, leading to accumulations east of Annapolis.

Mass CGR [mg /g HC]

2000

Condensate

1000

Gas only

0

Mass CGR compares the amount of condensate to the amount of gas for each cell that bears hydrocarbons in vapor phase (even for very small saturation).

This property demonstrates the likelihood of dry gas for nearly the whole Jurassic section up to the Lower Missisauga.

Hydrocarbons that migrate in the Middle Missisauga to Logan Canyon should be encountered primarily as vapor but with significant amounts of condensate.

API of Liquid from Liquid Phase

60 ***Gas only***

50 ***Condensate***

40 ***Light Oil***

30 ***Medium Oil***

20 ***Heavy Oil***

10

API Gravity of the liquid in the liquid phase is calculated for the cells in which liquid hydrocarbon are expected at reservoir conditions. The calculation is done for every cell that bears hydrocarbons (even for very small saturation).

In the distal part of the basin, this property demonstrates the likelihood of finding liquid hydrocarbons. This domain corresponds to the low maturity area of the Tithonian SR.

Solution GOR [ft³/stb]

2000

1000

0

Solution GOR is the ratio between the vapor and the liquid at the surface from the liquid at reservoir conditions. It is calculated in each cell of the model that bears liquid (even with very low saturation).

Figure 71: Migration results of the 3D model on a WE section passing through Balvenie, Annapolis and Tantallon

Migration Simulation – 2D Extraction – Saturation, HC Quality and GOR at present-day

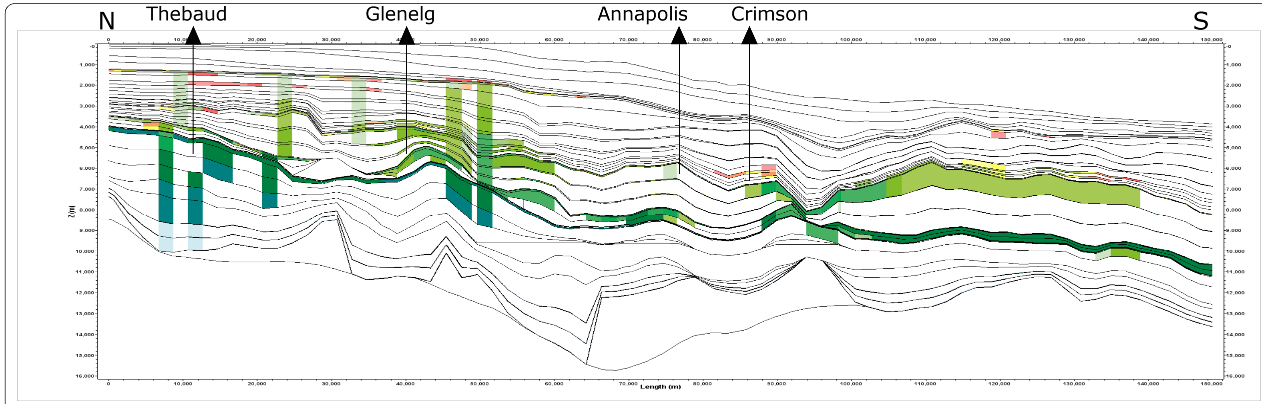

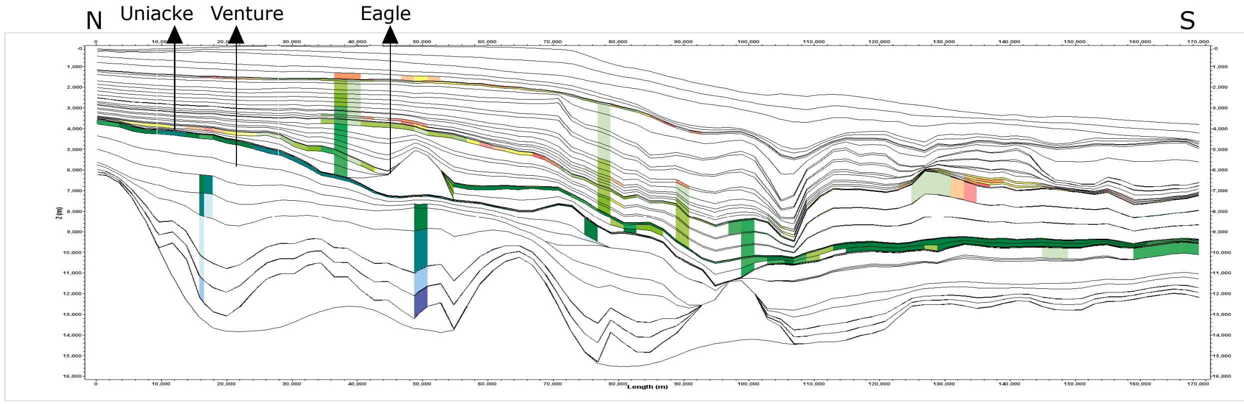

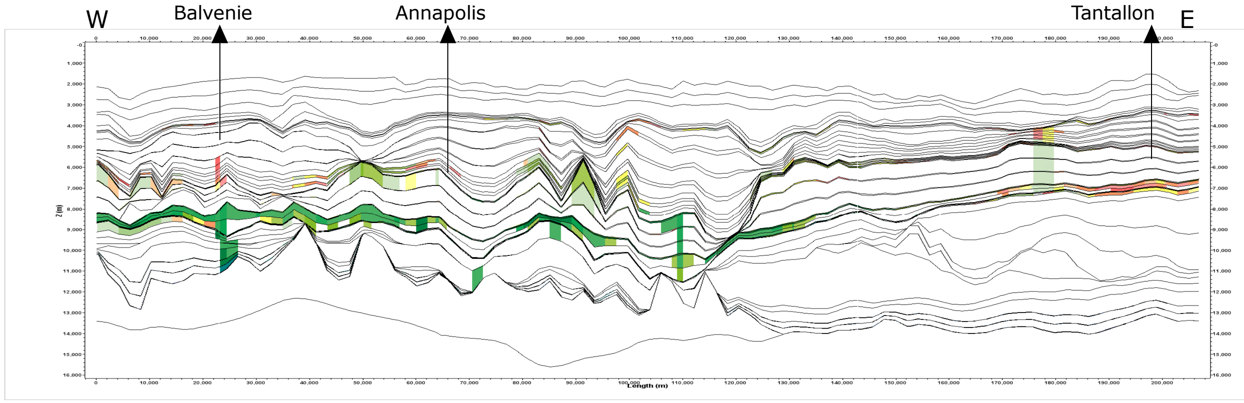

Figure 72: Age of the first HC saturation for two NS sections and one WE section extracted from the 3D block

Timing of Saturation [%]

The timing of saturation is computed to display the age at which a cell reaches a fixed threshold for hydrocarbon saturation. Using a very low value allows visualizing the age at which hydrocarbons start to flow through a given layer.

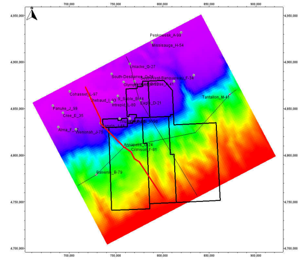

Both NS sections show a decoupling between the Lower Jurassic system and Upper Jurassic / Cretaceous.

Early migration takes place during the Upper Jurassic to Lower Cretaceous in the deeper strata.

Migration of hydrocarbons sourced in the Tithonian takes place in the Upper Cretaceous and Tertiary along fault corridors with vertical movements. Then reservoir layers are progressively invaded by hydrocarbons (lateral migration).

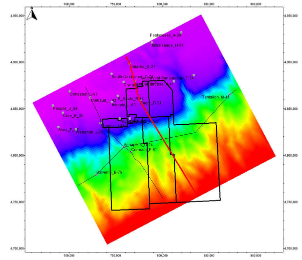

EW section does not clearly show the Lower Jurassic system as salt is more visible in this configuration.

On the contrary, migration in the Upper Jurassic to Upper Cretaceous is similar to the two NS sections: vertical migration in faulted areas followed by lateral migration in the reservoir layers.

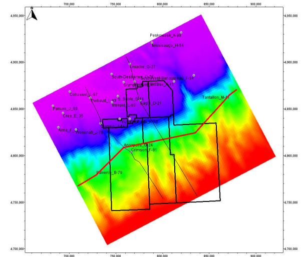

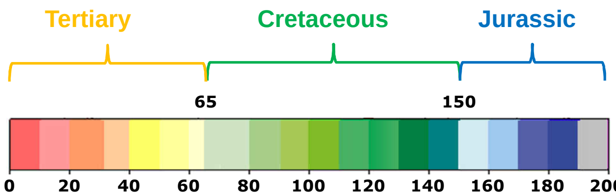

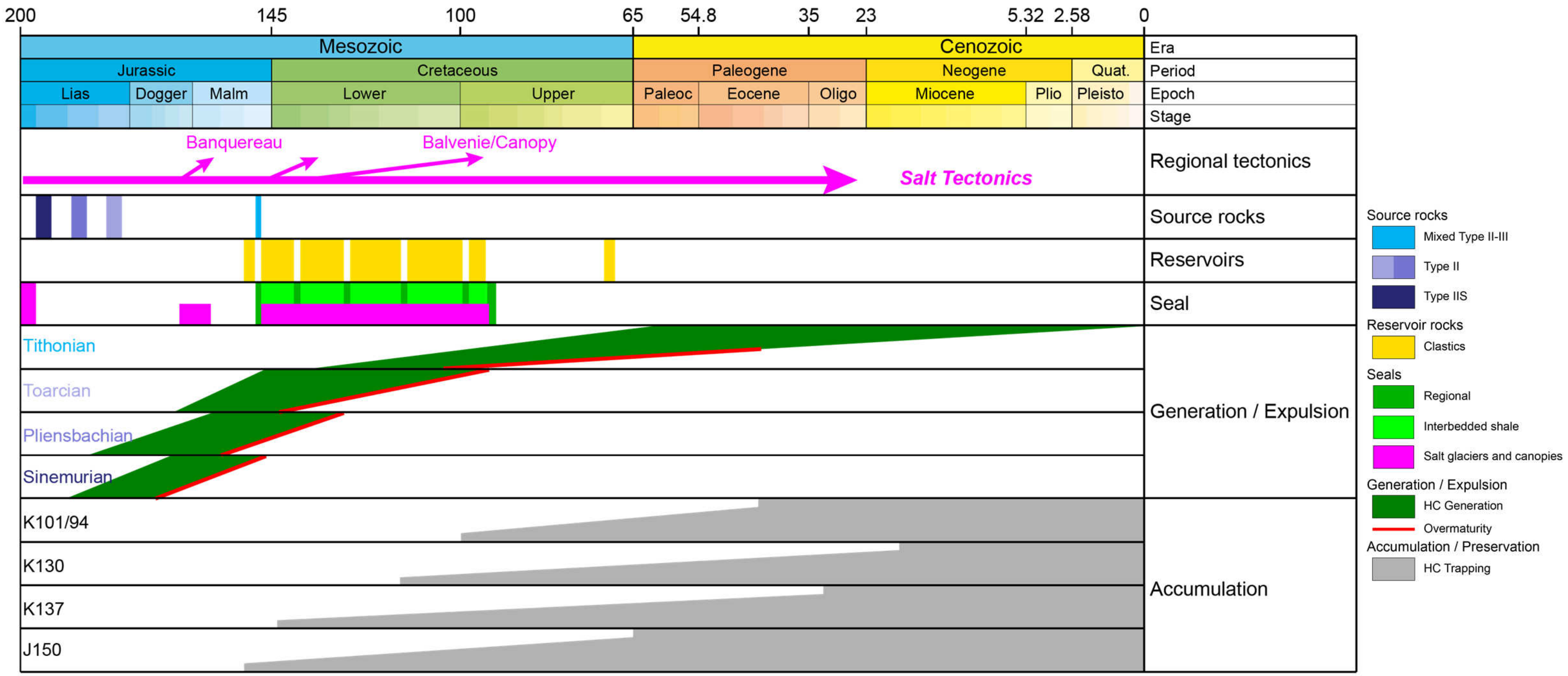

Petroleum System Chart

The Petroleum System Chart summarizes the results of expulsion and migration simulations. These results are integrated together with structural and sedimentological studies.

The horizontal axis corresponds to the geological age using the colors of the International Chronostratigraphic Chart. The width of each object (arrow or rectangle) indicates the duration of a particular episode. The inclination of a box reflects the spatial and temporal variations for a given process.

The sedimentary system encompasses the source rocks, reservoirs and seals that were assessed during the study.

The part 'Generation and Expulsion' presents the evolution of each source rock included in the model. The dark green areas correspond to the hydrocarbon generation period for each source rock. The red line highlights the occurrence of over-maturity. Note that the entrance in the oil or gas window is highly diachronous in the different parts of the study area.

The Lower Jurassic source rocks entered early into the oil generation window due to the rapid burial and high heat flow, a relict of the early rifting. Over-maturity was reached between 20 to 40 Ma later.

Tithonian source rock has been generating hydrocarbons during most of the Cretaceous and the Paleogene. Potential remains on the shelf and in the deep basin.

The play charge is symbolized by grey areas showing the beginning of hydrocarbons trapping in the reservoirs.

Figure 73: Petroleum System Chart summarizing the main results of expulsion and migration simulations.

Parcels	Mass Gas (Gkg)	Mass Oil (Gkg)	Total Mass (Gkg)	Total Mass 1_Oil Heavy (Mkg)	Total Mass 2_Oil Normal (Mkg)	Total Mass 3_Oil Condensate (Mkg)	Total Mass 4_Gas Thermogenic (Mkg)
Parcel 1	66	113	179	18440	49560	44971	65791
Parcel 2	8	14	22	2094	5946	5798	8363
Parcel 3	75	119	194	22703	51071	45726	74629
Parcel 4	47	123	171	30186	56238	36924	47302
Parcel 5	15	27	43	6307	11797	9222	15339
Parcel 6	30	47	77	5509	22544	18620	30356
Total Parcels	*242*	*444*	*685*	85239	197155	161260	241779

Table 8: Masses of hydrocarbons in the Play K94

Parcels	Vol Gas (tcf)	Vol Oil (MMbbl)	Total Volume (MMboe)	Vol Gas (bcf/km²)	Vol Oil (Mbbl/km²)	Total Volume (Mboe/km²)	GOR (scf/stb)	CGR (stb/Mscf)
Parcel 1	3.1	916	1457.4	13	3889	6187		232
Parcel 2	0.4	112.7	181.5	1	144	232		284
Parcel 3	3.6	964.9	1578.91	4	1030	1685		227
Parcel 4	2.3	943	1332	1	258	365	1833	346
Parcel 5	0.7	203	329	0.3	79	127	1815	315
Parcel 6	1.4	367.2	617.0	0.1	30	50	1828	380
Total Parcels	12	3507	5496	1	171	269	1826	297

Table 9: Volume of Hydrocarbon and Volume per Surface unit in the Play K94

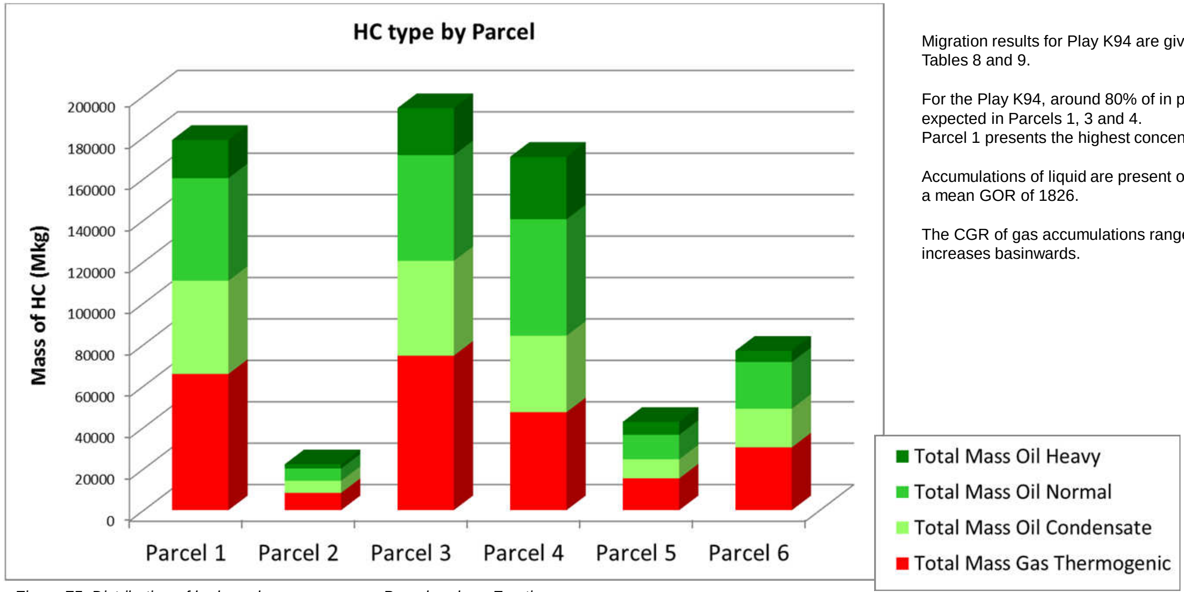

Figure 75: Distribution of hydrocarbons masses per Parcel and per Fractions

Migration results for Play K94 are given in Figures 74 and 75 and Tables 8 and 9.

For the Play K94, around 80% of in place hydrocarbons are expected in Parcels 1, 3 and 4.
Parcel 1 presents the highest concentration of hydrocarbons.

Accumulations of liquid are present only in Parcels 4, 5 and 6 with a mean GOR of 1826.

The CGR of gas accumulations ranges from 232 to 380 and increases basinwards.

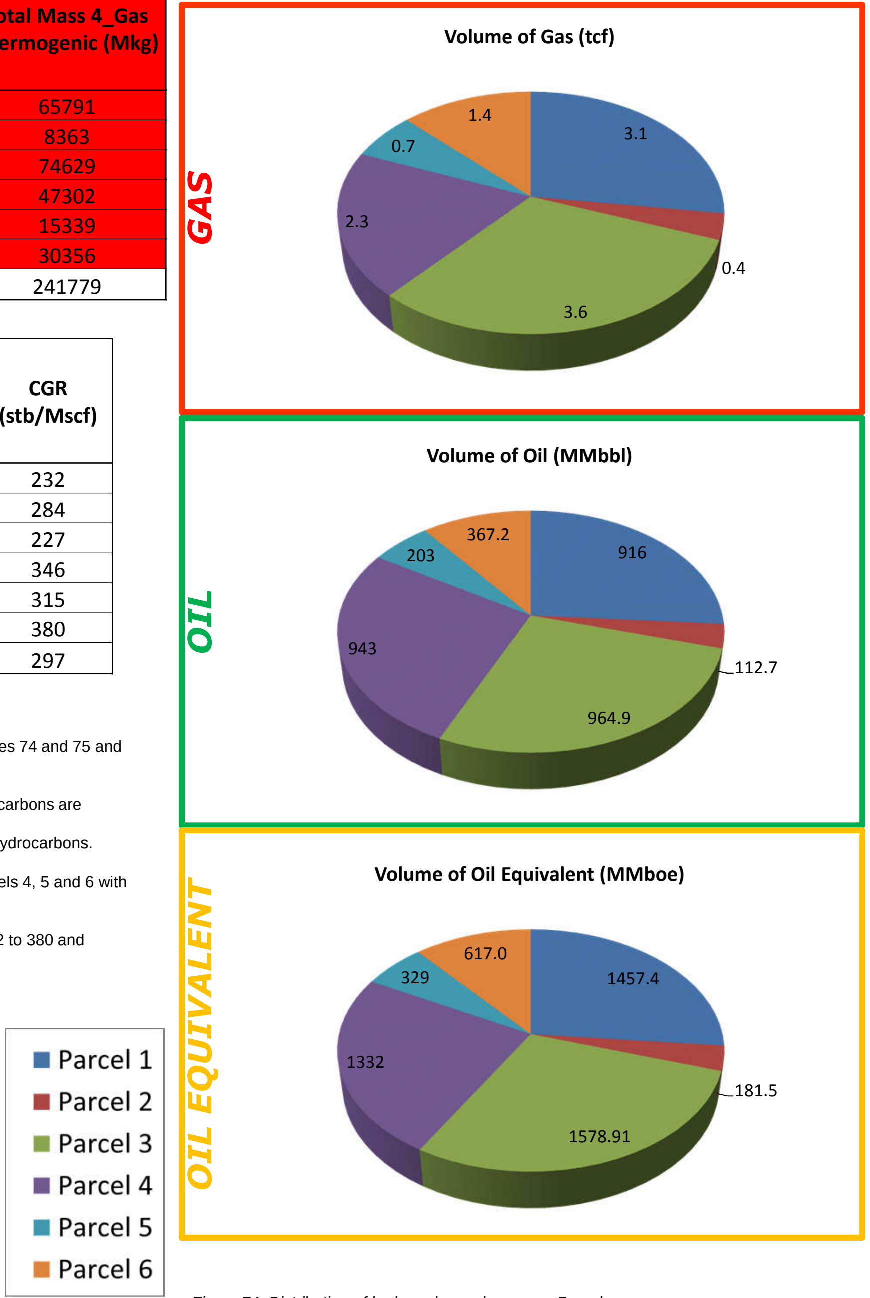

Figure 74: Distribution of hydrocarbon volumes per Parcel.

Parcels	Mass Gas (Gkg)	Mass Oil (Gkg)	Total Mass (Gkg)	Total Mass 1_Oil Heavy (Mkg)	Total Mass 2_Oil Normal (Mkg)	Total Mass 3_Oil Condensate (Mkg)	Total Mass 4_Gas Thermogenic (Mkg)
Parcel 1	11	19	30	1621	8921	8646	10990
Parcel 2	11	9	20	849	3147	5224	11063
Parcel 3	4	5	9	270	2058	2579	3780
Parcel 4	52	114	166	19737	53632	40436	52348
Parcel 5	35	101	137	25898	46702	28795	35451
Parcel 6	5	13	18	2310	5732	5252	5190
Total Parcels	*119*	*262*	*381*	50685	120192	90933	118824

Table 10: Masses of hydrocarbons in the Play K101

Parcels	Vol Gas (tcf)	Vol Oil (MMbbl)	Total Volume (MMboe)	Vol Gas (bcf/km^2)	Vol Oil ($Mbbl/km^2$)	Total Volume ($Mboe/km^2$)	GOR (scf/stb)	CGR (stb/Mscf)
Parcel 1	0.5	158	248.1	2	669	1053		301
Parcel 2	0.5	77.2	168.2	1	99	215		225
Parcel 3	0.2	40.9	71.99	0.2	44	77		275
Parcel 4	1.4	923	1164	0.4	253	319	2047	247
Parcel 5	1.7	752	1044	1	291	404	1230	312
Parcel 6	0.2	99.0	141.0	0.02	8	11	1357	340
Total Parcels	5	2050	2837	0.2	100	139	1544	283

Table 11: Volume of Hydrocarbon and Volume per Surface unit in the Play K101

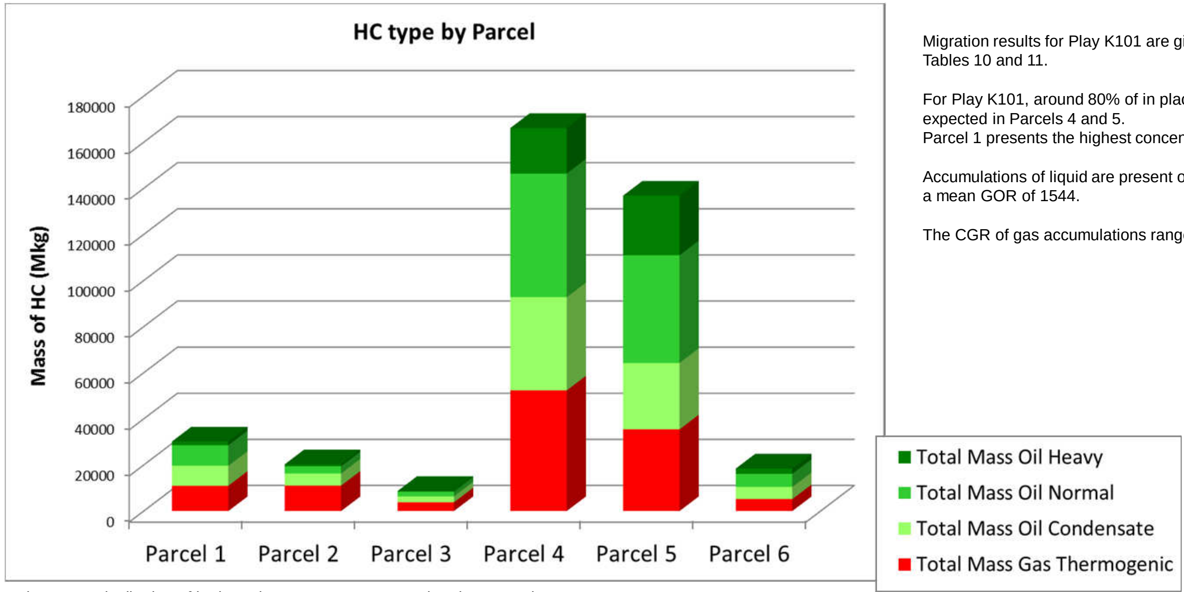

Figure 77: Distribution of hydrocarbons masses per Parcel and per Fractions

Migration results for Play K101 are given in Figures 76 and 77 and Tables 10 and 11.

For Play K101, around 80% of in place hydrocarbons are expected in Parcels 4 and 5.
Parcel 1 presents the highest concentration of hydrocarbons.

Accumulations of liquid are present only in Parcels 4, 5 and 6 with a mean GOR of 1544.

The CGR of gas accumulations ranges from 247 to 340.

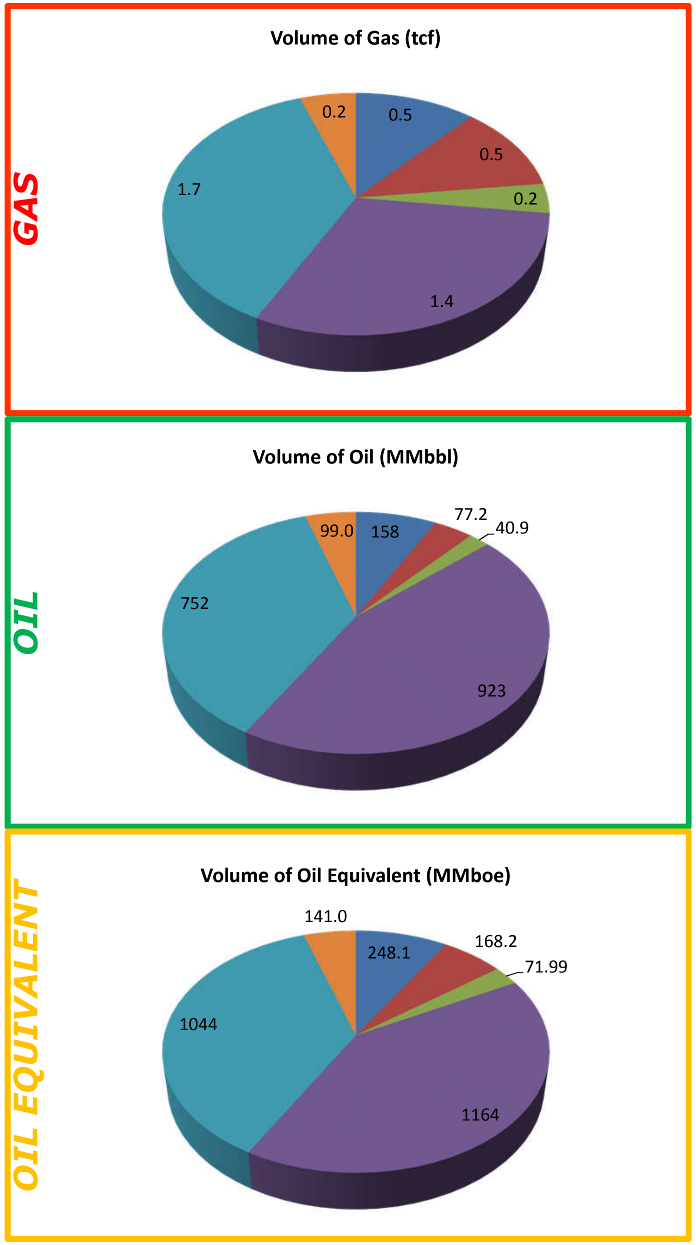

Figure 76: Distribution of hydrocarbon volumes per Parcel.

Parcels	Mass Gas (Gkg)	Mass Oil (Gkg)	Total Mass (Gkg)	Total Mass 1_Oil Heavy (Mkg)	Total Mass 2_Oil Normal (Mkg)	Total Mass 3_Oil Condensate (Mkg)	Total Mass 4_Gas Thermogenic (Mkg)
Parcel 1	8	10	18	45	3856	6018	7951
Parcel 2	15	9	24	7	1585	7612	14678
Parcel 3	10	6	15	59	1332	4256	9606
Parcel 4	68	113	181	19116	49390	44505	67926
Parcel 5	52	95	147	14768	40544	39964	51586
Parcel 6	70	153	223	28805	72884	51652	69697
Total Parcels	*221*	*386*	*608*	62800	169592	154008	221444

Table 12: Masses of hydrocarbons in the Play K130

Parcels	Vol Gas (tcf)	Vol Oil (MMbbl)	Total Volume (MMboe)	Vol Gas (bcf/km²)	Vol Oil (Mbbl/km²)	Total Volume (Mboe/km²)	GOR (scf/stb)	CGR (stb/Mscf)
Parcel 1	0.4	433.3	497.4	2	1840	2112		314
Parcel 2	0.7	178.8	300.5	1	228	384		269
Parcel 3	0.2	64.97	106.9	0.3	69	114		93
Parcel 4	3.2	1137	1696	1	312	465	1908	224
Parcel 5	2.4	1039	1460	1	402	565	1637	189
Parcel 6	3.3	1474	2048	0.3	120	167	1550	324
Total Parcels	10	4328	6110	1	212	299	1698	236

Table 13: Volume of Hydrocarbon and Volume per Surface unit in the Play K130

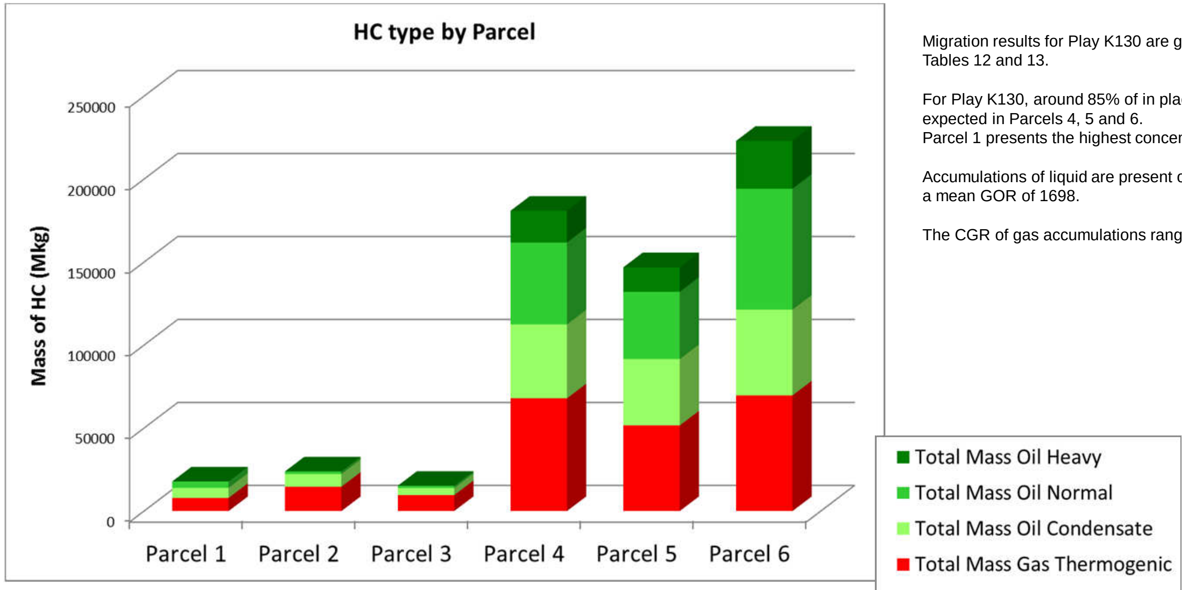

Figure 79: Distribution of hydrocarbons masses per Parcel and per Fractions

Migration results for Play K130 are given in Figures 78 and 79 and Tables 12 and 13.

For Play K130, around 85% of in place hydrocarbons are expected in Parcels 4, 5 and 6.
Parcel 1 presents the highest concentration of hydrocarbons.

Accumulations of liquid are present only in Parcels 4, 5 and 6 with a mean GOR of 1698.

The CGR of gas accumulations ranges from 93 to 324.

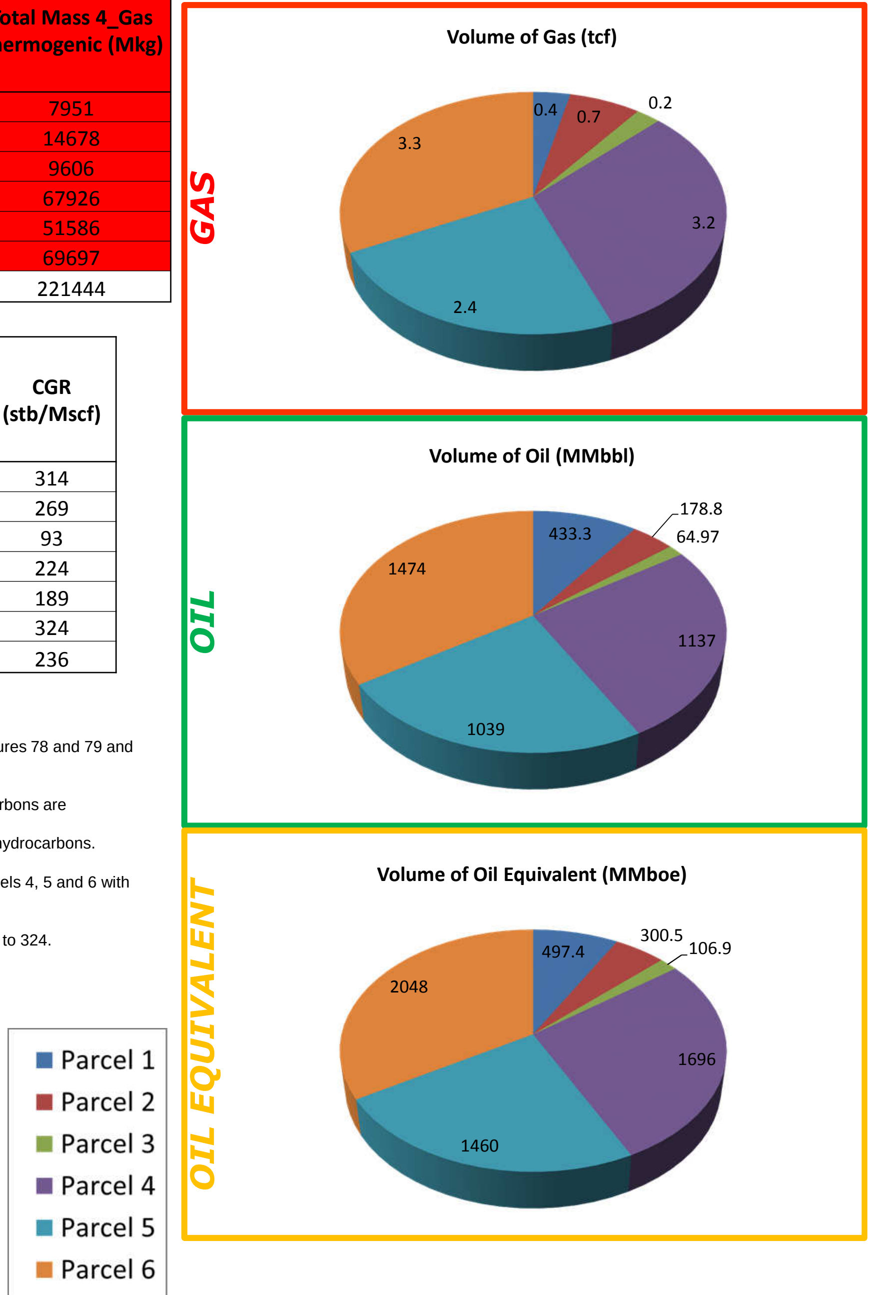

Figure 78: Distribution of hydrocarbon volumes per Parcel.

Parcels	Mass Gas (Gkg)	Mass Oil (Gkg)	Total Mass (Gkg)	Total Mass 1_Oil Heavy (Mkg)	Total Mass 2_Oil Normal (Mkg)	Total Mass 3_Oil Condensate (Mkg)	Total Mass 4_Gas Thermogenic (Mkg)
Parcel 1	13	1	14	0	0	521	13353
Parcel 2	41	3	43	0	0	2593	40860
Parcel 3	3	0	3	0	0	106	2776
Parcel 4	76	18	93	37	1344	16169	75627
Parcel 5	69	4	73	0	107	3798	68696
Parcel 6	122	76	198	741	22259	53333	121628
Total Parcels	*323*	*101*	*424*	778	23709	76520	322940

Table 14: Masses of hydrocarbons in the Play K137

Parcels	Vol Gas (tcf)	Vol Oil (MMbbl)	Total Volume (MMboe)	Vol Gas (bcf/km²)	Vol Oil (Mbbl/km²)	Total Volume (Mboe/km²)	GOR (scf/stb)	CGR (stb/Mscf)
Parcel 1	0.6	4.68	115	3	20	486		5
Parcel 2	1.9	23.3	359	2	30	459		11
Parcel 3	0.1	0.95	23.8	0.1	1	25		7
Parcel 4	3.6	156	778	1	43	213		67
Parcel 5	3.3	34.9	600	1	14	232		22
Parcel 6	5.8	655	1656	0.5	53	135		114
Total Parcels	15	875	3532	1	43	173		38

Table 15: Volume of Hydrocarbon and Volume per Surface unit in the Play K137

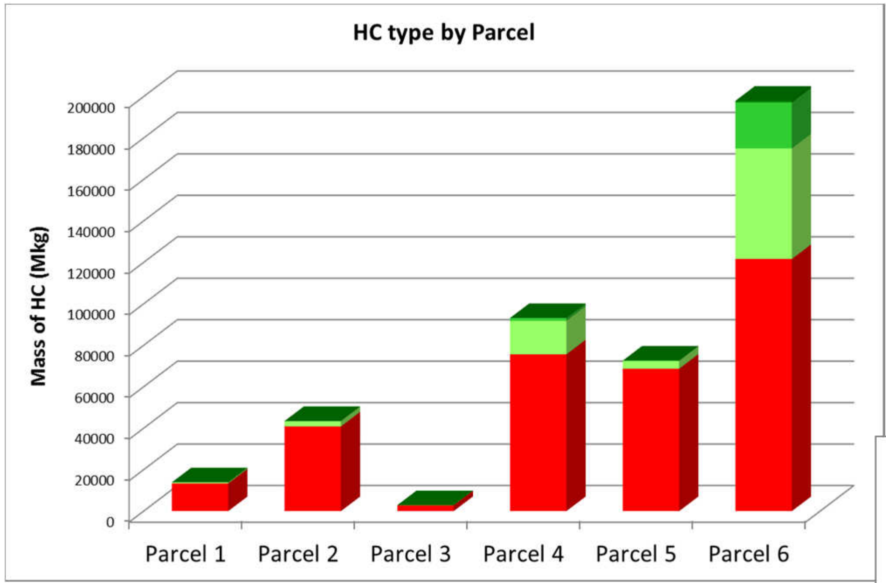

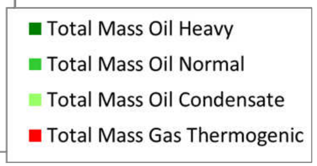

Migration results for Play K137 are given in Figures 80 and 81 and Tables 14 and 15.

For Play K137, around 85% of in place hydrocarbons are expected in Parcels 4, 5 and 6.
Parcels 1 and 2 present the highest concentration of hydrocarbons.

No accumulations of liquid at reservoir conditions are reported in the parcels for this play.

The CGR of gas accumulations ranges from 5 to 114.

Figure 81: Distribution of hydrocarbons masses per Parcel and per Fractions

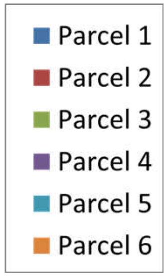

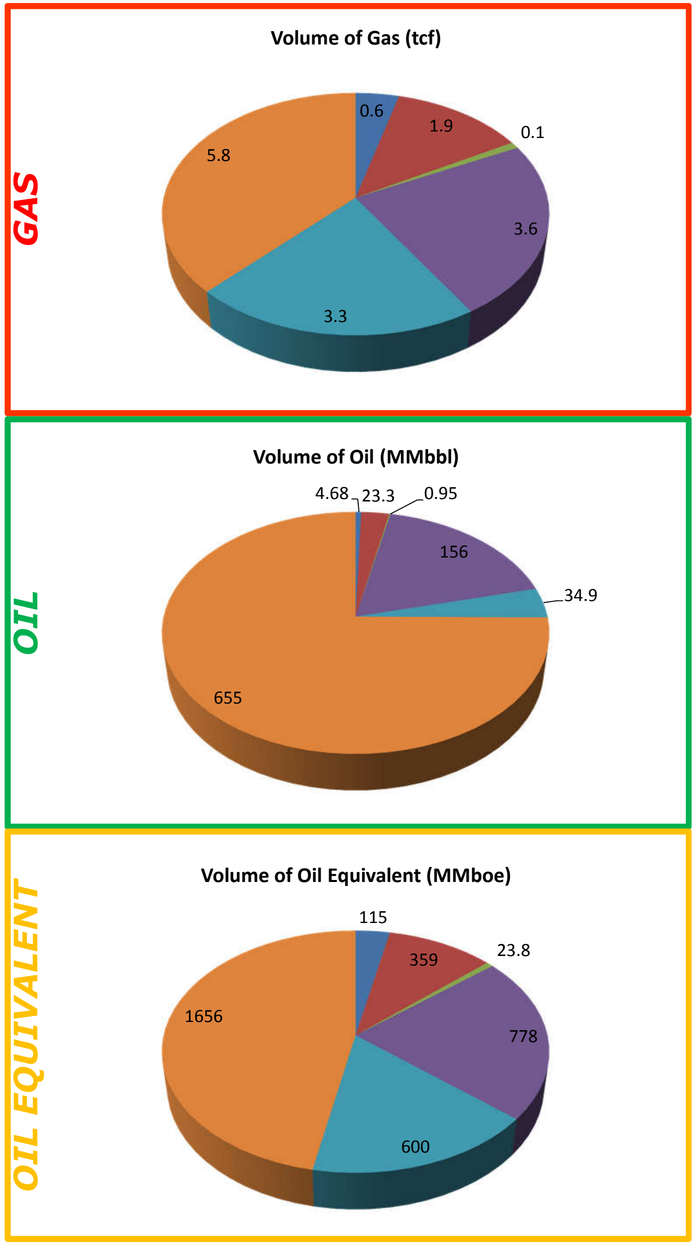

Figure 80: Distribution of hydrocarbon volumes per Parcel.

Parcels	Mass Gas (Gkg)	Mass Oil (Gkg)	Total Mass (Gkg)	Total Mass 1_Oil Heavy (Mkg)	Total Mass 2_Oil Normal (Mkg)	Total Mass 3_Oil Condensate (Mkg)	Total Mass 4_Gas Thermogenic (Mkg)
Parcel 1	54	0	54	0	0	6	53836
Parcel 2	83	0	83	0	0	21	82604
Parcel 3	9	0	9	0	0	3	9421
Parcel 4	365	68	433	423	6974	60721	364977
Parcel 5	146	4	150	0	29	3788	145797
Parcel 6	157	83	240	539	17226	65353	156900
Total Parcels	*814*	*155*	*969*	962	24230	129892	813535

Table 16: Masses of hydrocarbons in the Play J150

Parcels	Vol Gas (tcf)	Vol Oil (MMbbl)	Total Volume (MMboe)	Vol Gas (bcf/km²)	Vol Oil (Mbbl/km²)	Total Volume (Mboe/km²)	GOR (scf/stb)	CGR (stb/Mscf)
Parcel 1	2.6	0.05	443	11	0.2	1881		0
Parcel 2	3.9	0.19	680	5	0.2	868		0
Parcel 3	0.4	0.03	77.5	0.5	0.03	83		0
Parcel 4	17	602	3605	5	165	988		19
Parcel 5	7.0	34.3	1234	3	13	478		7
Parcel 6	7.5	723	2014	1	59	164		113
Total Parcels	39	1360	8054	2	66	394		23

Table 17: Volume of Hydrocarbon and Volume per Surface unit in the Play J150

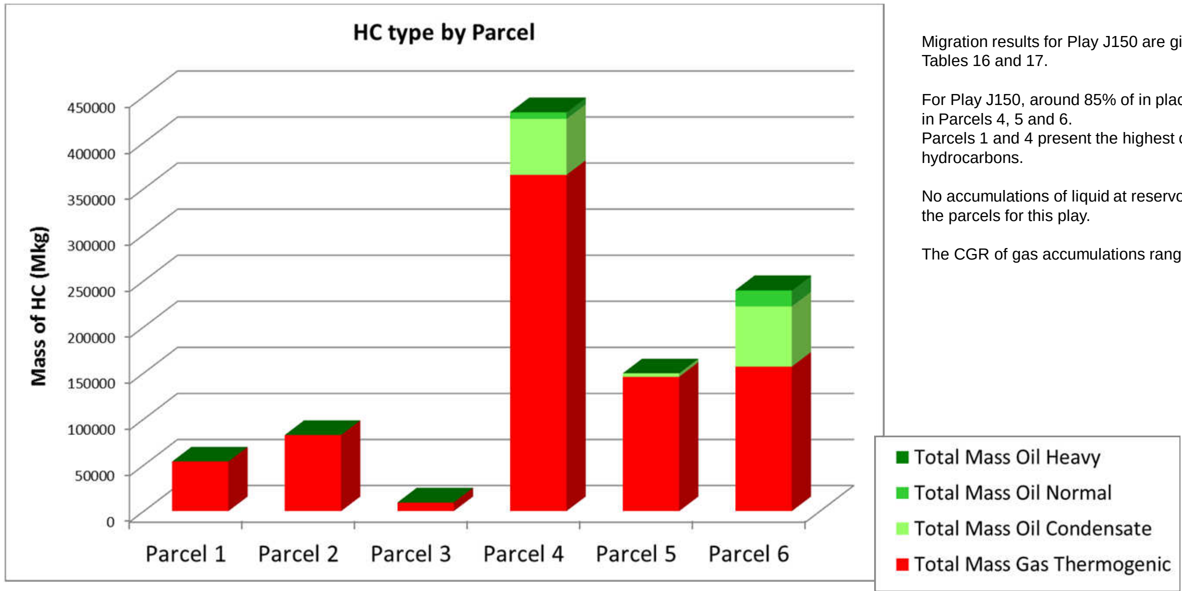

Figure 83: Distribution of hydrocarbons masses per Parcel and per Fractions

Migration results for Play J150 are given in Figures 82 and 83 and Tables 16 and 17.

For Play J150, around 85% of in place hydrocarbons are expected in Parcels 4, 5 and 6.
Parcels 1 and 4 present the highest concentration of hydrocarbons.

No accumulations of liquid at reservoir conditions are reported in the parcels for this play.

The CGR of gas accumulations ranges from 0 to 113.

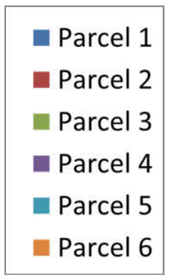

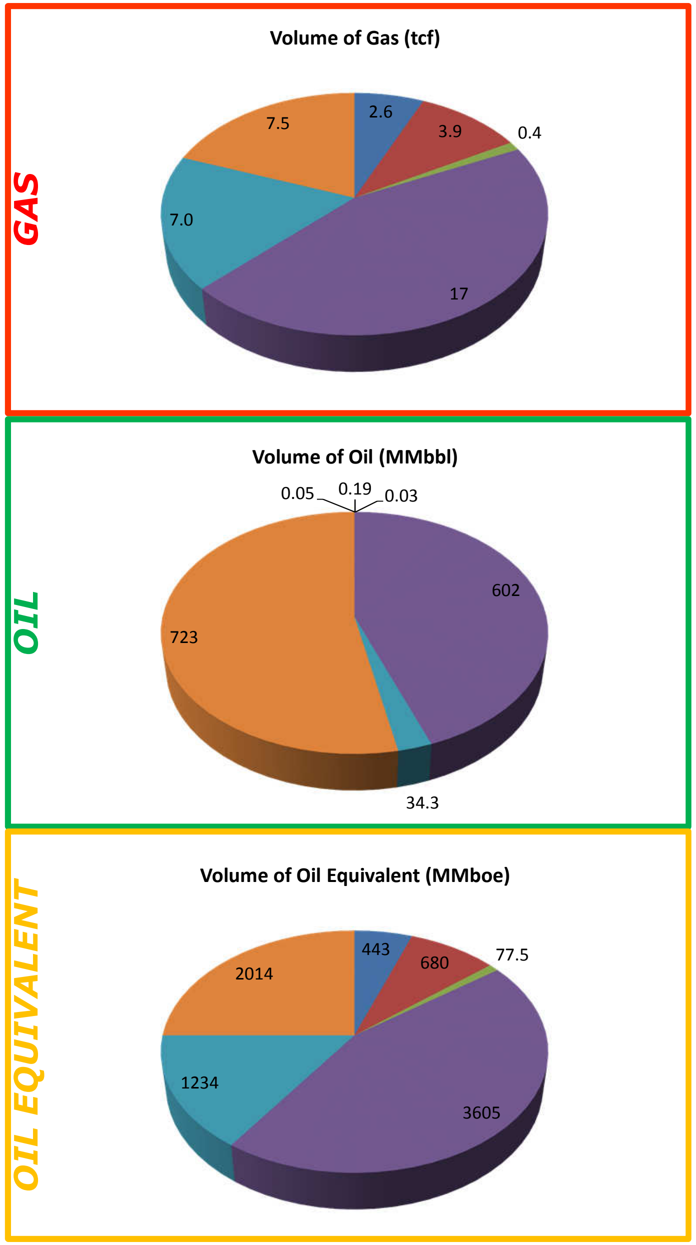

Figure 82: Distribution of hydrocarbon volumes per Parcel.

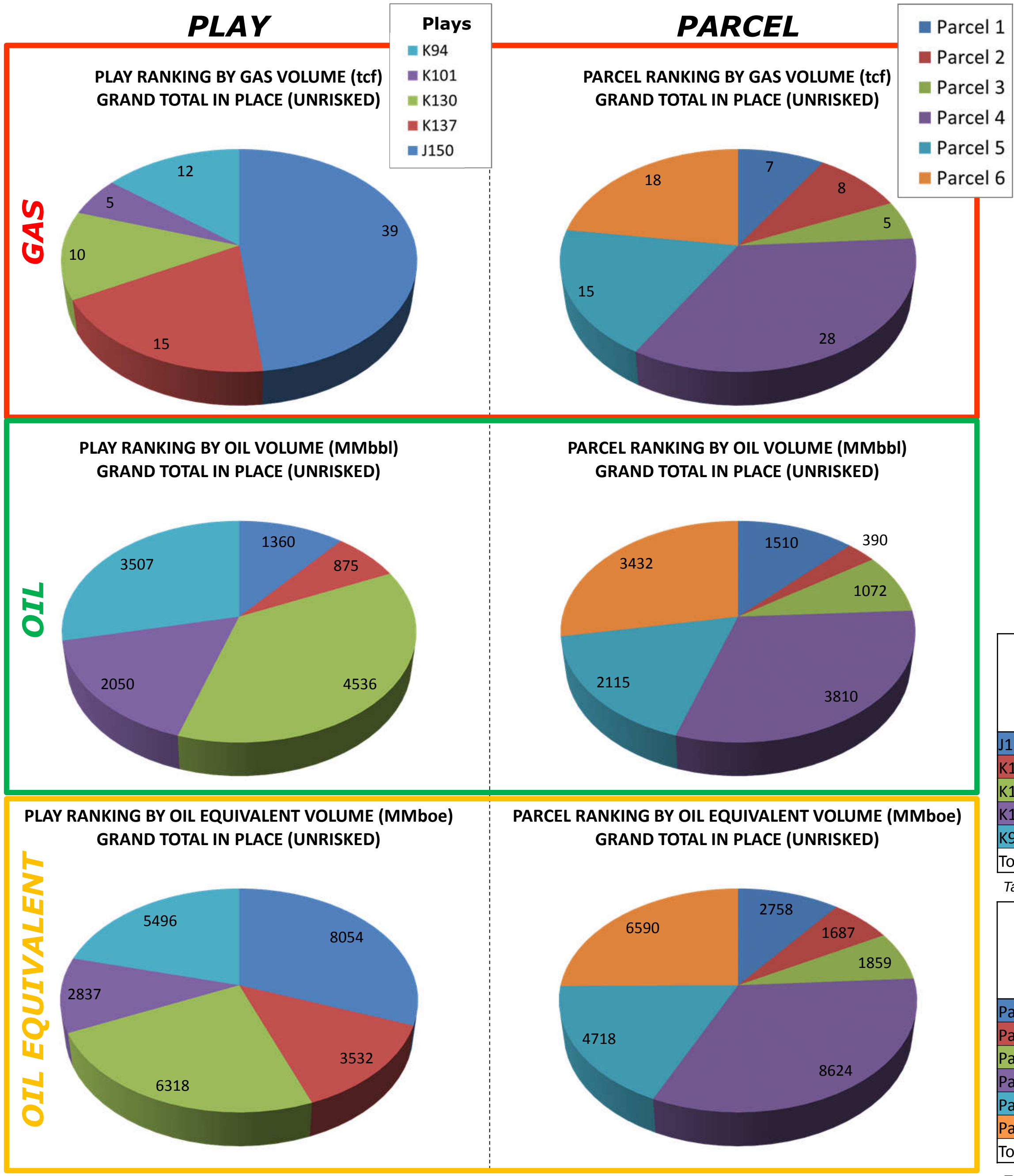

Figure 84: Distribution of hydrocarbon volumes per Play and per Parcel.

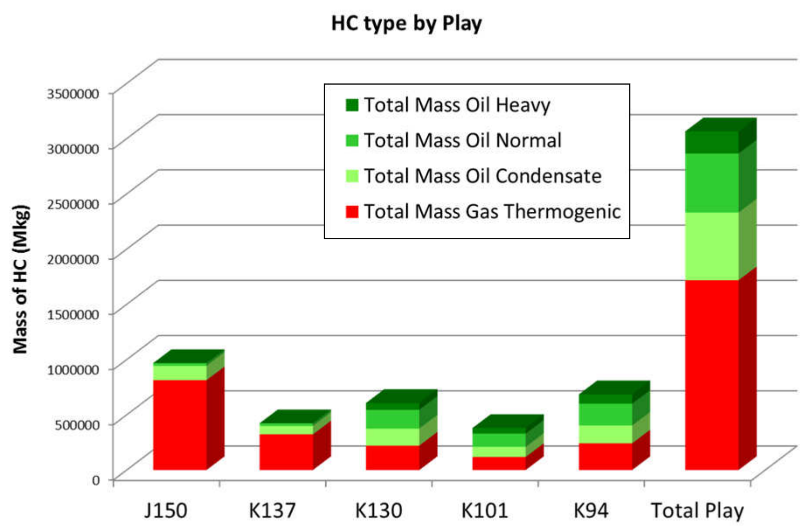

Figure 85: Distribution of hydrocarbons masses per Play and per Fraction.

Play	Grand Total: Vol Gas (tcf)	Grand Total: Vol Oil (MMbbl)	Grand Total: Total Volume (MMboe)	Volume per Surface Unit: Vol Gas (bcf/km²)	Volume per Surface Unit: Vol Oil (Mbbl/km²)	Volume per Surface Unit: Total Volume (Mboe/km²)
J150	39	1360	8054	2	66	394
K137	15	875	3532	1	43	173
K130	10	4536	6318	1	222	309
K101	5	2050	2837	0.2	100	139
K94	12	3507	5496	1	171	269
Total Play	81	12328	26236			

Table 18: Volume of Hydrocarbons and Volume per Surface Unit per Play

Parcels	Vol Gas (tcf)	Vol Oil (MMbbl)	Total Volume (MMboe)	Vol Gas (bcf/km²)	Vol Oil (Mbbl/km²)	Total Volume (Mboe/km²)
Parcel 1	7	1512	2760	31	6418	11718
Parcel 2	8	392	1689	10	501	2158
Parcel 3	5	1072	1859	5	1144	1984
Parcel 4	28	3762	8576	8	1031	2350
Parcel 5	15	2063	4667	6	799	1807
Parcel 6	18	3319	6477	1	270	528
Total Parcels	81	12120	26028	4	592	1272

Table 19: Volume of Hydrocarbons and Volume per Surface Unit per Parcel.

Play and Parcel Ranking – In Place - Unrisked

GAS

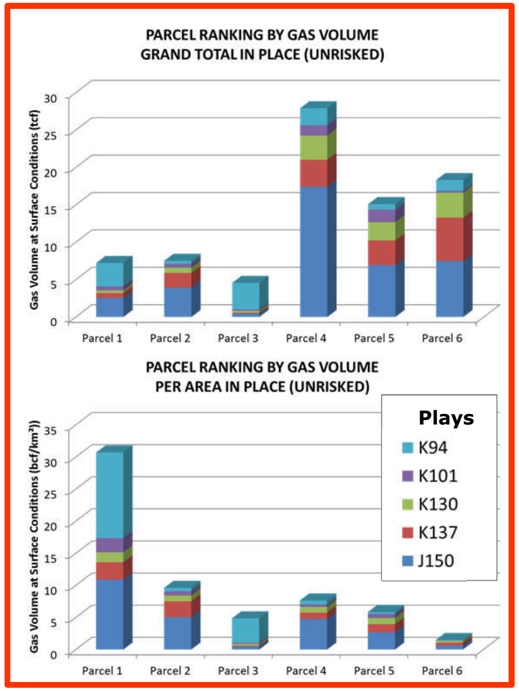

OIL

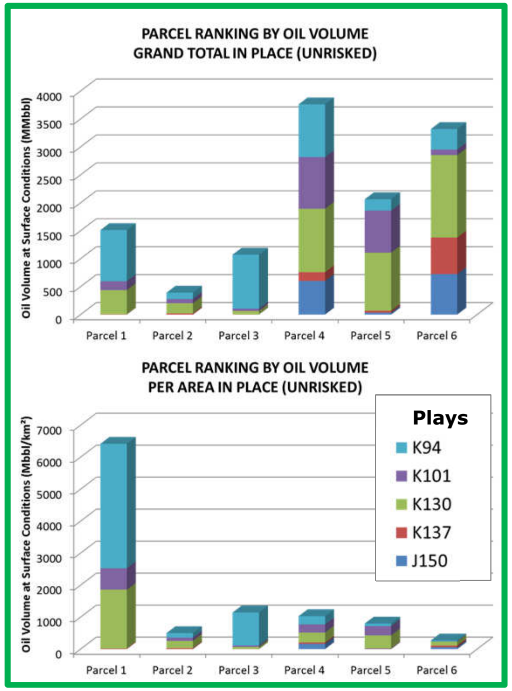

OIL EQUIVALENT

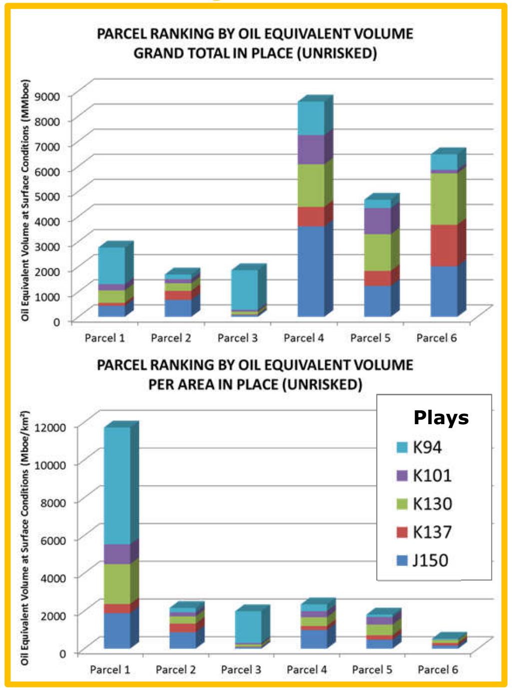

Figure 86: Distribution of hydrocarbons volume per Play and per Parcel

ZONE RANKING (Total Volume / Volume Per Area)

Assumptions

Volumes calculated by TemisFlow® are In Place and Unrisked.

Main assumptions are:

- Four potential source rocks are considered.
  - Tithonian SR, Toarcian SR, Pliensbachian SR and Sinemurian SR.
  - Source rock distribution, richness, and thickness are uncertain. Presence of organic-rich layers is not proven at the scale of the basin, particularly for the Lower Jurassic Complex.
- Five active play systems are considered.
  - Upper Cretaceous K94 and K101, Lower Cretaceous K130 and K137, Upper Jurassic (J150).
- Reservoir layer distribution, quality, and thickness are uncertain, particularly for Jurassic play system, and in deep water zones.

All closed structures (4 ways, traps against salt or faults) are considered if the porous volume exceeds 1E6 m^3, even subtle ones (in term of closure height and reservoir thickness). All reservoir layers, whether scattered in the play system or with low "net to gross", which may be considered as non economic and/or insignificant in production tests, are accounted for in the calculation of unrisked volumes of oil and gas in place. In addition, the volume calculation takes into account reservoir porosity whatever porosity, without discrimination by any sort of minimum porosity threshold above zero.

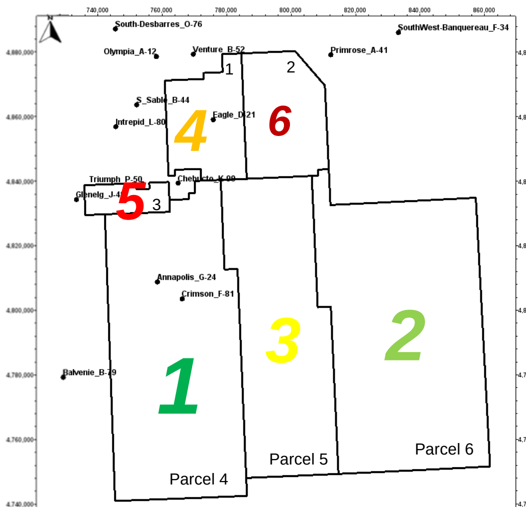

Ranking per Volume

Ranking is presented in Figures 86, 87 and 88.

Parcel 4 is the richest in terms of total hydrocarbon volume (oil equivalent) as it is ranked first for both gas and oil volume. Generally, the deep water parcels (4, 5 and 6) contain the highest volume of hydrocarbons because they contain the largest number of structures.
The large amount of gas in the deepest plays can be explained by both primary generation from gas prone Type II-III Tithonian SR and secondary cracking of oil generated by Lower Jurassic source rocks during its migration. The large amount of oil in the shallower plays results from the maturity level of the Tithonian SR.
The parcels on the shelf (1, 2 and 3) present limited amounts of oil and gas, oil being present in the shallower plays and gas being more distributed vertically.

If volumes are divided by surface areas of each zone ("volume per area" or "volume per surface unit"), Parcel 1 is ranked 1st for both oil and gas volumes. This means that Parcel 1 would contain the highest density of hydrocarbon accumulations.
Regarding the volume of oil equivalent, Parcels 2, 3, 4 and even 5 display values in the same range. This result for Parcels 1, 2 and 3 derives from fault density that scatters the accumulation with a possibility of high closure height.
In the Parcel 4, it is due to the relatively homogenous distribution of hydrocarbons in the different plays.

Parcel 6 appears the least prospective zone both for oil and gas in volume per area because of the low concentration of structures.

Figure 87: Ranking of the Parcels per volume of hydrocarbons (MMboe)

Figure 88: Ranking of the Parcels per volume of hydrocarbons per Area (Mboe).

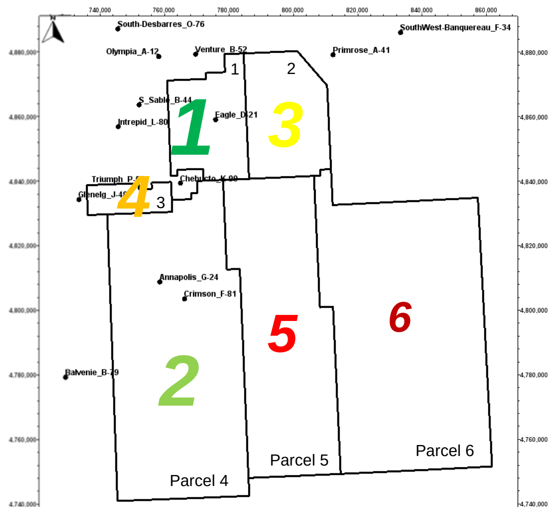

Ranking per Volume per Area